Dissertation

submitted to the

Combined Faculties for the Natural Sciences and for Mathematics

of the Ruperto-Carola University of Heidelberg, Germany

for the degree of

Doctor of Natural Sciences

presented by

Diplom-Ingenieur, MSc, MA, Andrés Carmona Gonzalez

born in Bogotá, Colombia

Oral examination: 25 July 2007

Observational Studies of Gas in Protoplanetary Disks

Referees: Prof. Dr. Thomas Henning

Dr. Mario E. van den Ancker

Abstract – Zusammenfassung

Observational studies of gas in protoplanetary disks

The gas dominates the mass and dynamics of protoplanetary disks. However, very few observational constraints exist about the physical properties of the gas in the planet forming region of the disks. This thesis presents an ensemble of new observational projects aimed at studying the gas in the disks of selected nearby Herbig Ae/Be stars (HAEBES) and classical T Tauri stars (CTTS). In the first chapter we present a search for CO 4.7 μm ro-vibrational emission from HAEBES using ISAAC, ESO's first generation VLT near-infrared spectrograph. In the second chapter, we describe a project in which we intended to probe the outer cold gas of protoplanetary disks, by measuring gas absorption features of the disk superimposed on the optical spectra of close (<1.5") visual companions of nearby HAEBES utilizing FORS2, ESO's VLT optical spectrograph. In the third chapter, we present a large observational effort to detect H_2 fundamental rotational emission at 12.278 and 17.035 μm from HAEBES employing VISIR, ESO's new high-resolution mid-infrared spectrograph. In the fourth chapter, we describe the first results of a sensitive search for near-infrared H_2 ro-vibrational emission at 2.1218, 2.2233 and 2.2477 μm in the CTTS LkHα 264 and the debris disk 49 Cet using CRIRES, ESO's new VLT near-infrared high-resolution spectrograph. From our observations (detections and non-detections), we derive important constraints on the physical properties of the studied disks (e.g. mass, column density, temperature, age, excitation mechanism, inclination). We show that high-resolution infrared spectroscopy is a crucial tool for future studies of the structure of protoplanetary disks.

Beobachtungen von Gas in protoplanetaren Scheiben

Gas dominiert die Masse und Dynamik von protoplanetaren Scheiben. Dennoch sind durch Beobachtungen erst sehr wenige Erkenntnisse über die physikalischen Eigenschaften des Gases in den Planetenentstehungsgebieten der Scheiben gewonnen worden. In dieser Arbeit präsentieren wir eine Anzahl von neuen Beobachtungsprojekten, die das Gas in den Scheiben ausgewählter Herbig Ae/Be Sterne (HAEBES) and klassischer T Tauri Sterne (CTTS) untersuchen. Im ersten Kapitel wird die Suche nach CO Emission (Rotations- und Schwingungsübergänge bei 4.7 μm) von HAEBES mit Hilfe von ISAAC, ESO's Nahinfrarot-Spektrographen der ersten Generation am VLT, erläutert. Im zweiten Kapitel beschreiben wir ein Projekt welches versucht, das äussere, kalte Gas der protoplanetaren Scheiben zu untersuchen. Dies wird erreicht durch die Messung der absorption durch Gas in der Scheibe. Die Absorption ist mit dem mit dem Spektrum eines engen (<1.5") visuellen Begleiters naher HAEBES überlagert. Für die Messungen wurde FORS2 benutzt, ein optischer Spektrograph am VLT. Im dritten Kapitel präsentieren wir ein grosses Beobachtungsprojekt zur Detektion der H_2 Emission (Rotationsübergang bei 12.278 und 17.035 μm) von HAEBES mit Hilfe von ESO's neuem, hochauflösenden Spektrographen für das mittlere Infrarot, VISIR. Im vierten Kapitel beschreiben wir erste Resultate einer sensitiven Suche nach Nahinfrarot-H_2-Emission (Rotations- und Schwingungsübergänge bei 2.1218, 2.2233 und 2.2477 μm) in der CTTS Scheibe LkHα 264 und der "debris disk" 49 Cet unter Verwendung des neuen VLT-Instruments CRIRES, eines hochauflösenden Nahinfrarot-Spektrographen. Basierend auf unseren Beobachtungsresultaten (Detektionen sowie auch gegebenfalls abgeleitete Obergrenzen für gewisse Parameter) können wir wichtige physikalische Eigenschaften der beobachteten Scheiben (z. B. Masse, Säulendichte, Temperatur, Alter, Anregungsbedingungen, Scheibenneigung) entscheidend eingrenzen. Wir zeigen, daß Infrarot-Spektroskopie ein unerlässliches Werkzeug für zukünftige Studien zur Struktur protoplanetarer Scheiben ist.

A la memoria de Beatriz González, mi madre, quien desafortunadamente falleció justo antes de finalizar esta tesis.
A mi padre José Emerio Carmona y su permanente apoyo.

Contents

Chapter 1

Introduction: From Clouds to Disks to Planets

Curiosity is an integral part of human nature. Although it is fair to admit that powerful personal, political and economical interests lay behind many of the titanic adventures of discovery of the natural world, we must also undoubtedly recognize that the sense of wonder is an integral part of our human experience. Our actual understanding of the Universe is the result of the collaborative effort of thousands of inquisitive human minds. An effort of women and men across time, breaking down geographical and cultural barriers.

The very fact of our existence brings us to the fundamental question of our origins. This question, and the related question of whether life is a common phenomena in the Universe as a whole, has been addressed in mythology, religion, philosophy and science. The method for attempting to solve such a fundamental issue, from the scientific perspective, it is to divide the great question into smaller interrelated questions and strive to answer them individually in the frame of a coherent picture. From the astronomical perspective, we start by supposing that life arises on planets, in particular, planets with similar conditions as the Earth. Then, we search to answer more and more detailed questions: do planets exist around other stars? what are they like? are they different to our solar system?, are there planets similar to the earth? how did the solar system form? how did other solar systems form? etc.

In the last decade, hundreds of extrasolar planets have been detected. We can confidently say *planets exist around other stars!*. However, the amazing physical properties of these newly discovered systems (see for example the review by Udry et al. 2007), opened more exciting questions that will keep us wondering for a long time. The heavens are full of new food for the human mind. The Extrasolar Planetary Systems differ greatly from our own Solar System. In the Solar System, the gas giant planets (i.e. Jupiter and Saturn) orbit in almost circular orbits at more than 5 times the distance from the Earth to the Sun (1 AU). In contrast, most of the Extrasolar Planets detected are gas giant planets orbiting at distances amazingly close to their parent stars (a fraction of an AU). In addition, the vast majority of them orbit in eccentric orbits. The impetus of these discoveries reinvigorated the astronomical community's interest in the field of planet formation.

In our present understanding of planet formation, planets form in the disk of gas and dust that surrounds the star when it is young (age < 10 Myr). Gas giant planets were formed from the vast reservoir of gas. Terrestrial planets were formed from the dust. The protoplanetary disk's mass and dynamics are almost entirely dominated by the gas (99%), and its chief constituent being molecular hydrogen (90% of the gas). The dust, an almost negligible constituent of the total mass, is, however, the main source of opacity. Dust regulates the thermodynamics of the disk and is the easiest observable disk constituent. For this reason most of our knowledge about protoplanetary disks (mass, geometry, size, composition) has been inferred from investigations of dust emission. In contrast, studies of the gas are relatively rare. Nevertheless, if we want to

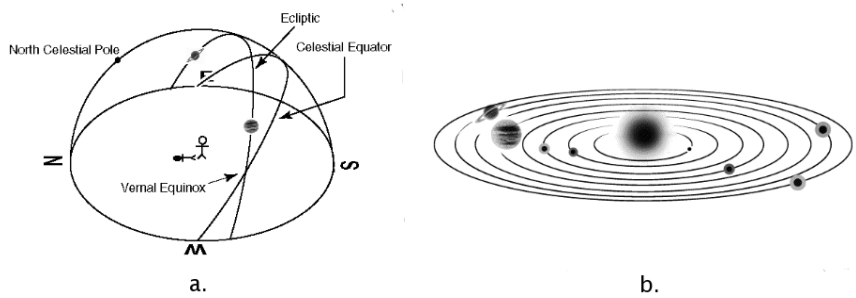

Figure 1.1: *Viewed from the Earth planets are located in an imaginary arc on the sky: the Ecliptic (a). This geometry implies that planets, including the Earth itself, orbit the Sun in the same plane (b). This and the fact that all the planets orbit in the same direction were the first hint that planets formed from a disk surrounding the young Sun.*

answer major questions in planet formation such as: How massive are the disks? how extended are the disks? and how long do protoplanetary disks last? we require information about the gaseous component of the disk. Specifically, there is important progress to be made in the study of warm gas in the inner disk (R < 50 AU), the region where gas giant planets form. The aim of this thesis has been to constrain the disk's gas properties observationally by employing spectroscopy in the optical, near and mid-infrared. But before discussing this thesis, lets start with a brief introduction to the general topic of star and planet formation.

1.1 How did we arrive at idea that planets form in disks?

On some clear nights we are fortunate to be able to see how the stars revolve magnificently over the celestial dome during the night, and perhaps, if we are more attentive, we realize that the constellations appearing in the sky slowly change from one season to another. We now know that these motions of the stars are due to the rotation of our own planet and its orbital motion around the Sun. The apparent distance between the stars does not noticeably change in the life span of a human being. However, in addition to the Moon and the Sun, there are five conspicuous bright objects that move with respect to the stars. The greeks called these lights $\pi\lambda\alpha\nu\eta\tau\nu\eta\zeta$ (planètès) a word that means "wanderer". Nowadays these objects are called Planets and their names are familiar to most of us: Mercury, Venus, Mars, Jupiter and Saturn. These objects have an interesting and fundamental characteristic: they are always located along or very close an imaginary arc on the sky named the Ecliptic (see Figure 1.1a). Their motions have a curious characteristic: they first move forward, then backwards, and forward again. The motion of the planets intrigued the human mind for eons.

It seems that one of the first people to understand this retrograde motion, and that planets and the Earth are objects orbiting the Sun, was Aristarco of Samos around 200 B.C. (Sagan 1980). Nevertheless, this conclusion needed to wait for Copernicus around 1500 and the untiring efforts of Johanes Kepler in 1600 to be widely accepted. Once the heliocentric model was accepted, another subtle, but fundamental property emerged: *all the planets orbit the Sun in the same plane, and in the same direction!* (see Figure 1.1b). This flattened orbital configuration inspired many

that tried to understand the origin of our planet and the Solar System. Two of them were the philosophers Immanuel Kant and later Pierre-Simon Laplace, who advanced, around the second half of the 18^{th} century, the idea that planets formed in a flat nebula surrounding the primitive Sun. We now know that their conclusion is fundamentally correct, but we should keep in mind that this theory was only one of several other possible theories proposed at the time. For example, the idea that the Solar System formed by a cataclysmic event, i.e. material stripped from the Sun by a close approach of a nearby star, was much more favored than the nebular hypothesis [1] until almost the first half of the 20^{th} century. The nebular hypothesis gained more support, and finally the status of paradigm, when astronomers searching to understand the process of star formation realized that disks are a natural product of this process. Therefore, before discussing planet formation theories and the observational evidence for disks, let us discuss how stars form.

1.2 Star Formation

With the determination of the distance between the Earth and the Sun [2] and the development of the theory of gravity[3], by end of the 17^{th} century the mass of the Sun was determined. Given the apparent size of the Sun, it was demonstrated that the Sun is composed of gas. On a clear and dark night some fuzzy extended structures can be observed, "Nebulae" as early astronomers named them. With the advent of telescopes, more of these "Nebulae" were discovered. Around the beginning of the 18^{th} century, William Herschel, who systematically catalogued the Nebulae, proposed based upon on the shapes and sizes of the Nebulae and stellar clusters, that Nebulae condensed due to gravitation and formed a star (or stars). Astronomical photography at the end of the 19^{th} century, showed that several "Nebulae" are in fact other kind of objects (galaxies and planetary nebulae among others). However, by that time it was clear that stars form from gas clouds[4].

Naked-eye observations of the Milky Way reveal that there are several regions which are obscured (i.e. where we do not see stars). These dark spots are regions where the light gets absorbed by material lying in the line of sight. Photographic images of the edges of obscured regions, the discovery that the color of distant stars is redder, and the fact that in several spectroscopic binaries the Na I absorption feature at 5890 Å remained constant through their period, pointed to the existence of important amounts of gas and dust between the stars, the so called Interstellar Medium (ISM)[5]. The existence of copious amounts of interstellar gas was dramatically confirmed later in the 1950's, when radio observations revealed the existence of giant molecular clouds.

A molecular cloud is a physical entity in equilibrium between two forces: the gravitational force, that tends to contract the cloud, and the pressure forces, that tend to expand the cloud. The gravitational and pressure forces are in equilibrium in a cloud. Gravity depends uniquely on the cloud mass, but pressure depends on many factors: turbulent motions, temperature and

[1] For example, Sir James Jeans, famous for his studies of gravitational collapse, did not believe the nebular hypothesis.

[2] In 1672 Giovanni Cassini and Jean Richer determined the distance to Mars and were thereby able to calculate the distance to the Sun.

[3] The *Principia* of Newton were published in 1687.

[4] For example by 1885 Paul & Posper Henry obtained the first images of the Pleaides, confirming the faint nebulosity long suspected by visual observations.

[5] The ISM is constituted ~99% from gas and ~1% from dust. Since the density of cold molecular gas is extremely low in the ISM, lower than the best vacuum obtained on earth, the extinction is caused by dust particles.

electromagnetic forces. At some point in the life of a molecular cloud the equilibrium is broken, the gravitational force wins over the pressure forces, and in special locations of high density, named cores, the cloud collapses due to its own gravity[6]. Since stars are observed to form in groups, it is very likely that these collapsing processes occur simultaneously in several regions of the cloud. Cores of different masses collapse giving birth to stars of different mass[7]. As most young stars are multiple, it is probable that large cores fragment to give birth to smaller cores and therefore to multiple systems. In an alternative scenario, small close cores accrete the material from the surroundings competitively.

Independent whether the core is massive or light, the collapse involves a change of dimension of almost five orders of magnitude. Since the angular momentum must be conserved during the collapse, the material can not fall directly to the center. Angular momentum should be lost by outer material in order to cause the central object to increase its mass. The conservation of angular momentum produces a flattened structure. Copious material from the collapsing cloud continues falling from an envelope onto the flattened structure, and from the flattened structure, the gas find its way to the central object. Since important amounts of angular momentum should be lost, during this stage, outflows and jets (exporting the angular momentum) are launched. Once the infall of material stops, the flattened structure evolves to an even flatter structure with a disk-like shape. The disk surrounding the newly formed star, a direct by-product of the star formation process, is the scene of the vicissitudes of the formation of planets. These protoplanetary disks are a source of wonder and astonishment for many contemporary astronomers that try to understand, how nature manages to form objects of thousands of kilometers in size from the microscopic dust grains and minuscule gas molecules of the ISM.

Since science is in part the art of creating a set of conceptual categories for describing events of the natural world and make sense of them with coherent models, based upon observations of the Spectral-Energy Distribution (SED)[8], a set of classes of objects describing the process of star formation has been introduced[9]. In Figure 1.2 we show a cartoon describing the process of single star formation (right), together with the SED characteristic of each stage (left). The history of a star starts with a clump or dense pre-stellar core that is only visible in the (sub)-mm. When the pre-stellar core is in process of collapse, we have a Class 0 object. Its SED displays only far-infrared ($\lambda > 24\ \mu$m) and (sub)-mm light emission. When the collapse ends and the object starts to be visible in the near-infrared, we have a Class I source. The SED displays the black body emission from the newly formed central source (that radiates by gravitational contraction) and the emission of the envelope that dominates the IR flux. A Class I object is an infrared protostar. When the accretion of the envelope ends and the star starts to be visible in the optical, we have a Class II object. The SED is now dominated by the black-body emission of the central source, and the near, mid-infrared and sub-mm flux over the photospheric level is emitted by a circumstellar

[6] For a detailed review of the process of single isolated star formation see Shu et al.(1987). For a more recent and more "dynamical" picture of the process where turbulence of the cloud is taken into account, see Ballesteros-Paredes et al. (2007).

[7] The Jeans mass defines the minimum critical mass for which a cloud collapses and the maximum mass for which the material can collapse but not fragment. It is very exiting to live in a time when the existence of objects with masses below the minimum Jeans mass, and massive cores well above the maximum Jeans mass has been demonstrated. How these objects form is question of fierce debate and research.

[8] An Spectral Energy Distribution (SED) is the amount of light that an astronomical object emits at each wavelength.

[9] In Lada (1988) the reader can find a very good description of the classes of young objects.

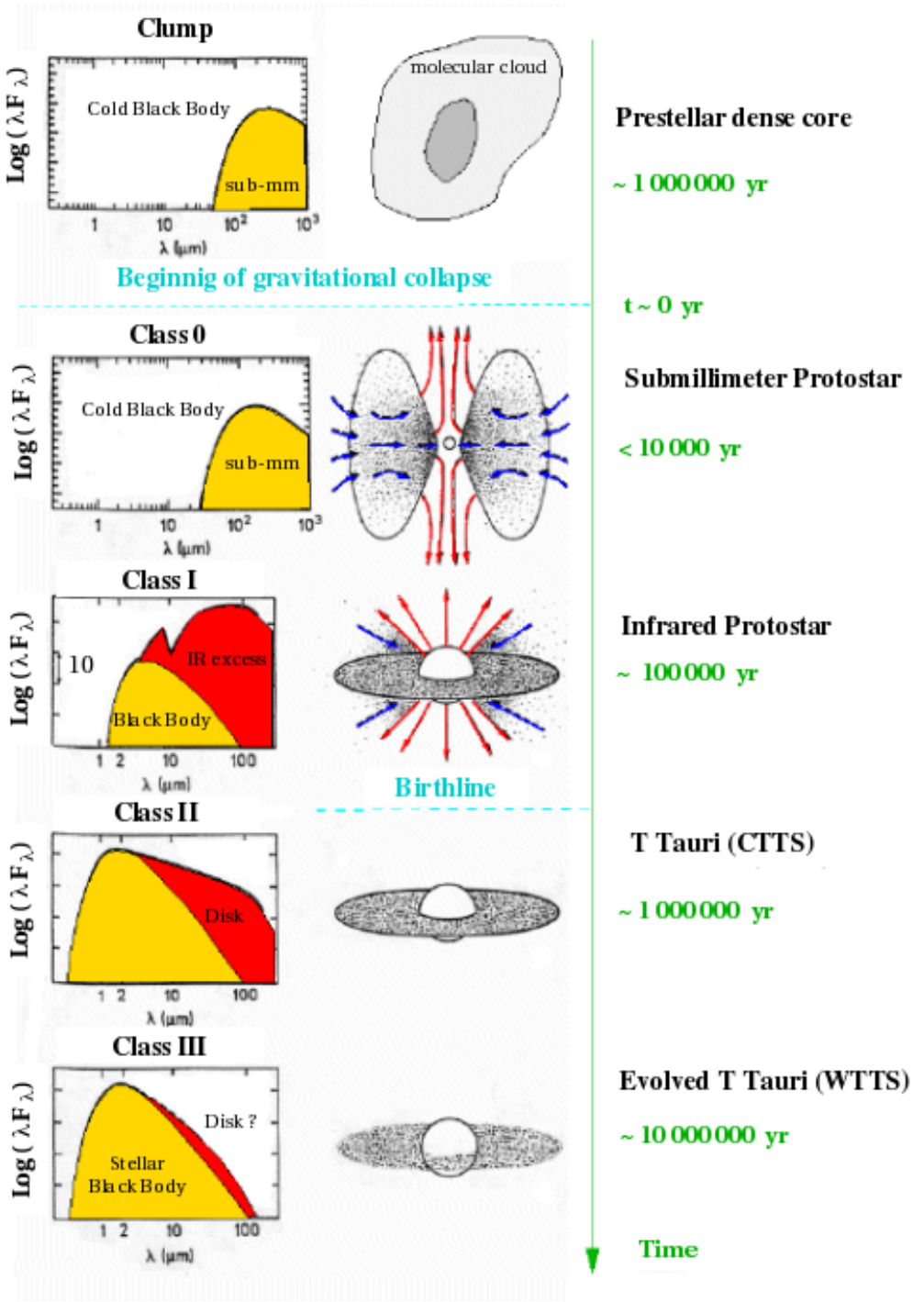

Figure 1.2: *Infrared/Submillimeter Young Stellar Objects classification. Image credit: CEA Service d'Astrophysique. Lada et al. (1988), Andrè et al. (1993).*

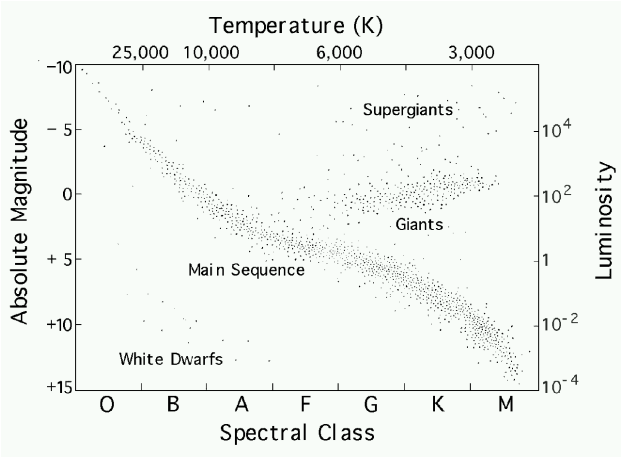

Figure 1.3: *Example of the HR diagram. Most of the stars are in the main-sequence phase.*

disk[10]. When the disk dissipates, we have a Class III source. Then, the SED is entirely dominated by the central star blackbody emission at all wavelengths.

The fact that circumstellar disks are a direct product of star formation strongly suggests that planet formation, or at least the initial conditions of planet formation, are a common phenomenon in the galaxy. If planets are common, it is not unlikely that life could arise in at least some of these worlds. Before beginning the discussion of the structure of protoplanetary disks, let us dedicate some lines describing their young host stars, and to discuss the observational signatures that allow one to identify them.

1.3 Pre-main sequence stars

Simple naked eye observations reveal that stars have diverse brightness, and colors. The advent of photographic plates in astronomy around the middle of the 19^{th} century, allowed the brightness and the colors of the stars to be systematically quantified the by imaging obtained with different sets of filters. The parallel development of spectroscopy permitted the realization that there is a link between the spectrum observed, the colors, and the photospheric temperature. At the beginning of 20^{th} century, when estimations of stellar distances (by parallax) and spectral types were available for a significant number of objects, stars were plotted in a two-dimensional diagram, relating their intrinsic brightness (i.e. the luminosity or total energy liberated per unit of area) and their spectral type (i.e. effective temperature). This diagram, the Hertzsprung-Russell diagram (see Figure 1.3), revealed that the vast majority of the stars lie in a diagonal band: the Main Sequence.

From the beginning of stellar spectroscopy, it was suspected that different spectral types corresponded to different stages of stellar evolution[11]. With the introduction of the H-R diagram, the idea was extended to the hypothesis that different positions should correspond to different stages

[10] In fact a disk-like structure is the only configuration that allows one to observe optical and infrared emission simultaneously. For example, a sphere-like shape will absorb all the visible light and we will see only an IR source.

[11] This is the historical reason why we refer to the O, B and A spectral types as early, and the spectral types G, K, and M as late.

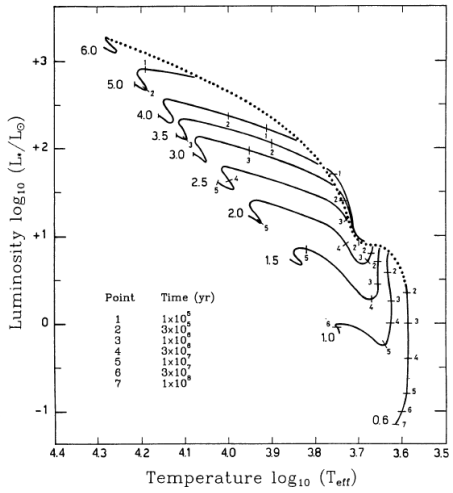

Figure 1.4: *Zoom on the HR diagram displaying the theoretical evolutionary tracks of the pre-main-sequence phase for stars of low- and intermediate-mass. Palla & Stahler (1993).*

of stellar evolution. Several evolutionary models were proposed, but it was only until it was determined that the source of energy are nuclear reactions, that the correct sequence was established. A main-sequence star is a star that is in equilibrium between the gravitation and the gas pressure generated by the energy released from nuclear fusion of hydrogen into helium. In most of its life a star is sustained by hydrogen burning. This is the reason why a large majority of stars, including the Sun itself, are located in the main-sequence.

Stars that have not yet started the fusion of hydrogen into helium are named pre-main-sequence stars (PMS). Correspondingly, the period between becoming visible in the optical (stellar birthline, see dotted line in Figure 1.4) and the main-sequence is called pre-main-sequence phase. During this phase the star for evolves from a Class I object to a Class III object. This period last up to 100 Myr for a 0.5 $M_\odot$ low-mass star, and is shorter for higher masses (see Figure 1.4). Pre-main sequence stars are fueled by gravitational contraction and deuterium burning. In low-mass ($M < 1.2M_\odot$) PMS stars, the energy is transported from the interior to the surface by convective motions[12]. For stars with higher masses, the transport of energy from the center to the surface is done by radiation.

1.3.1 T Tauri and Herbig Ae/Be stars

Historically, it was known that some bright stars exhibited peculiar behavior, they are variable. Follow-up optical spectroscopy of some of these objects revealed that their spectra were different: they exhibited strong emission lines (especially of hydrogen). Systematic surveys for variable stars combined with narrow band imaging in Hα and follow up optical spectroscopy, revealed that in well defined regions of the sky (e.g. Taurus, Ophicius, Orion) there existed groups of these variable stars with emission lines. These objects were labeled as T Tauri stars (Joy, 1945), based on the name the first of their type discovered. When plotted in the HR diagram, all of them are located in pre-main sequence region.

[12]When a low-mass PMS star gets close to the main sequence, the energy begins to be partially transported by radiation.

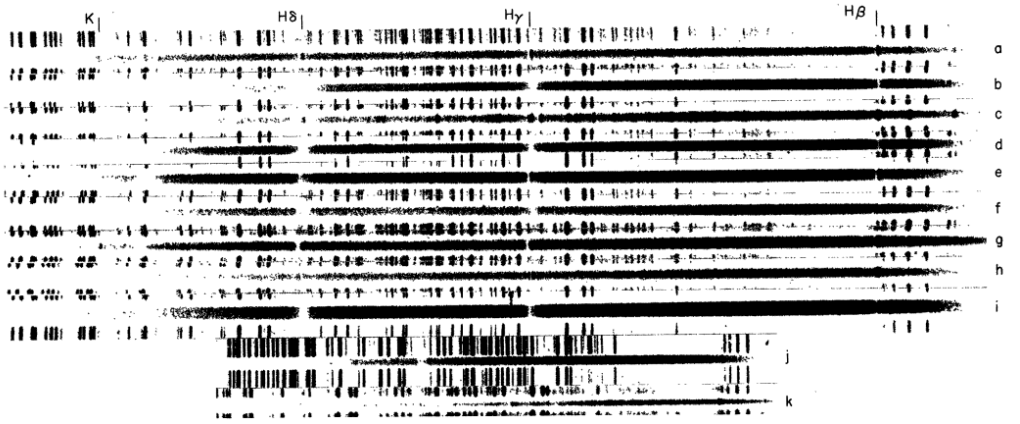

Figure 1.5: *Spectra of Herbig Ae/Be stars from Herbig's 1960 paper: a) +61° 154; b) T Ori; c) V380 Ori; d) RR Tau; e) HD 250550; f) LkHα 15; g) Z Canis Majoris; h) +40°4124; i) +46° 3471; j) MWC 497; k) MWC 1080.*

Emission lines, in particular the H_α line at 6563 Å, the Na line at 5890 Å and the Ca triplet at 8000 Å , indicate the presence of gas at temperatures hotter than the photosphere of the star. Developments in the last two decades (see for example the book by Hartmann 2001), convincingly suggest that these lines are the imprint of accretion of gas from the disk to the central object. Other signs of youth are present in their spectrum. For stars with masses < 1.2 $M_\odot$, the presence of Lithium in absorption at 6728 Å is an additional indicator of youth (Skumanich 1972). Lithium is present in the molecular cloud that forms the star. As the star's center reaches high temperatures the Lithium starts to get burned. Convective motions transport the Li from the colder outer layers to the interior where it is processed. At their arrival on the main sequence, low-mass stars have depleted their Li and the line at 6728 Å is not observed in their photospheres anymore.

In the 1960s, Herbig (Herbig 1960) suggested that the equivalent of the low-mass T Tauri stars should exist for the intermediate mass (2-8 $M_\odot$) range. He found several stars of spectral types A and B exhibiting emission lines (H_δ, H_γ, H_β, see Figure 1.5) situated close to reflection nebula. These intermediate mass pre-main sequence objects are now called Herbig Ae/Be stars [13].

Later on, in the 70s and the 80s the development of IR astronomy revealed that T Tauri and Herbig Ae/Be stars have emission excess over the photospheric level in the infrared (e.g. Rucinski 1985). Then, the evidence that T Tauri stars should be surrounded by a disk became stronger and stronger. Developments of UV astronomy, revealed that T Tauri stars exhibit an UV excess too. Also in the 80s (e.g. Hartmann & Kenyon 1985) it was advanced that the UV excess, the emission lines and the veiling[14] can be understood as the signatures of magnetospheric accretion of gas from the disk onto the central star.

The development of X-ray astronomy revealed that T Tauri stars are strong emitters of X-rays as well (e.g. Feigelson & Decampli 1985). In addition, in the same regions of the sky where emission-line T Tauris are located, X-rays surveys revealed the existence of other pre-main-sequence objects with similar X-ray activity, but their spectra exhibited weak emission lines or no

[13] For an introductory review see Waters & Waelkens (1998).

[14] Continuum emission that fill-up absorption lines in the optical spectra of T Tauri stars. Its net effect is to make the spectra look flat.

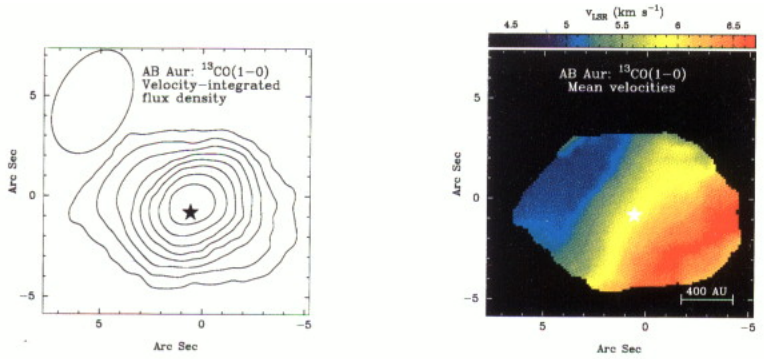

Figure 1.6: *Spatially resolved CO emission at sub-mm wavelengths demonstrated that Herbig Ae/Be stars are surrounded by disks. Mannings & Sargent (1997).*

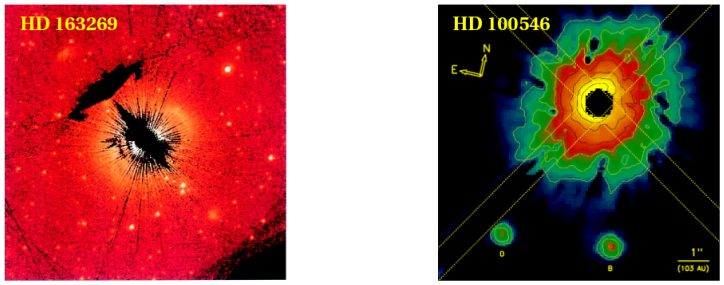

a) **b)**

Figure 1.7: *HST coronographic imaging of dust-scatered light confirmed the disk-like shape of the circumstellar material around Herbig Ae/Be stars. a) HD 163296 Grady et al. (2000). b) HD 100546 Augereau et al. (2001).*

emission at all. Since their SED do not exhibit IR excess, it was proposed that these new objects are devoid of disks. They are named weak-lined T Tauri stars (WTTS), and they are thought to be the evolved counterparts of the emission-line "classical" T Tauri stars (CTTS).

The geometry of the material around Herbig Ae/Be stars, was debated for a long time. SED models with disks or spherical envelopes of small dust particles fitted the SED's equally well. Their emission lines can be explained with an accretion model or by a wind model too. Given that the Herbig Ae/Be stars are much brighter that their low mass T Tauri counterparts and that their spectra are almost featureless, the UV excess and veiling produced by accretion could not be discerned to favor the accretion scenario. In the 1990s spatially resolved cold dust emission and spatially resolved cold gas CO emission revealed that the circumstellar material should have a disk geometry (e.g. Mannings & Sargent 1997, see Figure 1.6). In the last decade, coronographic imaging of scattered-light revealed unambiguously the disk-like shape of the circumstellar material around Herbig Ae/Be stars (e.g. Grady et al. 2000, Augereau et al. 2001 see Figure 1.7).

Given that accretion is as important as the reprocessing of the stellar light in the energy balance in disks around T Tauri stars, we call these disks *active disks*. In Herbig Ae/Be stars, the main source of energy in the disk is the reprocessing of the stellar light. We call their disks *passive disks*. Having briefly discussed the observational signatures of their host stars, we can start our

discussion about the observational study of protoplanetary disks. However let us discuss first some basic issues concerning planet formation theories.

1.4 Planet Formation

How nature manages to form planets from the small micron size particles present in the interstellar medium is an intriguing question. At the present, we have some ideas, however, the issue is still far from being concluded. For attacking the problem, first we should recall that there are three kinds of planets in the Solar System. The terrestrial planets (Mercury, Venus, the Earth, Mars) are relatively small ($R_\oplus \sim 0.01 R_\odot$), dense and composed mostly of rock. The gas giant planets (Jupiter, Saturn) are large ($R_J \sim 0.1 R_\odot$), light and composed mostly of gas. The ice planets (Uranus, Neptune) have an intermediate size ($R_N \sim 0.04 R_\odot$) and are composed principally of ice. The process of planet formation should reflect the different kinds of planets in our Solar System, and the characteristics of the Extrasolar Planets detected (i.e. gas planets in close orbits to the star and large eccentricities).

1.4.1 Terrestrial Planet Formation

Globally there is consensus on the way terrestrial planets form. Terrestrial planets form from the dust particles in the inner disk. The details of how this occurs are however still in development. The first problem is the initial step of growth, from micron to cm size grains. In a hydrostatic and non-turbulent disk, dust particles grow in size by collisions and settle down to the mid-plane of the disk (Safronov 1966). The process of growing to a cm size particle is relatively fast (less than 10^5 years, see Dullemond & Dominik 2005). The growth from cm dust pebbles to km sized planetesimals is also terra incognita because of the quick radial drift of m-sized bodies (Weidenschilling 1977) and poor sticking efficiency of pebbles and boulders (Benz 2000). One suggestion is that planetesimals form by the gravitational instability of a mid-plane sedimentary layer of dust (Safronov 1966, Goldreich & Ward 1973). However, turbulence prevents the formation of the very thin mid-plane layers that are necessary for such a process to occur (Goldrecih & Ward 1973, Weidenschilling & Cuzzi 1993). Newer findings nevertheless show that turbulence can also concentrate solids (Johansen, Klahr, & Henning 2006) so that the formation of planetesimals by self-gravity remains viable. When solid bodies reach km size, gravitational focusing starts becoming important (Stewart & Wetherill 1988). Few of these embryos will experiment run away-growth emptying their zones of gravitational influence (feeding zones). These embryos will suffer further collisions until they arrive at the terrestrial planet mass regime. However, if the gaseous disk has not been dissipated at the time they form, their inexorable destiny will be to plunge into their parent star, by the tidal interaction with the disk (Goldreich & Tremaine 1980, Ward 1997). Another intriguing question is the role of the presence of a migrating giant-planet in evolution of the terrestrial planets. At the time of writing it is not well understood whether giant planet migration inhibits or perturbs terrestrial planet formation, or by the contrary, if it enhances it (Mandell et al. 2007).

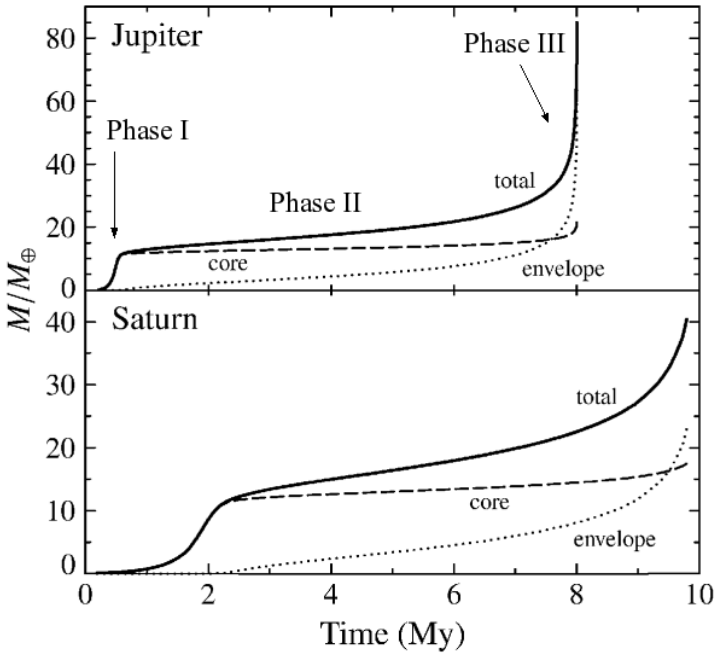

Figure 1.8: *Evolution of the masses of Jupiter and Saturn as a function of time in the context of the core accretion model (Pollack et al. 1996).*

1.4.2 Giant Planet Formation

The formation of giant planets is an area of strong debate in our time. The gas in the nebula should suffer an instability for increasing its density by a factor of five in forming a giant planet. The source of this instability is the center of the debate. In one scenario, the Gravitational Instability (GI) scenario (Kuiper 1951, Cameron 1978, Boss 1997), the gas is cold and dense enough in some regions of the disk that it becomes gravitationally unstable. The gas collapses by its own gravity and forms a giant planet in a time scale comparable to the dynamical time scale of the disk ($\sim$ 1000 yr). This scenario requires a disk that is cold and massive. Massive disks are perfectly possible, especially in the early stages of disk evolution. A very effective cooling mechanism is required to lower the temperature to the instability limit and to continue cooling the disk once the instability is turned on (Gammie 2001). However, no convincing mechanism for cooling has been found to date. Gas cooling by line emission, for example, is far too slow to provide the cooling that GI needs. An additional concern with this scenario is the metal enriched chemical composition of giant planets with respect to solar abundances. Accretion of planetesimals has been proposed as possible solution to this issue, however, accretion rates need to be large to explain Jupiter's composition. A final concern is that it is still needed to be convincingly demonstrated that clumps and banana shaped zones of enhanced density found in the simulations can survive enough time to produce a planet, in other words, it is necessary to establish that they are not transient phenomena in an unstable disk.

In a second scenario, the Core Accretion model (Safronov 1966, Pollack 1996), the source of instability in the gaseous disk is the presence of a core of $\sim$ 12 Earth ($M_\oplus$) masses. This core,

expected to be formed in a time scale shorter than 1 Myr (Phase I), starts to accrete the gaseous material in its surroundings forming a gaseous envelope slowly (Phase II). At the moment in which the envelope reaches a mass comparable to the central core, a phase of run-away gas accretion begins (Phase III) and in a very short time scale the mass grows from ~ 30 $M_\oplus$ to a Jupiter mass (318 $M_\oplus$, see Figure 1.8). The main concern of this scenario is the time scale (> 10 Myr) required for Phase II. Protoplanetary disks, as we will see in next section, seem to disappear in a time scale shorter than the time scale required by Phase II. In addition, modeling of the interior of giant planets based on space craft data suggest that Jupiter has a small core, or no core at all (it depends strongly on the equation of state chosen, Guillot & Chabrier 1999). The core-accretion mechanism is the favored mechanism for planet formation in the literature. It can explain the chemical composition of Jupiter, does not require a very narrow set of disk conditions to happen, and naturally explains the higher detection rate of extrasolar planets in stars with high-metallicity (Kornet et al. 2005). However, the time scales required are strongly related to unknown opacities and the initial swarm of planetesimal chosen. In addition, in this scenario is hard to form giant planet more massive than 5 M_J or located at distances much larger than 5 AU.

1.4.3 Some additional open issues

Besides the incertitude of the mode of giant planet formation, and the caveats and limitations of each model, there are other fundamental issues that still need to be resolved. For example the migration stopping mechanism. A large number of extrasolar planets orbit very close to their parent stars. The tidal interaction of the disk with the planet causes the orbital drift of the planet towards the star (Goldreich & Tremaine 1980). This migration phenomena has been suggested as explanation for the close-in extrasolar planets detected (Lin et al. 1996). In Type I migration, planetesimals and low mass planets drift very fast inwards and they are quickly depleted because they fall onto the star. In Type II migration, a planet of 1 M_J opens a gap in the disk, and the tidal interaction with the disk moves it inwards in a time scale of 10^5 years. Without a migration stopping mechanism, most giant planets will end up engulfed by their parent stars. But, if most planets migrate, one natural question is, why did Jupiter stay where it was formed?.

Another fundamental issue are the eccentricities. The vast majority of the Extrasolar Planets have eccentric orbits. Only the closest planets, that have been tidally circularized, appear to have circular orbits, almost all of the rest have an eccentricity. To date there is not a convincing explanation for this. In addition, recent detections of extrasolar planets by the transit method, revealed that extrasolar giant planets have an unexpected variety of densities. Finally, although it is well established that a great majority of the stars are part of a binary or multiple system, that the multiplicity fraction increases as the stars are younger (Duquenoy & Mayor 1991) and that radial velocity surveys revealed the planets are also present in multiple systems (see review by Desidera et al. 2007), the real effect that multiplicity has in the formation of planetary systems still needs to established.

After briefly discussing the theories of planet formation, we realize that it is important to understand the protoplanetary disk structure and evolution to be able to constrain possible planet formation scenarios. In the next section we will discuss the observational study of disks.

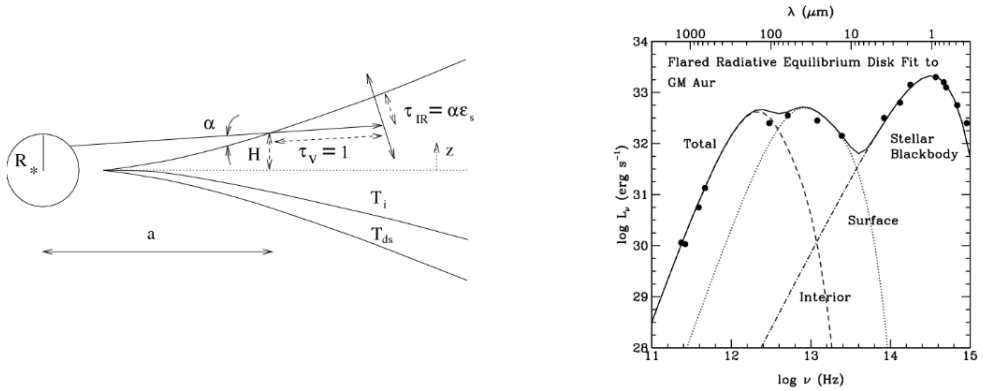

a) **b)**

Figure 1.9: *Chiang & Goldreich (1997) two-layer model of a protoplanetary disk. a) The radiation of the star strikes the surface at an angle α and it is absorbed within visible optical depth of unity. Dust particles are superheated in the surface layer at a temperature T_{ds}. About half of the emission from the surface layer emerges as dilute blackbody radiation. The remaining half heats the interior to a lower temperature T_i. b) Two-layer model fit to the SED of the classical T Tauri star GM Aur. The contributions of stellar blackbody, the surface and the interior are indicated in solid, dot-dashed and dashed lines respectively.*

1.5 The observational study of protoplanetary disks

1.5.1 Modeling of the Spectral Energy Distribution

The primary indication of the existence of disks is the infrared emission excess over photospheric levels in pre-main sequence stars with emission lines (e.g. Medoza, 1966). Therefore, the first attempts to understand the structure of the disks were based on the modeling of the Spectral Energy Distribution (SED). At first, it was assumed that the disk had a flat geometry, that it was composed of dust with ISM composition and size distribution and that the gas-to-dust ratio was 100 (e.g. Adams et al. 1987). The SED was fitted with a disk of decreasing surface density as a function of radius obeying a power law with index -1.5. However, the infrared emission at 3 microns and the mid-infrared emission were systematically underestimated by this model. The next idea suggested that the disk was a passive disk in hydrostatic equilibrium and that it flared as a consequence of the heating of the disk surface by the radiation of the central source (Kenyon & Hartman 1987, Chiang & Goldreich 1997). The SED was then understood as the emission of superheated small dust particles in the hot surface layer of the disk (Chiang & Goldreich 1997, see Figure 1.9). This two-layer disk model is able to successfully reproduce the mid-infrared emission; however, the origin of the 3 micron "bump" observed in Herbig Ae/Be stars remained unsolved. Most recent developments extended the two-layer model, introducing an inner rim at the dust sublimation radius (T~ 1500K, Dullemond et al. 2001). The inner-rim is directly heated by stellar radiation, and its vertical scale height is increased. The hot dust in the rim is responsible for the 3 μm emission (see Figure 1.10 panels a and b). The existence of the inner rim introduced the possibility of having two flavors of disks: i) The self-shadowed disks, where the inner rim

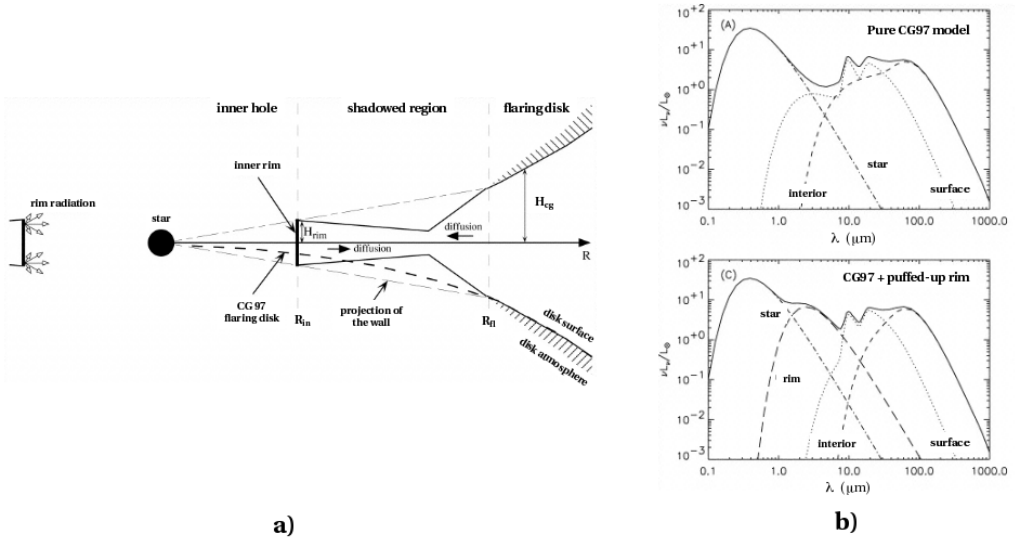

Figure 1.10: *a) The puffed-up inner rim hypothesis introduced by Dullemond et al. (2001) in the CG97 two-layer model explained the emission bump at 3μm observed in Herbig Ae stars.*

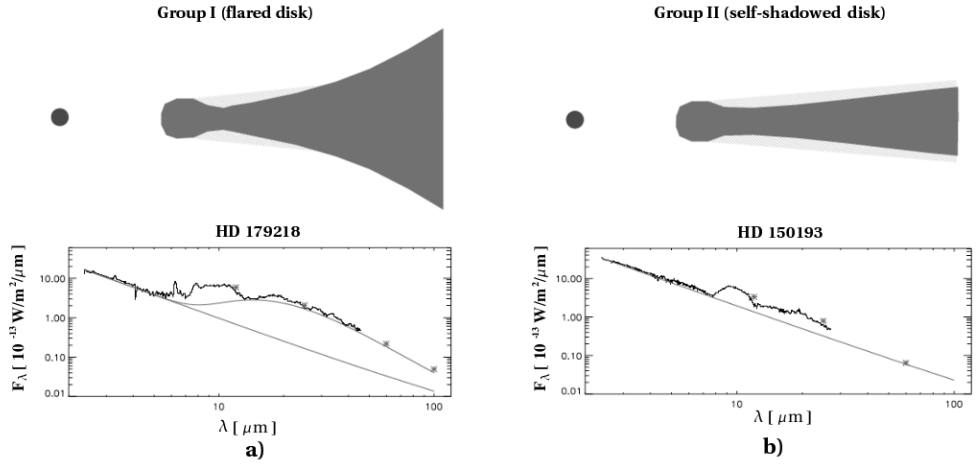

Figure 1.11: *The puffed-up inner rim model permitted us to understand the two groups of SED (rising and flat) observed by Meeus et al. (2001) as flared disks (group I) and self-shadowed disks (group II). Dullemond and Dominik (2004).*

shadows the outer part of the disk, and ii) the flared-disks, where the disk flares just after the inner rim (Dullemond & Dominik 2004, see Figure 1.11 panels a and b). These two kinds of disk geometries are able to explain the two classes of SED (flat and rising) that were observed towards Herbig Ae/Be stars by the Infrared Space Observatory (Meuss et al. 2001). Group I sources are sources with rising SEDs (flared disks, see Figure 1.11a) and Group II sources are sources with flat SEDs (self-shadowed disks, see Figure 1.11b).

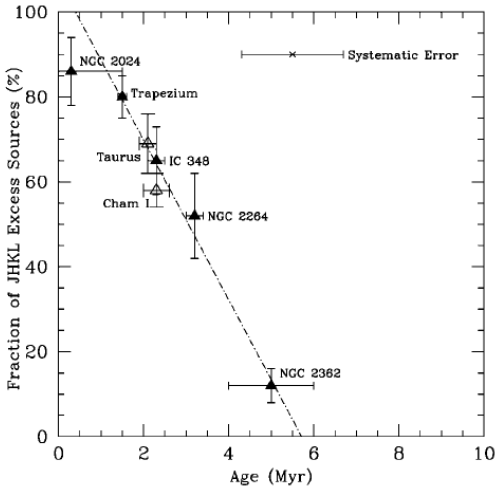

Figure 1.12: *JHKL excess/disk fraction as a function of cluster age (Haisch et al. 2001)*

1.5.2 The disk dissipation time scale

In surveys of a large number of sources, the primordial sign of a disk presence is the location in the JHK color-color diagram. Sources with infrared excess occupy a particular area in such a diagram. When clusters of young stars of diverse ages[15] were studied in near-infrared surveys, it was noticed that the fraction of sources with JHK IR excess (i.e. with disk) decreased as a function of the cluster age. When the fraction of sources with disks is plotted against the cluster's age and the plot is extrapolated, it is found that disks should disappear in a time scale of 6 Myr (Haisch et al. 2001, see Figure 1.12). This time scale is shorter than the giant-planet formation time scale by the core accretion mechanism. Therefore there is a conflict between the disk's life time and the time scale for giant planet formation. However, we should keep in mind that the NIR excess only probes small hot dust particles in the surface layer in the innermost part of the disk. The lack of NIR excess could be explained as the result of a distribution of large dust grains (i.e. an opacity gap) or by the opening of a gap in the inner disk (i.e. a physical gap). One important question that needs to be addressed observationally is whether the dust dissipation time scale deduced from the NIR is similar to the dissipation time scale of the gas. We do know, that special sources exist in which the NIR signature of the disk has disappeared, but they exhibit MIR excess at 24 and 70 micron. Some of these transitional objects exhibit H_α in emission, suggesting the presence of warm gas in the inner disk (Sicilia-Aguilar et al. 2006), while other sources (e.g. 49 Cet) show CO emission at sub-mm wavelengths (Dent et al. 2005), indicating a reservoir of cold gas in the outer disk. The study of transitional objects is important in order to understand the late evolution of the disk and the earliest times of planetary systems.

[15]The age is calculated by locating the cluster members in the HR diagram.

1.5.3 The disk's mass

Dust particles responsible for the near- and mid-infrared excess are small heated particles in the upper layers of the disk. However, most of the disk's mass is in cold material. Cold gas and dust are located in the disk's mid-plane and the outer disk (R>50 AU). Cold material emits at (sub)-mm wavelengths. Disks are optically thin in the (sub)-mm, therefore, dust continuum emission can be used to derive the total disk's mass. Assuming an interstellar medium gas-to-dust ratio of 100, the dust continuum flux measured at 1.3 mm can be directly translated into an estimate of disk mass:

$$M_{disk} = \frac{F_{1.3\mathrm{mm}}\, D^2}{\kappa_{1.3\mathrm{mm}} T} \tag{1.1}$$

Where $F_{1.3\mathrm{mm}}$ is the measured flux, $\kappa_{1.3\mathrm{mm}}$ the dust opacity and T the dust temperature. Using this technique, the mass of an important fraction of protoplanetary disks has been estimated (e.g. Beckwith et al. 1990, Henning et al. 1994, Osterloh & Beckwidth 1995, André et al. 1995). The disk's masses range from a tenth of Jupiter mass up to a few hundred Jupiter masses.

We should note that besides the uncertainty in κ and T, this technique has a strong limitation: the gas-to-dust ratio is expected to change in the disk as planets form, and the amount of dust grains at mm wavelengths is not representative of all the solid material. For example, if the gas to dust ratio is smaller than 100, the technique overestimates the disk's mass. Alternatively, if most of the solid material in the disk has sizes larger than a few cm; we will severely underestimate the total gas mass. Therefore, independent estimations of the gas mass are crucial for establishing the total mass of the disk (we will discuss the studies of the disk gas in section 1.5.6).

1.5.4 Direct evidence for disks

In previous sections we discussed that by modeling the dust continuum emission (i.e. the SED) we can learn a great deal about the structure and geometry of protoplanetary disks. But, is there direct evidence for disks?. Yes there is plenty of direct evidence. The first image of a circumstellar disk was obtained more than 20 years ago in 1984 by coronographic [16] observations of the debris disk β Pictoris (Smith & Terrile 1984, see Figure 1.13a) shortly after IRAS discovered far-infrared excess in the star (Aumann et al. 1984). Coronography is a technique designed to detect the scattered light of the small dust particles present in the surface of the disk. It has been widely used with the Hubble Space Telescope for imaging protoplanetary disks around nearby stars (see, for a review, Grady et al. 2005, Figure 1.7). In recent years, coronagraphy has been used in large telescopes equipped with Adaptive Optics as well (e.g. Fukagawa et al. 2004). This technique has been mostly used for studying the disks of nearby face-on Herbig Ae/Be stars. We learned that their disks can extend as much as 400 AU and that they are not uniform. The images reveal rings and spiral structures. A similar technique (in some lucky cases) consist of using the inclination of the disk as a natural coronograph. In edge-on disks, the dust in the disk occults the central source and the disk-scattered light is observable. The result: a beautiful butterfly shape (e.g. Burrows 1996, McCaughrean 1998, Stapelfeldt et al. 1998, Padgett et al. 1999, see Figure 1.13b).

Another technique used is to observe the disk not in emission, but in absorption against a bright background. Dust particles in the disk absorb background light and the disks are detected

[16] Coronography consists of masking the light of the bright central source and integrating long enough until the tenuous light from the surroundings is obtained.

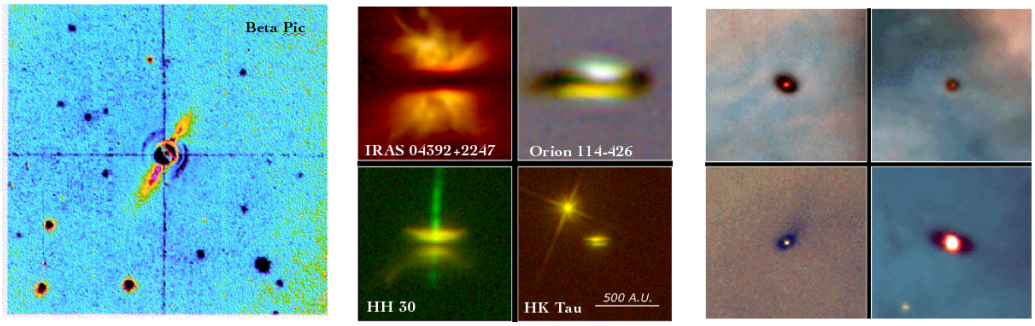

Figure 1.13: *Direct evidence of circumstellar disks. a) First image of a circumstellar disk using coronography (β Pic, Smith & Terrile, 1984). b) HST images of edge-on disks (Padgett et al. 1999, McCaughrean et al. 1998, Burrows et al. 1996, Stapelfeldt et al. 1998). c) HST images of disks in absorption against the bright background in Orion (McCaughrean et al. 1996).*

as dark shadows against the bright surroundings. In this way, an impressive confirmation of the disk paradigm has been achieved by the discovery of a significant number of protoplanetary disks in Orion (e.g. O'dell et al. 1993, McCaughrean et al. 1996). Protoplanetary disks are observed as black spots against the bright emission from the background cloud (see Figure 1.13c). From measurement of disk sizes in Orion (Vicente & Alves 2005), it was confirmed that disks extend several hundred of AU (the distribution peaks at 200 AU).

Finally, the emission of cold dust and gas the in outer part of the disk has been spatially resolved with sub-mm interferometry (e.g. Mannings and Sargent 1997, see Figure 1.6). From sub-mm observations we learned that disks can extend up to 1000 AU and that the gas in the outer cold disk is rotating with a Keplerian velocity profile.

1.5.5 Disk dust composition and mineralogy

The study of mid-infrared spectra of protoplanetary disks allows us to disentangle the mineralogy of the emitting grains. By modeling mid-infrared spectra of Herbig Ae/Be stars, it was found that grain sizes in the disks can differ significantly from those in the interstellar medium (ISM). Amorphous silicates were found to make up the bulk of the dust mass. However, the shape of the 10 μm emission feature shows that in several sources crystalline silicates are an important constituent as well. ISO spectra revealed that other minerals as such as fosferite, magnetite, olivine, and piroxens should be present in disks as well (Bouwman et al. 2000, see Figure 1.14a). One astonishing discovery made by ISO showed that the mid-infrared spectrum of an evolved Herbig Ae star (HD 100456) closely resembles the spectrum of the comet Hale-Bop (Malfait et al. 1998, see Figure 1.14b). This result suggests that the same kind of elements present in our Solar System are common in other planetary systems in the process of formation. Recent developments in high spatial resolution interferometry in the mid-infrared (MIDI at ESO-VLT) revealed that the dust composition in disks around Herbig Ae/Be stars varies as a function of the distance to the central object. The dust in the inner part of the disk is rich in crystalline silicates, while the dust in the outer part of the disk is rich in amorphous silicates (van Boekel et al. 2004, see Figure

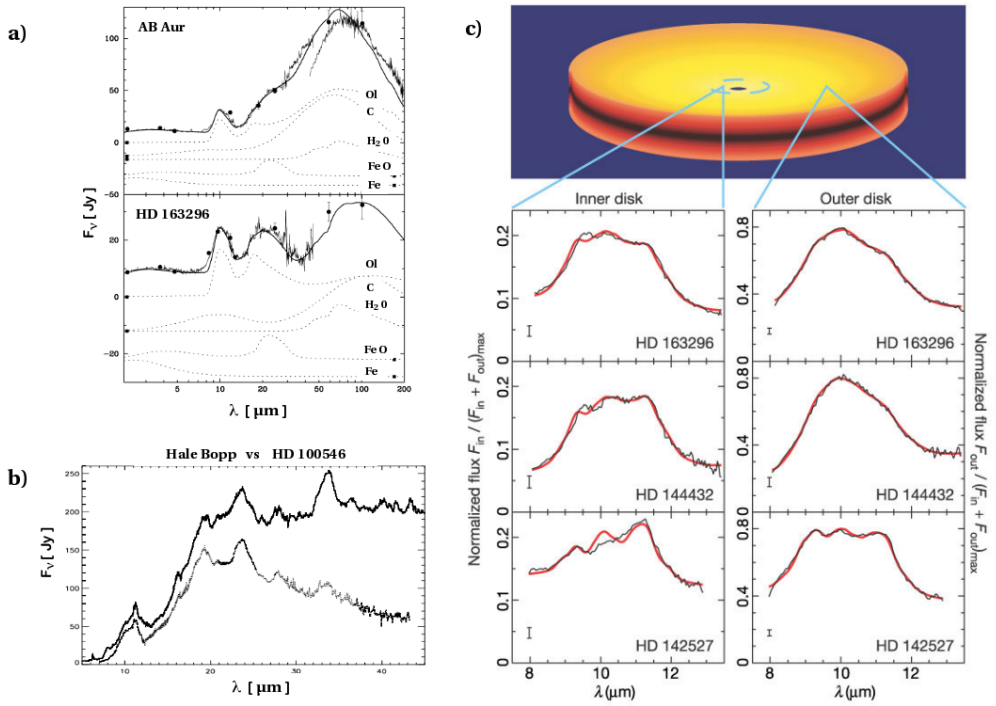

Figure 1.14: *a) Dust species employed to model the ISO mid-infrared spectra of the Herbig Ae stars HD 163296 and AB Aur (Bouwman et al. 2000). b) The ISO spectra of the Herbig Ae star HD 100546 is very similar to the spectra of the comet Hale-Bopp (Malfait et al. 1998) c) Mid-infrared interferometry at ESO-VLI revealed that the dust composition varies as a function of radius in Herbig Ae stars. The inner disk is rich in crystalline silicates. The outer disk is rich in amorphous silicates (van Boekel et al. 2004).*

1.14c). This discovery indicates that the dust is considerably reprocessed in the disk. Finally, the combined analysis of mid-infrared spectra and SED modeling in a large sample of Herbig Ae stars show that a correlation exists between the geometry of the disk (flared or self-shadowed) and the dust size. Self-shadowed disks have, on average, larger grains than flared disks (Acke et al. 2004).

1.5.6 The study of the gas

Interesting insights on the physics of disks have been obtained employing the dust. However, fundamental issues remain unanswered because of intrinsic limitations in the study of the dust. These limitations include: (1) *Dust is not the chief constituent of the material in the disk.* Any conclusion regarding disk dissipation time scales, or the disk mass will be limited by the assumptions made concerning dust composition and the gas-to-dust ratio. If we are interested in knowing when the disk disappears, we need to establish when the disk is depleted of gas. If we are interested in determining the mass of the disk, we need to measure how much molecular hydrogen is in the disk. 2) *Dust spectral features are broad,* therefore, any information about the disk's dynamics is lost. In summary, gas studies are necessary to complement the dust studies in our quest for understanding protoplanetary disks.

The study of gas in the disks is in its infancy. Just in the last few years, with the advent of

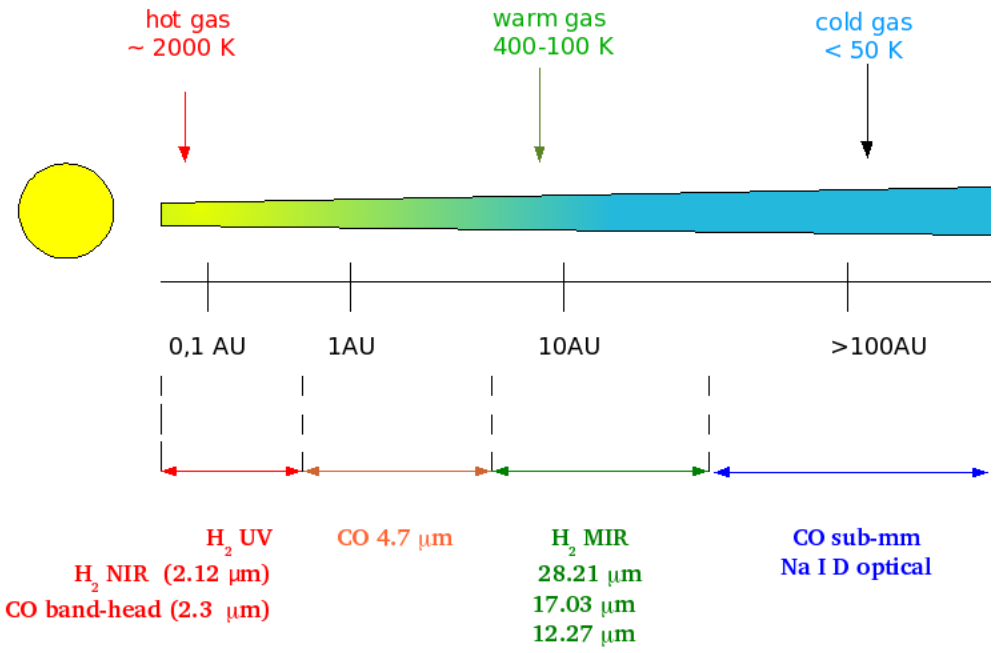

Figure 1.15: *The gas in the disk is studied employing diverse diagnostics according to the gas temperature.*

high-resolution spectrographs, the study of the gas has started in a systematic way. Given that the disk's temperature varies as a function of radius across the disk, several disk diagnostics exist. Each diagnostic probes a particular region in the disk. In Figure 1.15 we present a brief summary of gas diagnostics that can be used for the study of the disk's gas. The innermost ($R <$ few AU) hot ($T >$ 1000K) region of the disk is probed in the ultraviolet and in the near-infrared. The outermost ($R >$ 10 AU) cold (T <50 K) regions are studied in the sub-mm. The intermediate warm region (few AU < R < 50) is investigated in the mid-infrared.

The chief technique for studying the gas is spectroscopy. In general, we search for emission lines of the gas. Emission lines have the imprint of the physical conditions of the media where they were produced. From the strength of the transitions we can determine how many gas molecules are in the state that produces the emissions thereby measuring the density of the gas. From the relative strength between different emission lines of one molecular species and by using rotational diagrams, we can deduce the temperature of the gas. By the line ratios, we can infer the physical process that excites the emission. From the shape of the emission lines and velocity shift with respect to the source, we can infer the dynamics of the gas that produces the emission. In the particular case of protoplanetary disks, **molecular and atomic line emission in the optical and infrared is produced in the surface layers of the disk where the media is optically thin**. These lines are observed because the surface layer of the disk is hotter than the optically thick interior layer. In the (sub)-mm, almost the entire disk is optically thin. Therefore, using (sub)-mm observations we can gain an insight of what is happening in the cold mid-plane and in the outer

disk.

In the following sub-sections we will discuss one-by-one several gas disk diagnostics and what we can learn from them. They are presented in increasing wavelength.

H_2 absorption lines in the UV

If the orientation of the disk is close to edge-on, H_2 gas can be seen in absorption. UV observations measure the column density of the gas in the line of sight. Disk are observed by UV space observatories (i.e. IUE , FUSE)[17]. This technique allowed the measurement of circumstellar gas around a few Herbig Be stars (HD 76534, HD 259431, HD 250550, Martin et al. 2004). Its principal limitations are: i) this technique can only be applied to a small number of sources with the right orientation, ii) only the gas along the line of sight is probed, and iii) the detections could be explained as gas observed in a flared disk, or in a circumstellar envelope/halo surrounding the star.

H_2 emission lines in the UV

This emission can only be observed from space observatories (e.g. HST, IUE, FUSE). Longward of Lyα fluorescent H_2 lines dominate the far-ultraviolet spectrum of classical T Tauri stars (Valenti et al. 1993). These fluorescent H_2 lines are photoexcited by the Lyα emission produced by the accretion shock. The velocity shift of the lines with respect to velocity of the star (up to 20 km s^{-1}) reveals that in most of the cases the origin of the emission is stellar outflows (e.g. Ardila et al. 2002) or emission of shocked gas surrounding ambient molecular material (e.g. Walter et al. 2003). However, at least in three cases (TW Hya, DF Tau, and V836 Tau) the lines observed by HST STIS and FUSE most likely come from a circumstellar disk (Herczeg et al. 2002, 2006, Bergin et al. 2004). From the detected lines the temperature and the column density of hot emitting H_2 can be derived. For example, in the case of TW Hya, detailed modeling of the UV H_2 lines (Herczeg et al. 2004) indicates that a molecular layer with a kinetic temperature of 2500 K and a column density of log N(H_2) = 18.5 absorbs Lyα radiation in the surface layer and inner edge of the TW Hya's disk within 2 AU.

Hα at 6563 Å

H_α is not exactly a direct probe of the properties of the gas in the disk, but it is the prime indicator of gas in protoplanetary disks. H_α emission with large velocity wings (> 100 km/s) provide evidence for accretion. Naturally, for having accretion phenomena gas is required. In addition, if the Hα profile is of typeI P Cygni profile, then the disk inclination can be constrained to be less than 30°. When any other gas diagnostic fails or that the source does not exhibit JHK excess, H_α emission tells us unambiguously that there is gas in the disk (e.g. Sicilia-Aguilar et al. 2006). The opposite scenario - to have a gaseous disk but no H_α emission- is rare, but has been observed. For example 49 Cet, a debris disk, exhibits CO emission in the sub-mm but not H_α. The disk of this object most probably has an inner hole.

[17] IUE = International Ultraviolet Explorer, FUSE = Far Ultraviolet Spectroscopic Explorer

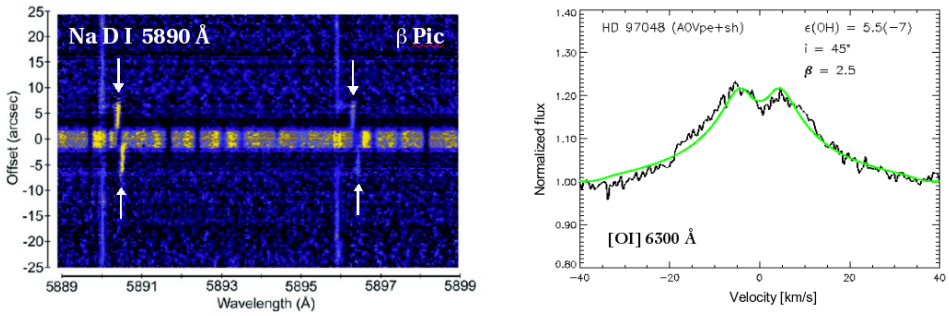

a) **b)**

Figure 1.16: *a) Na I D emission at 5890 Å towars β Pictoris revealed cold gas in keplerian rotation (Olofsson et al. 2001). b) [OI] forbidden emission at 6300 Å probes the ionized surface layer of disks around several Herbig Ae stars. The double peaked profile observed is characteristic of gas rotating in a disk. In green, the model of the spectra is presented (Acke et al. 2005).*

Na I D emission and absorption at 5890 Å

Observed in emission towards the debris disk β Pictoris (see Figure 1.16a), spatially resolved Na I D emission at 5890 Å permitted the discovery of cold gas in keplerian rotation (Olofsson et al. 2001). Monitoring of the Na I D absorption profile towards the edge-on disk of the Herbig Ae star UX Ori revealed a clumpy gaseous structure (Grinin et al. 1994). In the case of having a background source shining through the disk of a nearby source viewed close to pole-on, it is possible to observe the cold gas of the disk superimposed in absorption in the optical spectra of the background object. In Chapter 3 of this thesis we present a project in which we aimed to measure the gas in outer disks of nearby Herbig Ae/Be stars using this technique employing the optical spectrograph FORS2 at ESO-VLT.

[OI] forbidden line at 6300 Å

High energy UV photons and X-rays emitted from the central source ionize the upper layers of the disk. Ionized material at low densities emit forbidden emission lines. One of these atoms is oxygen, which has a forbidden emission line at 6300 Å . High-spectral resolution spectroscopy of this line towards a sample of Herbig Ae/Be stars, revealed a double peaked profile consistent with gas in keplerian rotation (Acke et al. 2005, see Figure 1.16b). Detailed combined modeling of the [OI] line at 6300 Å and the SED in HD 100456 provided evidence supporting the idea that there is a low-mass companion around this Herbig Ae star (Acke & van den Ancker 2006).

H_2 emission at 2.12 and 2.22 μm

In the inner few AU of protoplanetary disks, intense UV or X-ray heating can bring the gas temperatures to a few thousand Kelvin. At these high temperatures, ro-vibrational transitions of H_2 are excited and a rich spectrum of H_2 lines in the near-infrared is expected to be produced. The study of H_2 quiescent ro-vibrational emission permit us to address the question of the presence of hot gas in the disk by probing the temperature and density in the innermost regions where terrestrial planets are expected to form. Usually, the H_2 $\nu = 1 - 0$ S(1) line at 2.1218 μm (one of the

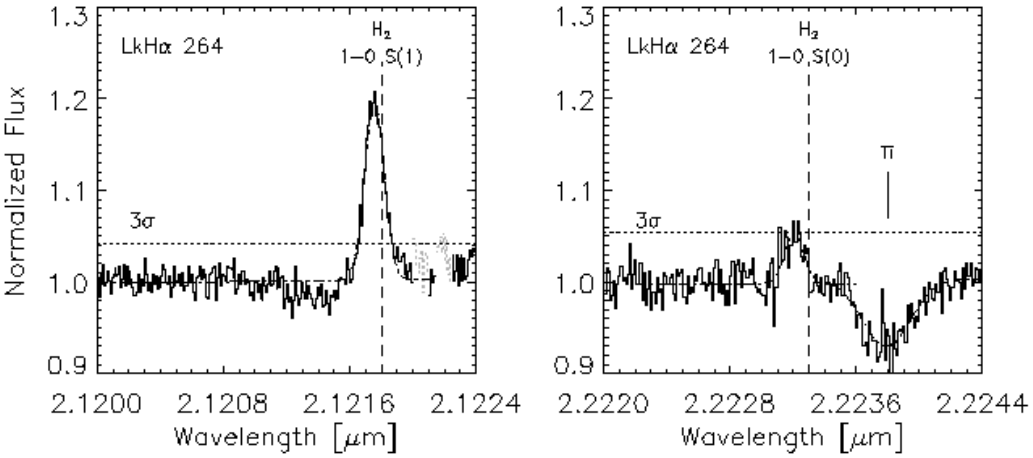

Figure 1.17: *H_2 ro-vibrational emission from the disk around the classical T Tauri star LkHα 264 (Carmona et al. 2007)*

strongest H_2 ro-vibrational lines) is searched for. This line is sensitive to a few lunar masses of gas. The non-presence of the line is strongly suggestive of little or no hot gas in a system. Other lines searched for include the H_2 $\nu = 1 - 0$ S(0) line at 2.2233 μm and the H_2 $\nu = 2 - 1$ S(1) line at 2.2477 μm. In Figure 1.17 we present an example of observations of the 1-0 S(0) and 1-0 S(1) line in the classical T Tauri star LkHα 264. H_2 emission can be the result of thermal (collisions) and non-thermal (radiative decay from excited electronic states) excitation mechanisms. In the thermal case, the gas is heated either by shocks, X-rays or UV-photons. In this case, the H_2 spectrum is characterized by a single excitation temperature typically between 1000 and 2000 K. In the non-thermal case, the electronic excitation results from the absorption of a UV photon in the Lyman-Werner band (912-1108 Å) or the collisions with a fast electron due to X-ray ionization. The $\nu = 1 - 0$ S(0)/$\nu = 1 - 0$ S(1) and the H_2 $\nu = 2 - 1$ S(1)/$\nu = 1 - 0$ S(1) line ratios permit us to constrain the excitation mechanism of the gas. Finally, modeling of the shape of the H_2 $\nu = 2 - 1$ S(1) line allow us to constrain the inclination of the disk. The H_2 $\nu = 1 - 0$ S(1) line has been detected in several classical T Tauri stars and a few weak-lined T Tauri stars (Weintraub et al. 2000, Bary et al. 2003, Itoh et al. 2003, Ramsay Howat & Greaves 2007, Carmona et al. 2007). H_2 ro-vibrational lines are relatively weak lines that require high-resolution infrared spectroscopy to be detected and analyzed. The advent of a new generation of infrared spectrographs in large aperture telescopes such a CRIRES at ESO-VLT will permit the systematic study of the H_2 near-infrared emission from disks in the near future. In this thesis, we dedicate Chapter 5 for discussing a project in which we studied the H_2 near-infrared emission in the classical T Tauri star LkHα 264 and the debris disk 49 Cet employing CRIRES.

CO bandhead emission at 2.3 μm

If the CO gas in the inner part of the disk is hot and dense, emission of CO $\nu = 2 - 0$ transitions are expected. Since the material is rotating at high velocity in the inner region of the disk, the line profiles become severely distorted and overlap with each other. The net combination of the rotational distorted profiles results in the bandhead profile observed (see Figure 1.18). These

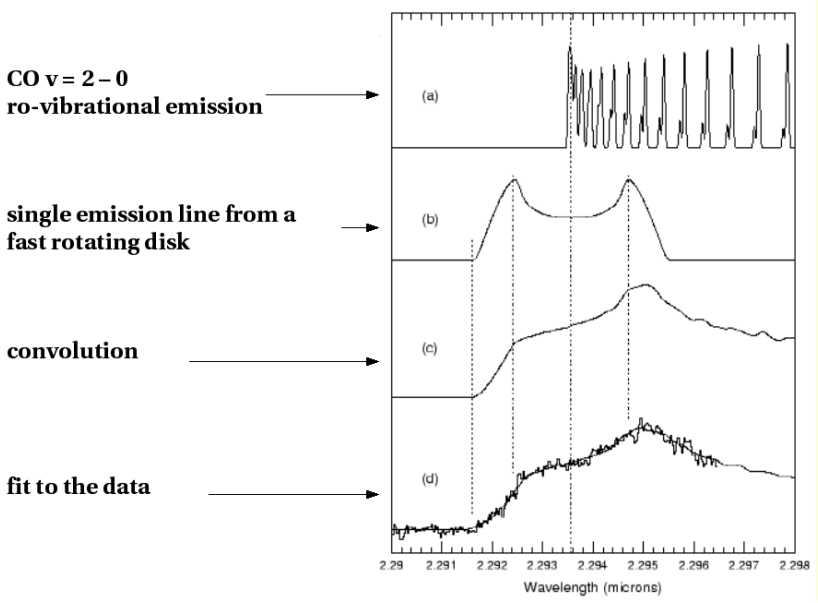

Figure 1.18: *CO $v = 2 - 0$ bandhead emission probes very hot gas in the inner disk. It was one of the first diagnostics employed for studying the dynamics of the gas in the inner-disk (Carr et al. 1993).*

observations tell us about the innermost part of the disk, in the regions close to the accretion funnel flows and the corotation radius of the star and the disk. Since the $v = 2 - 0$ requires a non-thermal mechanism for excitation (i.e. strong UV or X-ray pumping), the CO bandhead is observed in a very small fraction of objects. This diagnostic was one of the first diagnostics confirming that the inner gaseous disk is rotating (Carr et al. 1993). It is important because, it probes the regions of the disk where the dust has been sublimated.

CO ro-vibrational emission at 4.7 μm

The high densities and high temperatures characteristic of the disks in the the inner 5 AU are the medium in which a rich spectrum of CO ro-vibrational transitions are expected. This diagnostic, observed towards an increasing number of Herbig Ae/Be and T Tauri stars (e.g. Najita et al. 2003, Blake and Boogert. 2004, Brittain et al. 2003, 2007, see Figure 1.19a) by the rotational diagram (see Figure 1.19b), tell us about the temperature of the gas in the inner 5 AU (the region where terrestrial planets form). When high spectral resolution is combined with high-spatial resolution (i.e. Adaptive Optics) the region emitting the CO 4.7 emission can be resolved (see Figure 1.19c), and the lines allow us to constrain the dynamics of the inner disk (Goto et al. 2006, see Figure 1.19d). This diagnostic is not only promising for studying the inner regions of disks around T Tauri and Herbig Ae/Be stars, but it would also permit the study of transitional disks and determine if the gap deduced from the SED is a physical gap in the gas distribution or an opacity gap due to change in the optical properties of the dust (i.e. growth and settling). Since CO lines lie extremely close to atmospheric absorption features, CO ro-vibrational emission demands observations with the highest spectral resolution in the near-infrared. Targets need to be observed in periods of high velocity shift to minimize the impact of telluric absorption. New facilities such as CRIRES at

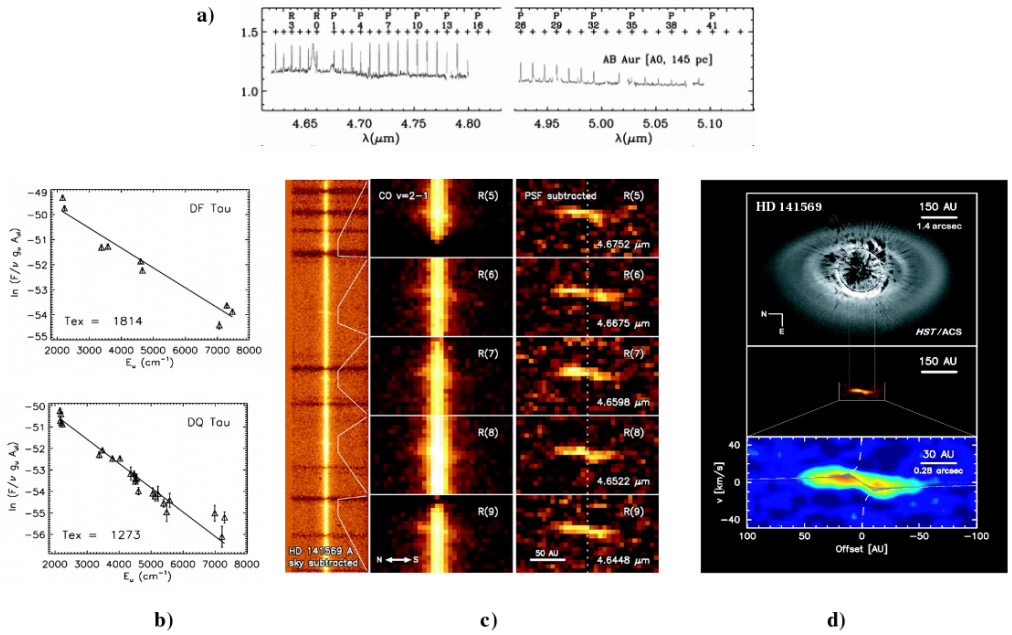

Figure 1.19: *a) CO ro-vibrational emission is identified as a forest of lines around 4.7μm (Blake and Boogert 2004). b) Rotational diagrams of the detected CO lines allow to constrain the temperature of the emitting gas (Najita et al. 2003). c) When the emission is spatially resolved, the dynamics of the emitting gas can be constrained.(d) The observed lines are consistent with gas in keplerian rotation (Goto et al. 2006).*

ESO-VLT will allow the systematic study of the CO ro-vibrational emission in protoplanetary disks. In Chapter 2 of this thesis we discuss a project in which we searched for ro-vibrational emission of CO at 4.7μm in a sample of nearby Herbig Ae/Be stars employing the near-infrared spectrograph ISAAC at ESO-VLT.

H_2 fundamental emission at 28, 17 and 12 μm

The chief constituent of the protoplanetary disk is molecular hydrogen (H_2). Emission from its first rotational states is observable in the infrared (J=2-0 at 28.218 μm, J=3-1 at 17.035 μm, J=4-2 at 12.278 μm). H_2 pure rotational emission probes the warm and hot gas ($150 < T < 1000$ K) present in the inner 50 AU of the disk. These transitions are important because they provide information about the temperature and mass of gas in the zone where giant planets form. Other gas diagnostics are either not sensitive to the total amount of warm gas (e.g. the near-IR H_2 and the NIR and (sub)-mm CO lines), or only measure the column of gas in the line of sight towards the star (all absorption line studies, e.g. H_2 lines in the UV). In addition, such diagnostics are highly model-dependent when trying to deduce a total gas mass, or do not probe the H_2 (bulk of the gas mass) directly, and therefore are highly dependent on fractional abundances of the tracer in question and thus on the details of the disk chemistry.

The principal limitation of the H_2 rotational lines is that they are extremely weak and challenging to detect. H_2 transitions are electric quadrupole in nature, and thus posses small Einstein coefficients. In addition, in protoplanetary disks, the weak H_2 emission has to be detected on

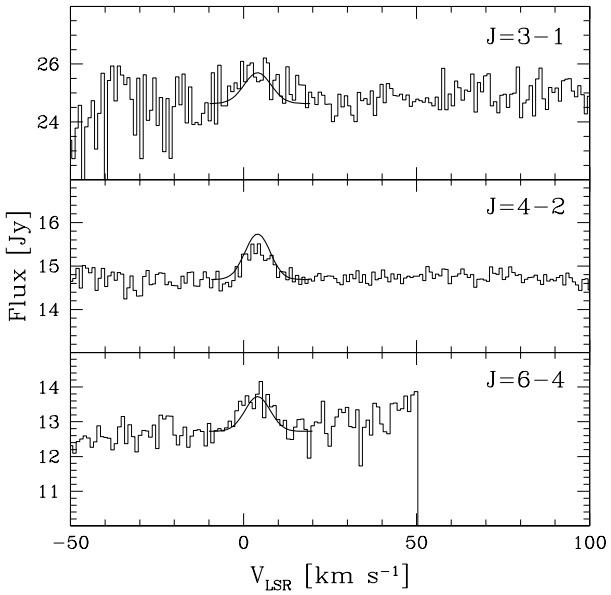

Figure 1.20: *a) H_2 pure rotational emission observed towards the Herbig Ae star AB Aur (Bitner et al. 2007).*

the top of strong continuum emission of the dust. High spectral resolution in the mid-infrared is therefore required for observing this line. So far H_2 emission in the mid-infrared has been detected and confirmed only towards the Herbig star AB Aur[18] (Bitner et al. 2007, see Figure 1.20). The small rate of detections of the line suggest that the intrinsic levels of H_2 thermal emission in optically thick disks are very low. Theoretical calculations of the expected H_2 thermal fluxes from the upper layers of disks in Herbig Ae stars (Carmona et al. 2007c) and T Tauri stars (Nomura et al. 2005, 2007) suggest that the thermal line fluxes are one to two orders of magnitude lower than the sensitivity limits of current instrumentation. In Chapter 4 we discuss a large and sensitive survey for H_2 emission at 17 and 12 micron in nearby Herbig Ae stars performed with VISIR, the new-high resolution mid-infrared spectrograph at ESO-VLT.

CO emission in the (sub)-mm

The most widely used gas diagnostic is the CO emission of cold gas at sub-mm wavelengths. Initially detected with observations performed by single disk telescopes, the observed double peaked profiles revealed gas in rotation around the central star. Follow up observations with (sub)-mm interferometers spatially resolved the emission and convincingly proved that the gas is in a disk-like shape (Mannings and Sargent 1997, see Figure 1.6). The most remarkable advantage of CO (sub)-mm emission is that it is detectable. CO fundamental transition have a large einstein coefficients, thus the lines are very strong once the gas is excited. The principal limitation of this diagnostic is that it probes very cold gas in the outer regions of the disk, a region were giant

[18]ISO reported the detection of H_2 rotational lines towards several Herbig Ae stars, T Tauri stars and debris disks (Thi et al. 2001). However, none of these detections has been confirmed by ground observations (Richter et al. 2002, Sheret et al. 2002, Sako et al. 2005).

planets are not believed to form. Since the CO gets frozen onto dust surfaces and the abundance of CO with respect to H_2 is very uncertain ($\sim 10^{-4}$), CO observations in the (sub)-mm could not be used for determining the total gas mass. The masses deduced from CO observations are far too low with respect to the disk masses deduced from mm dust continuum emission.

Other molecules observed in (sub)-mm observations

Numerous gaseous species (e.g. CO, CN, HCO^+, HCN, DCN, C_2H, CS, etc) have been observed towards protoplanetary disks using (sub)-mm observations (for a recent review see Bergin et al. 2007). The study of emission from diverse molecular species is of paramount importance for understanding the chemistry in protoplanetary disks.

1.5.7 This Thesis

The fundamental goal of the projects comprising this thesis was to observationally constrain the properties of gas in protoplanetary disks. We focused on the study of disks around nearby (d < 400 pc) Herbig Ae/Be stars (HAEBES) and a few classical T Tauri stars. The thesis consists of four chapters, each chapter describes a self-consistent project in which we used one observational technique for studying gas in the disk. The chapters are presented in chronological order. From our observations (detections and non-detections), we derive important constraints on the physical properties of the studied disks (e.g. mass, column density, temperature, age, excitation mechanism, inclination). We show that high-resolution infrared spectroscopy is a crucial tool for future studies of the structure of protoplanetary disks.

In the first chapter, we present a search for emission of hot and warm gas ($T = 100 - 1000$ K) in the inner 50 AU of protoplanetary disks. We observed a sample of five nearby HAEBES and searched for the ro-vibrational emission band of CO at 4.7 micron with ISAAC, the first generation near-infrared spectrograph at ESO VLT[19].

In the second chapter, we describe a project in which we intended to use a novel technique to probe the outer cold gas (T < 50) of protoplanetary disks. We obtained VLT-FORS2 optical spectroscopy of stars close (<1.5") to a sample of nearby HAEBES. Our goal was to measure absorption gas features of the Herbig disk superimposed on the spectra of the close visual companion[20].

In the third chapter, we present a large observational effort to detect H_2 fundamental emission at 12.278 and 17.035 μm from the disks around six nearby Herbig Ae/Be stars and one T Tauri spectroscopic binary. In this project we employed VISIR, ESO's foremost high-resolution mid-infrared spectrograph.

In the fourth chapter, we present the first results of a sensitive search for near-infrared H_2 emission from protoplanetary disks using CRIRES, ESO's new VLT near-infrared high-resolution spectrograph. We searched for the H_2 $\nu = 1 - 0$ S(1) line at 2.1218 μm, the H_2 $\nu = 1 - 0$ S(0) H_2 emission at 2.2233 μm and the H_2 $\nu = 2 - 1$ S(1) H_2 emission at 2.2477 μm towards LkHα 264, a

[19] At the time of our ISAAC observations, ISAAC was the most powerful near-infrared spectrograph at ESO.

[20] We discovered that the companions are in fact physically associated emission-line pre-main sequence stars (CTTS and WTTS). Given this discovery, the absorption lines detected could not be attributed unambiguously to the gas disks surrounding the primaries. However, since the companions are close and physically associated with the primaries, this allowed us to constrain the ages of the Herbig Ae/Be primaries, and to realize that binarity could be an important factor in the longevity of the disks.

gas-rich classical T-Tauri star, and 49 Cet, a debris disk with evidence of large reservoirs of cold gas at sub-mm wavelengths

In the fifth, and closing chapter, we present our summary and conclusions, and discuss future perspectives in the observational study of gas in protoplanetary disks.

1.6 References

Acke, B., et al. 2004, A&A, 422, 621
Acke, B., van den Ancker, M. E., & Dullemond, C. P. 2005, A&A, 436, 209
Acke, B., & van den Ancker, M. E. 2006, A&A, 449, 267
Adams, F. C., Lada, C. J., & Shu, F. H. 1987, ApJ, 312, 788
Andre, P., Ward-Thompson, D., & Barsony, M. 1993, ApJ, 406, 122
Andre, P., & Montmerle, T. 1994, ApJ, 420, 837
Ardila, D. R., Basri, G., Walter, F. M., Valenti, J. A., & Johns-Krull, C. M. 2002, ApJ, 567, 1013
Augereau, J. C., et al. 2001, A&A, 365, 78
Aumann, H. H., et al. 1984, ApJL, 278, L23
Ballesteros-Paredes, J., Klessen, R. S., Mac Low, M.-M., & Vazquez-Semadeni, E. 2007, in Protostars and Planets V., Edited by B. Reipurth, D. Jewitt, and K. Keil. University of Arizona Press, Tucson, 2007
Bary, J. S., Weintraub, D. A., & Kastner, J. H. 2003, ApJ, 586, 1136
Beckwith, S. V. W., Sargent, A. I., Chini, R. S., & Guesten, R. 1990, AJ, 99, 924
Benz, W. 2000, Space Science Reviews, 92, 279
Bergin, E., et al. 2004, ApJL, 614, L133
Bergin, E. A., Aikawa, Y., Blake, G. A., & van Dishoeck, E. F. 2007, in Protostars and Planets V., Edited by B. Reipurth, D. Jewitt, and K. Keil. University of Arizona Press, Tucson, 2007
Bitner, M. A., et al. 2007, ApJL, 661, L69
Blake, G. A. & Boogert, A. C. A. 2004, ApJ, 606, L73
Boss, A. P. 1997, Science, 276, 1836
Bouwman, J., de Koter, A., van den Ancker, M. E., & Waters, L. B. F. M. 2000, A&A, 360, 213
Brittain, S. D., et al. 2003, ApJ, 588, 535
Brittain, S. D., et al. 2007, ApJ, 659, 685
Burrows, C. J., et al. 1996, ApJ, 473, 437
Cameron, A. G. W. 1978, Moon and Planets, 18, 5
Carmona, A., van den Ancker, M. E., Thi, W.-F., Goto, M., & Henning, T. 2005, A&A, 436, 977
Carmona, A., van den Ancker, M. E., & Henning, T. 2007, A&A, 464, 687
Carmona, A., van den Ancker, M. E., Henning, T., Ya. Pavlyuchenkov, C.P. Dullemond, M. Goto, W.F-.Thi, J.Bouwman, & L.B.F.M. Waters. 2007, submitted to A&A.
Carmona, A., van den Ancker, M.E., Henning, T., Goto, M., Fedele, D., & B.Stecklum. 2007, submitted to A&A.
Carr, J. S., Tokunaga, A. T., Najita, J., Shu, F. H., & Glassgold, A. E. 1993, ApJL, 411, L37
Chiang, E. I., & Goldreich, P. 1997, ApJ, 490, 368
Desidera, S., & Barbieri, M. 2007, A&A, 462, 345
Dent, W. R. F., Greaves, J. S., & Coulson, I. M. 2005, MNRAS, 359, 663

Dullemond, C. P., Dominik, C., & Natta, A. 2001, ApJ, 560, 957
Dullemond, C. P., & Dominik, C. 2004, A&A, 417, 159
Dullemond, C. P., & Dominik, C. 2005, A&A, 434, 971
Duquennoy, A., & Mayor, M. 1991, A&A, 248, 485
Feigelson, E. D., & Decampli, W. M. 1981, ApJL, 243, L89
Fukagawa, M., et al. 2004, ApJL, 605, L53
Gammie, C. F. 2001, ApJ, 553, 174
Guillot, T., Chabrier, G., Morel, P., & Gautier, D. 1994, Icarus, 112, 354
Goldreich, P., & Tremaine, S. 1980, ApJ, 241, 425
Goldreich, P., & Ward, W. R. 1973, ApJ, 183, 1051
Goto, M., et al. 2006, ApJ, 652, 758
Grady, C. A., et al. 2001, AJ, 122, 3396
Grady, C. A. 2005, in The Nature and Evolution of Disks Around Hot Stars, ASPC, 337, 155
Grinin, V. P., et al. 1994, A&A, 292, 165
Haisch, K. E., Jr., Lada, E. A., & Lada, C. J. 2001, ApJL, 553, L153
Hartmann, L., & Kenyon, S. J. 1985, ApJ, 299, 462
Hartmann, L. 2001, Accretion Processes in Star Formation, Cambridge, UK: Cambridge University Press, January 2001.
Henning, T., Launhardt, R., Steinacker, J., & Thamm, E. 1994, A&A, 291, 546
Herbig, G. H. 1960, ApJS, 4, 337
Herczeg, G. J., et al. 2002, ApJ, 572, 310
Herczeg, G. J., et al. 2004, ApJ, 607, 369
Herczeg, G. J., et al. 2006, ApJS, 165, 256
Itoh, Y., Sugitani, K., Ogura, K., & Tamura, M. 2003b, PASJ, 55, L77
Johansen, A., Henning, T., & Klahr, H. 2006, ApJ, 643, 1219
Joy, A. H. 1945, ApJ, 102, 168
Kenyon, S. J., & Hartmann, L. 1987, ApJ, 323, 714
Kornet, K., Bodenheimer, P., Różyczka, M., & Stepinski, T. F. 2005, A&A, 430, 1133
Kuiper, G. P. 1951, Proceedings of the National Academy of Science, 37, 1
Lada, C. J. 1988, NATO ASIC Proc. 241: Formation and Evolution of Low Mass Stars, 93
Lin, D. N. C., Bodenheimer, P., & Richardson, D. C. 1996, Nature, 380, 606
Malfait, K., et al. 1998, A&A, 332, L25
Mandell, A. M., Raymond, S. N., & Sigurdsson, S. 2007, ApJ, 660, 823
Mannings, V., & Sargent, A. I. 1997, ApJ, 490, 792
Martin, C., Bouret, J.-C., Deleuil, M., Simon, T., & Catala, C. 2004, A&A, 416, L5
McCaughrean, M. J., & Stauffer, J. R. 1994, AJ, 108, 1382
McCaughrean, M. J., et al. 1998, ApJL, 492, L157
Mendoza V., E. E. 1968, ApJ, 151, 977
Meeus, G., et al. 2001, A&A, 365, 476
Najita, J.,Carr, J. S., & Mathieu, R. D. 2003, ApJ, 589, 931
Nomura, H., & Millar, T. J. 2005, A&A, 438, 923
Nomura, H., et al. 2007, ArXiv Astrophysics e-prints, arXiv:astro-ph/0702030.
O'dell, C. R., Wen, Z., & Hu, X. 1993, ApJ, 410, 696
Olofsson, G., Liseau, R., & Brandeker, A. 2001, ApJL, 563, L77
Osterloh, M., & Beckwith, S. V. W. 1995, ApJ, 439, 288

Padgett, D. L., et al. 1999, AJ, 117, 1490
Palla, F., & Stahler, S. W. 1993, ApJ, 418, 414
Pollack, J. B., et al. 1996, Icarus, 124, 62
Ramsay Howat, S. K., & Greaves, J. S. 2007, ArXiv e-prints, 705, arXiv:0705.4601
Richter, M. J., Jaffe, D. T., Blake, G. A., & Lacy, J. H. 2002, ApJL, 572, L161
Rucinski, S. M. 1985, AJ, 90, 2321
Safronov, V. S. 1966, The Protoplanetary cloud and its evolution, AZH 43, 817
Sagan, C. 1980, COSMOS, New York: Random House.
Sako, S., et al. 2005, ApJ, 620, 347
Sheret, I., Ramsay Howat, S. K., & Dent, W. R. F. 2003, MNRAS, 343, L65
Shu, F. H., Adams, F. C., & Lizano, S. 1987, ARA&A, 25, 23
Sicilia-Aguilar, A., et al. 2006, AJ, 132, 2135
Skumanich, A. 1972, ApJ, 171, 565
Smith, B. A., & Terrile, R. J. 1984, Science, 226, 1421
Stapelfeldt, K. R., et al. 1998, ApJL, 502, L65
Stewart, G. R., & Wetherill, G. W. 1988, Icarus, 74, 542
Thi, W. F., et al. 2001, ApJ, 561, 1074
Udry, S., Fischer, D., & Queloz, D. 2007, in Protostars and Planets V., Edited by B. Reipurth, D. Jewitt, and K. Keil. University of Arizona Press, Tucson, 2007
van Boekel, R., et al. 2004, Nature, 432, 479
Valenti, J. A., Basri, G., & Johns, C. M. 1993, AJ, 106, 2024
Vicente, S. M., & Alves, J. 2005, A&A, 441, 195
Walter, F. M., et al. 2003, AJ, 126, 3076
Waters, L. B. F. M., & Waelkens, C. 1998, ARA&A, 36, 233
Ward, W. R. 1997, ApJL, 482, L211
Weintraub, D. A., Kastner, J. H., & Bary, J. S. 2000, ApJ, 541, 767
Weidenschilling, S. J. 1977, MNRAS, 180, 57
Weidenschilling, S. J., & Cuzzi, J. N. 1993, Protostars and Planets III, 1031

Published as: A. Carmona, M.E van den Ancker, W.-F. Thi, M. Goto, and Th. Henning – *"Upper limits on CO 4.7 μm emission from disks around five Herbig Ae/Be stars"* Astronomy & Astrophysics 2005, 436, 977C

Chapter 2

Upper limits on CO 4.7 μm emission from disks around five Herbig Ae/Be stars

Abstract

We present the results of medium-resolution spectroscopy of five nearby Herbig Ae/Be stars at 4.7 μm: UX Ori, HD 34282, HD 50138, V380 Ori, HK Ori. The goal was to search for CO fundamental ro-vibrational emission. None of the targets show CO features, either in absorption nor in emission. We derive a 5σ *upper limit of* $< 10^{-12}$ cm^{-2} *to the column density of hot CO (*$T \approx 1500$ *K) in the sources. These upper limits are considerably lower than the values of Herbig Ae/Be stars for which warm and hot CO emission has been reported. The non-detection of CO* $v = 1 - 0$ *emission in these five targets suggest that Herbig Ae/Be stars are not a homogeneous group with respect to the structure of the gaseous disk and/or the amount of CO in the inner 50 AU of their disks.*

2.1 Introduction

Circumstellar disks around pre-main sequence stars are the likely place for planet formation. Present theoretical models predict that planets are formed in the inner 50 AU of such disks. Terrestrial planets are thought to be made from hierarchical growth of planetesimals (e.g. Ida & Lin 2004). Two major classes of models exist for the formation of gas giant planets: a) the gravitational instabilities model (Boss 2004; Mayer et al. 2004), b) the core accretion model (Pollack 1996; Alibert et al. 2004; Kornet et al. 2002). The knowledge of fundamental disk properties such as temperature and density profile, geometry and dissipation time scales, gas and dust composition, is paramount to constrain planet formation models.

Giant planets in our Solar System and giant extrasolar planets (Vidal-Madjar et al. 2004) are composed mainly of gas. Current models predict that they are formed in the inner 50 AU of the protoplanetary disk (Ida & Lin 2004; Alibert et al. 2004; Boss 2004). However, the observational study of the gas in the planet forming region of the disks only started recently with the advent of space observatories (e.g. Bergin et al. 2004; Thi et al. 2001; Lecavellier des Etangs et al. 2003) and high-resolution infrared spectrometers mounted on large aperture telescopes (e.g. Richter et al. 2002; Bary et al. 2002, 2003; Brittain & Rettig 2002; Brittain et al. 2003; Najita et al. 2000, 2003; Blake & Boogert 2004).

Intermediate-mass Herbig Ae/Be stars (HAEBES) and low-mass classical T Tauri stars are pre-main sequence stars characterized by strong optical emission lines (e.g. Hα) and infrared excess. These properties are consistent with the idea that they are young stars surrounded by a circumstellar disk. The strong emission lines are interpreted as the signature of gas accretion onto the central star, and the infrared excess as the emission of the warm dust in the disk (see reviews

by Waters & Waelkens 1998 and Bertout 1989). These disks have been imaged from the NIR to the (sub-)millimetre (e.g Grady et al. 2004; Mannings & Sargent 1997, 2000; Henning et al. 1998). Nearby HAEBES and T Tauri stars are natural laboratories for studying the process of planet formation.

Pure rotational CO emission from circumstellar disks is commonly seen at millimeter and submillimeter wavelengths (e.g. Qi et al. 2004; Ceccarelli et al. 2002; Mannings & Sargent 2000; Thi et al. 2004). However, these wavelengths are only sensitive to the cold gas (T < 50K) in outer regions of the disk (R > 50 AU).

Theoretical models and recent observational evidence suggest that in the inner 50 AU, temperatures can be relatively high ($T \geq 150K$) (Willacy et al. 1998; Dullemond et al. 2001; Markwick et al. 2002; Kamp & Dullemond 2004). Under these conditions, molecules such as water and CO are in the gas phase, and a rich emission spectrum from their rotational and vibrational transitions is expected. However, the relatively large column densities in the inner 50 AU (1500 g cm $^{-2}$ at 1 AU for the minimum-mass solar nebula) could preclude the observability of such transitions, because the disk is optically thick in the continuum (Najita et al. 2003) .

Nevertheless, in some circumstances, parts of the inner circumstellar disk could be optically thin, and warm CO emission becomes detectable. Carr et al. (2001), Brittain & Rettig (2002) and Rettig et al. (2004) detected $\nu = 1 - 0$ emission of warm CO and suggested that it originates in a disk gap or in a inner low-density region; Najita et al. (2000, 2003) and Blake & Boogert (2004) reported the detection of CO fundamental ro-vibrational band, and postulated that warm CO emission is produced in a disk's atmosphere when the stellar radiation of the host star induces a temperature inversion (disk atmosphere hotter than the disk mid-plane); Brittain et al. (2003) found $\nu = 1 - 0$ emission of hot and warm CO in AB Aur and suggested that it is produced by IR pumping (resonant scattering). The same authors reported the detection of $\nu = 2 - 1$ and $3 - 2$ emission of CO in HD 141569, and pointed out that it originates by UV pumping in the inner rim of the disk.

This chapter describes our search for CO fundamental ro-vibrational emission from a selected number of Herbig Ae stars known to be surrounded by a disk. Meeus et al. (2001) devised a classification scheme for the spectral energy distributions (SED) of Herbig Ae/Be stars. In their classification scheme, group I sources have a SED that is strongly double-peaked in the near to mid-infrared, whereas the SED of group II sources can be described by a power-law at those wavelengths. Dullemond (2002) has identified this empirical classification with two different disk geometries: flared (group I) and self-shadowed (group II). We observed objects belonging to both groups. UX Ori, V380 Ori, HK Ori (group I) are likely to have a flared disk, and HD 50138 and HD 34282 (group II) a self-shadowed disk. We used ISAAC at the VLT at R∼10,000 to search for the CO emission band at 4.7 μm. We report here our non detection in all the objects observed in April 2004. We discuss how the stringent upper limits derived from our deep search set constrains the physical properties of the observed disks.

The chapter is organized as follows. In Section 2.2 the observational set-up and data reduction procedure are described, in Section 2.3 the spectra obtained and the estimation of the upper limits to the hot (T ≈ 1500 K) CO column density are presented, finally in Section 2.4 the meaning of our results in the context of the structure of the disk is discussed.

2.2 Observations

Medium-resolution spectra in the 4.6 – 4.8 μm range were obtained for five Herbig Ae/Be stars (UX Ori, HD 34282, HD 50138, V380 Ori and HK Ori) between the 2^{nd} and 20^{th} of April 2004 using ISAAC at the First Unit Telescope ANTU of the ESO-VLT at Cerro Paranal, Chile. These targets were selected to maximize the shift in velocity between the expected position of the CO emission in the targets and the telluric CO absorption at the time of observation. A medium-resolution grating and the narrowest available slit (0.3") were used to provide spectra of resolution 10,000. The slit has been oriented in the North-South direction. Sky background was subtracted by chopping each exposure by 15 " in the direction of the slit. Asymmetrical thermal background of the telescope was subtracted by nodding the telescope by 15". In each nodding position the telescope has been randomly jittered in order to record the raw spectra in different regions of the detector, minimizing the influence of bad pixels. In order to correct telluric absorption and obtain absolute flux calibration, spectroscopic standard stars were observed the same night at airmasses close to that of the science targets. Dome flat fields were obtained at the beginning and at the end of each observing night.

2.2.1 Data Reduction

Chopped raw frames of each nodding position were first corrected for the detector non-linearity. Since half-cycle frames were not recorded, the median value of each frame was subtracted to obtain an approximation to the half-cycle frame intensity subject to non-linearity. The residual raw frame was corrected for non-linearity using the expression

$$F_c = f_{rr} + 1.05 \times 10^{-6} \times f_{rr}^2 + 0.85 \times 10^{-10} \times f_{rr}^3$$

in which F_c refers at the corrected frame, and f_{rr} is the residual raw frame [1]. Once this correction for detector non-linearity is made, the median previously subtracted is added back to the frame.

The second step in the data reduction procedure is to correct all the frames for tilt in the spatial direction using Ar Xe arc lamp frames taken the same day of the observations. A second order polynomial deduced from the arc file is used for this correction. Individual exposures are corrected for differences in the detector sensitivity by dividing them by normalized dome flat fields.

Flat-fielded frames were combined using the Eclipse[2] jittering procedure. The procedure consists in classifying the set of data in groups having the nodding sequence form ABBA. In each group, the frames in the A position and B position are averaged, the averaged frames are subtracted from each other, divided by 2, and a combined frame is generated ($F_{combined} = (\bar{A} - \bar{B})/2$). The ensemble of combined frames, one for each ABBA group, are stacked in one single final 2D frame. During this process, combined frames are shifted in such a way that the addition of all the spectra is located in the center of the the final frame. This shifting procedure optimizes the subtraction of sky and telescope background emission.

One-dimensional spectra are extracted from the 2D frame, averaging the pixel counts in the PSF direction. These spectra are then divided by the exposure time defined by

$$E_{time}[s] = \mathrm{DIT} \times \mathrm{NDIT} \times 2 \times \mathrm{Chopcycles}$$

[1] Values taken from the ISAAC data reduction manual, see www.eso.org/instruments/isaac/#Documentation
[2] www.eso.org/eclipse

Here DIT is the Detector Integration Time (1.84 s in our case), NDIT is the number of DIT and Chopcycles is the number of chopping cycles (8) per DIT.

The one-dimensional spectrum of the standard star is corrected for the differences in airmass and air pressure with the science target using,

$$I_{STD_{corrected}} = I_0 \ \exp\left(-\tau \ \frac{\bar{X}_{TARGET}}{X_{STD}} \ \frac{\bar{P}_{TARGET}}{P_{STD}}\right)$$

Here $\bar{X}$ is the average of the airmass and $\bar{P}$ is the average of the air pressure. The continuum I_0 has been defined as uniform with a value equal to the mean plus three standard deviations ($I_0 = \bar{I}_{\rm obs} + 3\sigma_{I_{\rm obs}}$). The optical depth τ has been calculated from the measured data using $\tau = \ln\,(I_{obs}/I_0)$.

Employing a synthetic model of the earth atmosphere, the extracted one-dimensional spectra of the target and the standard star were subject to a precise wavelength calibration involving a correction for differences in the spectral resolution of both stars (Goto et al. 2003).

Finally, the science target spectrum is flux calibrated and corrected for atmospheric absorption by dividing it by the corrected spectrum of the standard star. Absolute flux calibration is obtained by multiplying the telluric corrected spectra by a theoretical SED model (Kurucz 1991) of the standard star.

We estimate the uncertainty in the flux calibration of our spectra to be between 10% and 20%. The principal source of noise in the spectra is due to imperfections in the correction for telluric absorption. The 4.7 μm band is particularly challenging in this aspect given the presence of strong CO absorption in the earth's atmosphere. Although the standard stars were observed with airmasses close to those of the science targets, and the extracted spectra were corrected for differences in airmass, air pressure and spectral resolution, in the regions of poor atmospheric transition the correction for the telluric absorption is not perfect. The noise present in the spectra is mostly due to systematic errors in this correction.

2.3 Results

Flux calibrated spectra of the five Herbig Ae/Be stars are presented in Figure 2.1. The $\nu = 1 - 0$ ro-vibrational band of CO was not detected in any of our targets, neither in absorption nor in emission. The only notable feature in all the spectra (except HD 34282) are recombination lines of H I: Pf β, Hu ε. A summary of the H I observations is presented in Table 2.1. In the case of HD 293782 and HK Ori the Pf β line shows a strong red/blue asymmetry. This phenomenon is likely associated with infalling gas (Najita et al. 1996). HD 50138 and V380 Ori show symmetric Pf β profiles. In these two systems the Hu ε emission line has a strong blue/red asymmetry and extended blue wings. This line most likely originates in a similar region as the balmer lines of H I, which are believed to come from a wind either from the disk or the central star (see Bouret & Catala 1998, 2000).

We derived upper limits to the flux in the CO emission line taking a conservative 5σ (standard deviation) of the intensity in the continuum ($\sigma_{I_{obs}}$). Given that the minimum FWHM of the instrument is 4.7×10^{-4} μm, we obtained upper limits ranging from 2.2×10^{-17} to 5.9×10^{-17} W m^{-2} for UX Ori, HD 34282, HK Ori, V380 Ori, and 4.2×10^{-16} W m^{-2} for HD 50138 (see Table 2.2).

From the upper limit to the CO flux, and supposing that CO is excited by infrared fluorescence (resonant scattering), we estimated the upper limit to the column density of hot CO using Brittain

Table 2.1: *H I lines detected in the 4.6 – 4.8 μm spectra of our targets*

		UX Ori	HD 34282[a]	HD 50138	V380 Ori	HK Ori
Line		Pf β	–	Pf β	Pf β	Pf β
Central Wavelength (λ)	[μm]	4.655	–	4.656	4.655	4.655
FWHM	[km s^{-1}]	255	–	156	176	233
Equivalent Width (EW)	[Å]	−7.4	–	−11.7	−12.7	−5.1
Line Flux (F$_\lambda$)	[W m^{-2}]	2.3×10^{-16}	–	5.1×10^{-15}	1.5×10^{-15}	1.1×10^{-16}
Line		Hu ε	–	Hu ε	Hu ε	–
Central Wavelength (λ)	[μm]	4.674	–	4.675	4.673	–
FWHM	[km s^{-1}]	60	–	142	116	–
Equivalent Width (EW)	[Å]	−3.2	–	−6.7	−4.1	–
Line Flux (F$_\lambda$)	[W m^{-2}]	1.0×10^{-16}	–	3.0×10^{-15}	4.7×10^{-16}	–

[a]No H I lines were detected in the ISAAC spectra of HD 34282

et al. (2003)[3]:

$$N = \frac{4\pi F_{line}}{\Omega\, g_{line}\, h\, c\, \tilde{\nu}}$$

Here F_{line} is the $\nu = 1 - 0$ line flux, Ω is the solid angle,$h\, c\, \tilde{\nu}$ is the energy per photon, and $g_{line} = P_J\, g_{1-0}$ is the fluorescence efficiency for the $1 - 0$ ro-vibrational transition by IR pumping.

Brittain et al. (2003) estimated a g_{1-0} at 0.6 AU of 1.1 photons molecule^{-1}s^{-1} for AB Aur, and calculated a column density of observed hot CO of 2×10^{13} cm^{-2}. Given that UV pumped (ν = 2- – 1) transitions were not detected in the wavelength range observed (4.6 - 4.8 μm), and assuming that our observed HAEBES have an inner disk configuration similar to AB Aur, we scaled the g_{1-0} coefficient for each star based on the IR luminosity ($L_{\mathrm{IR}_\star}$) at 4.7μm and the distance ($d_\star$) employing [4]

$$g_{1-0\,\star} = g_{1-0_{\mathrm{AB\,Aur}}}\, \frac{d_\star^2 \times L_{\mathrm{IR}_\star}}{d_{\mathrm{AB\,Aur}}^2 \times L_{\mathrm{IR}_{\mathrm{AB\,Aur}}}}$$

With this estimate of g_{1-0} for each of our targets and the upper limit for the line flux we calculated the hot CO column density. Our results are summarized in Table 2.2 We find upper limits to the column density of hot CO ranging from 1.5×10^{12} to 8.0×10^{12} cm^{-2}. In the case of HD 34282 the upper limit calculated is 8.9×10^{13} cm^{-2}. However, this is not a representative limit since the signal to noise of the spectra is low (S/N=7).

2.4 Discussion

Najita et al. (2003), Brittain et al. (2003), Blake & Boogert et al. (2004), and Rettig et al. (2004) showed how the study of warm and hot CO emission could be used as a powerful tool for probing disk surfaces and for assessing the density and temperature profiles of the inner 50 AU

[3]originally in DiSanti et al. (2001)

[4]AB Aur is a 144 pc and has a 4.7 μm intensity of 1.47×10^{-12} W m$^{-2}\mu$m^{-1}.

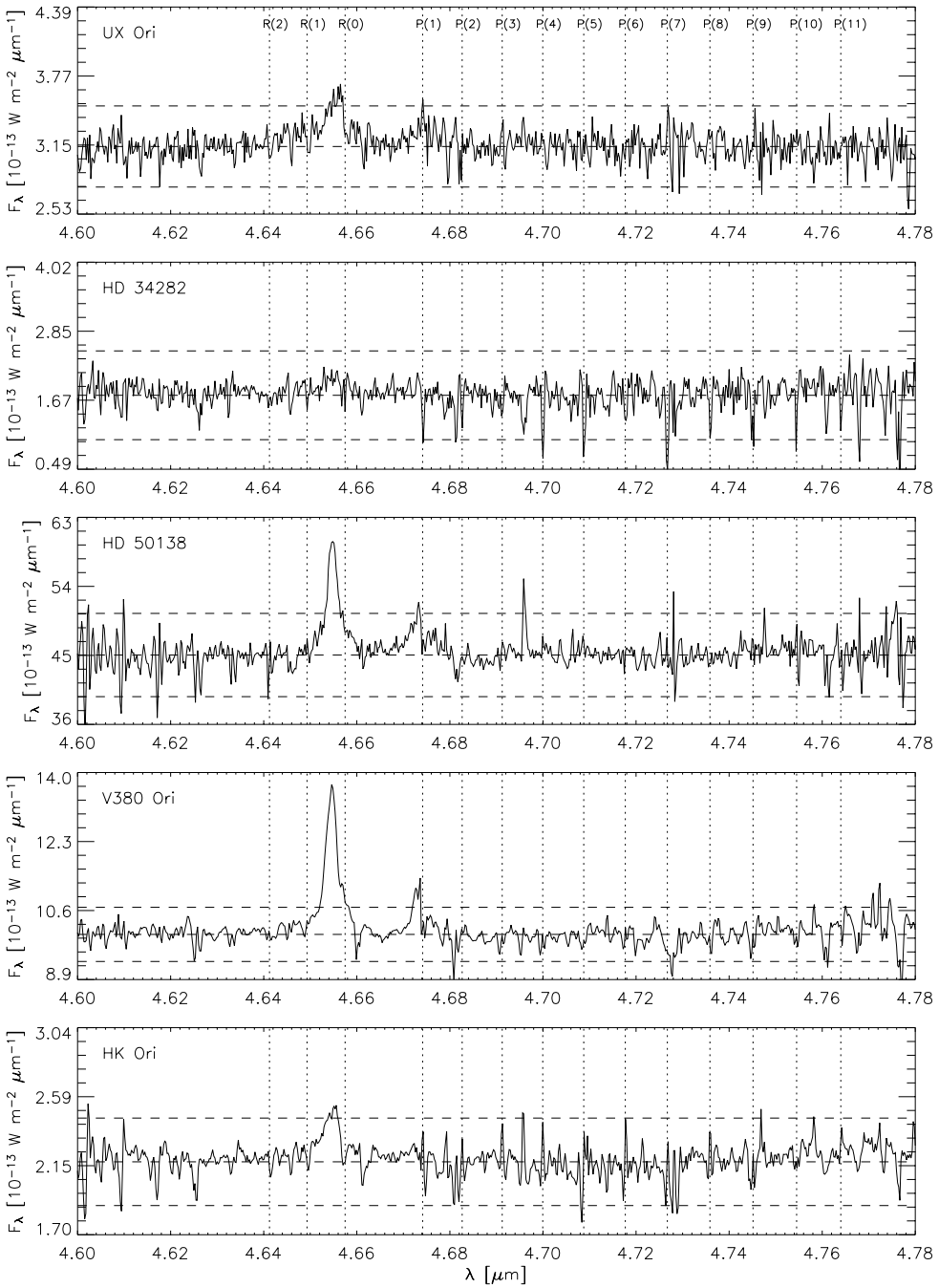

Figure 2.1: *ISAAC spectra of our five target stars. The strong emission seen at 4.65 μm and 4.67 μm are the Pf β and Hu ε recombination lines of H I. The noise in the spectra is mostly due to systematic errors in the telluric correction in this region of poor atmospheric transmission. Vertical dotted lines show the CO v = 1 − 0 transitions. Horizontal dashed lines show the 3σ limits of the intensity.*

Table 2.2: *Summary of CO ν = 1–0 emission characteristics of our sample stars.*

		UX Ori	HD 34282	HD 50138	V380 Ori	HK Ori	AB Aur [a]
Distance [b]	[pc]	400	164	290	500	500	144
Average Intensity	[10^{-13} W m^{-2} μm^{-1}]	3.1	1.8	44.7	10.0	2.2	14.7
5σ	[10^{-13} W m^{-2} μm^{-1}]	0.6	1.3	9.0	1.1	0.5	–
S/N		25	7	25	45	23	–
Instrument FWHM	[10^{-4} μm]	4.7	4.7	4.7	4.7	4.7	–
Line Flux upper-limit	[10^{-17} W m^{-2}]	< 2.9	< 5.9	< 42	< 5.2	< 2.2	8.6
scaled g_{1-0}	[pho mol^{-1} s^{-1}]	1.8	0.2	13.6	9.0	2.0	1.1
Column density of hot CO (1500K)	[10^{12} cm^{-2}]	< 4.1	< 89	< 8.0	< 1.5	< 2.9	20

[a] Values for AB Aur are listed for reference (Brittain et al. 2003)

[b] For HD 34282, HD 50138 and AB Aur the distance is estimated using Hipparcos data. UX Ori, V380 Ori and HK Ori have been assumed to be associated with the Orion OB1a (UX Ori) and OB1c (V380 Ori, HK Ori) star-forming regions.

of the circumstellar disk independent of SED models. These authors reported the detection of the $\nu = 1 - 0$ transition of CO in several Herbig Ae/Be stars.

Our estimates of the upper limit to the CO line fluxes are within the range of the detections of CO $\nu = 1 - 0$ emission fluxes measured. For example in AB Aur Brittain et al. (2003) observed a CO $R(1)$ line flux of 8.6×10^{-17} W m^{-2} in AB Aur and Blake & Boogert (2004) detected a CO $P(2)$ line flux of 10.4×10^{-17} W m^{-2} in the same star. The upper limits to the hot CO column density calculated (except for HD 34282 that presented a low S/N spectrum) are well below the 2×10^{13} cm^{-2} value reported for AB Aur by Brittain et al. (2003). From the upper limits deduced from our observations, we conclude that if our targets would had equal column densities of hot CO, or had presented CO $\nu = 1 - 0$ emission fluxes of the magnitude reported in the literature, we would have detected this emission within our ISAAC data.

Previous studies suggested that CO emission is produced by UV pumping or by IR fluorescence (resonant scattering). The nature of the excitation mechanism is revealed from the CO transitions present in the spectra. The $\nu = 2 - 1$ and $3 - 2$ emission bands indicate that the principal source of excitation is UV pumping. On the other hand, the $\nu = 0 - 1$ band indicates that the excitation mechanism is thermal (i.e. IR resonant scattering). Our upper limits are small enough that they are in the detection range of the $\nu = 2-1$ and $3-2$ emission band previously reported in the Herbig star HD 141569 by Brittain et al. (2003), F_{3-2} =1.1×10^{-17} W m^{-2}). The non-detection of UV excited CO transitions within our data suggests that UV radiation is scattered by the dust in the disk's inner rim and that the CO is probably shielded. However, the inner part of the disk (R < 50 AU) could also be optically thick in the continuum, precluding the observability of such transitions.

Meeus et al. (2001) in their study of the spectral energy distribution (SED) of a large sample of Herbig Ae/Be stars suggested that they could be classified in two groups according to the SED shape. Detailed modeling of the dust emission by Dullemond (2002) found that the 3 μm bump observed in many SEDs could be interpreted as evidence for the existence of a dusty "puffed-up" inner disk rim, and that the Meeus et al. classification could be understood as corresponding to two inner disk geometries: flared disk, and self-shadowed disk.

Using this geometrical classification, Brittain et al. (2003) interpreted the two temperature CO $\nu = 1 - 0$ profiles deduced from the rotational diagrams of AB Aur in the following way. They suggested that the hot (1500 K) CO originates just beyond the "puffed-up" inner rim by IR resonant scattering at 0.6 AU, and that the cold CO (70 K) is emitted by IR fluorescence in the

surface of the flared disk at 8 AU.

Following this classification method, our targets fall in both groups of disks: UX Ori, V380 Ori, HK Ori are likely to have a flared disk, and HD 50138 and HD 34282 a self-shadowed disk. Their SEDs indicate that all of them should have a "puffed-up" inner rim. The non-detection of $v = 1 - 0$ emission in our targets suggests that there is no strong correlation between the disk geometry and CO emission properties.

Recent work by Rettig et al. (2004), shows the detection of optically thin warm (T ≈ 140 K) CO emission in the classical T Tauri star TW Hydrae. These authors ascribed the non detection of hot CO (T > 1000 K) as evidence for a cleared inner disk region out to a radial distance of ≈0.5 AU, and proposed that the warm CO emission is produced in a dissipating gaseous disk. In view of this interpretation, we could conclude that the non-detection of hot CO in our targets is consistent with the idea that our stars cleared of gas in their inner gaseous disks. However, the presence of strong emission lines in the optical spectra of HAEBES testifies to the occurrence of accretion. Both results could be compatible under a scenario where accretion and clearing are episodic and that a replenishment mechanism is active.

In summary, the non-detection of CO $v = 1 - 0$ emission in these five targets suggests that, *despite the relative similarity of the dust emission in Herbig Ae/Be stars, they are not a homogeneous group with respect to gas emission, and in particular to hot and warm CO emission.* This heterogeneity could be interpreted as the result of (1) differences in the structure of their inner gaseous disk leading to differences in the inner disk CO temperature, or (2) true differences in the amount of warm CO, either due to chemical effects (selective CO depletion implying a variable CO/H_2 ratio in the disk) or due to variations in the amount of bulk gas in the inner 50 AU (assuming a constant CO/H_2 ratio). The last scenario is particularly intriguing. True variations in the the bulk of H_2 in the inner disk are consistent with the idea that in these stars giant planets have already formed. Unfortunately, the present data do not allow us to confirm such a tantalizing hypothesis. Future instruments with improved spectral resolution like CRIRES at the VLT will help us to address such ideas quantitatively.

Acknowledgements. We would like to thank C.P. Dullemond and A. Bik for several fruitful discussions. The authors wish to thank the ESO-VLT staff at Paranal observatory and in Garching that performed the service-mode observations presented in this chapter. This research has made use of the SIMBAD database, operated at CDS, Strasbourg, France.

2.5 References

Aikawa, Y., et al. 2002, A&A, 386, 622
Alibert, Y., Mordasini, C., & Benz, W. 2004, A&A, 417, L25
Bary, J. S., Weintraub, D. A., & Kastner, J. H. 2002, ApJ, 576, L73
Bary, J. S., Weintraub, D. A., & Kastner, J. H. 2003, ApJ, 586, 1136
Bergin, E., et al. 2004, ApJ, 614, L133
Bertout, C. 1989, ARA&A, 27, 351
Blake, G. A. & Boogert, A. C. A. 2004, ApJ, 606, L73
Bouret, J.-C. & Catala, C. 1998, A&A, 340, 163
Bouret, J.-C. & Catala, C. 2000, A&A, 359, 1011
Boss, A. P. 2004, ApJ, 610, 456

Brittain, S. D. & Rettig, T. W. 2002, Nature, 418, 57
Brittain, S. D., et al. 2003, ApJ, 588, 535
Carr, J. S., Mathieu, R. D., & Najita, J. R. 2001, ApJ, 551, 454
Ceccarelli, C., et al. 2002, A&A, 395, 863
DiSanti, M. A., et al. 2001, Icarus, 153, 361
Dullemond, C. P., Dominik, C., & Natta, A. 2001, ApJ, 560, 957
Dullemond, C. P. 2002, A&A, 395, 853
Goto, M., et al. 2003, ApJ, 598, 1038
Grady, C. A., et al. 2004, ApJ, 608, 809
Habart, E., Natta, A., & Krügel, E. 2004, A&A, 427, 179
Henning, T., Burkert, A., Launhardt, R., Leinert, C., Stecklum, B. 1998, A&A,336, 565
Ida, S., & Lin, D. N. C. 2004, ApJ, 616, 567
Jonkheid, B., et al. 2004, A&A, 428, 511
Kamp, I. & Dullemond, C. P. 2004, ApJ, 615, 991
Kornet, K., Bodenheimer, P., & Różyczka, M. 2002, A&A, 396, 977
Kurucz, R. L. 1991, BAAS, 23, 1047
Lecavelier des Etangs, A., et al. 2003, A&A, 407, 935
Mannings, V. & Sargent, A. I. 1997, ApJ, 490, 792
Mannings, V. & Sargent, A. I. 2000, ApJ, 529, 391
Markwick, A. J., Ilgner, M., Millar, T. J., & Henning, T. 2002, A&A, 385, 632
Martin, C., Bouret, J.-C., Deleuil, M., Simon, T., & Catala, C. 2004, A&A, 416, L5
Mayer, L., Quinn, T., Wadsley, J., & Stadel, J. 2004, ApJ, 609, 1045
Meeus, G., et al. 2001, A&A, 365, 476
Najita, J.,Carr, J. S., & Tokunaga, A. T. 1996, ApJ, 456, 292
Najita, J. R., Edwards, S., Basri, G., & Carr, J. 2000, Protostars and Planets IV, 457
Najita, J.,Carr, J. S., & Mathieu, R. D. 2003, ApJ, 589, 931
Pollack, J. B., et al. 1996, Icarus, 124, 62
Qi, C., et al. 2004, ApJ, 616, L7
Rettig, T.W., et al. 2004, ApJ,616, L163
Richter, M. J., Jaffe, D. T., Blake, G. A., & Lacy, J. H. 2002, ApJ, 572, L161
Thi, W. F., et al. 2001, ApJ, 561, 1074
Thi, W.-F., van Zadelhoff, G.-J., & van Dishoeck, E. F. 2004, A&A, 425, 955
Vidal-Madjar, A., et al. 2004, ApJ, 604, L69
Waters, L. B. F. M. & Waelkens, C. 1998, ARA&A, 36, 233
Willacy, K., Klahr, H. H., Millar, T. J., & Henning, T. 1998, A&A, 338, 995

Published as: A. Carmona, M.E van den Ancker, Th. Henning – *"Optical spectroscopy of close companions to nearby Herbig Ae/Be and T Tauri stars."* Astronomy and Astrophysics, 2007, A&A, 464, 687C.

Chapter 3

Optical spectroscopy of close companions to nearby Herbig Ae/Be and T Tauri stars

Abstract

We present VLT-FORS2 optical (5700 - 9400 Å) spectroscopy of close (r < 1.5") companions to three nearby (d < 200 pc) Herbig Ae/Be stars (HD 144432, HD 150193, KK Oph) and one T Tauri star (S CrA). We report the detection of Li I (6707 Å) in absorption and emission lines (H_α, Ca II triplet) in the spectra of the companions. Our observations strongly suggest that the companions are physically associated pre-main-sequence stars. The spectral type derived for the companions is K5Ve for HD 144432 B, F9Ve for HD 150193 B, and G6Ve for KK Oph B. S CrA A and B were observed simultaneously. The spatially resolved spectra indicate that S CrA A (primary, north) is a G star and that S CrA B (secondary, south) is a K star. Using photometry from the literature and estimations of the R and I magnitude derived from the spectra, we localized primaries and companions in the HR diagram, derived their masses and assuming coevality constrained the age of the systems. KK Oph B (7 Myr) and S CrA B (2 Myr) are actively accreting T Tauri stars and are very likely surrounded by disks. HD 150193 B (10 Myr) and HD 144432 B (8 Myr) are weak-line T Tauri stars. Three of the four systems studied (HD 144432, HD 150193, KK Oph) have ages > 7 Myr. These systems retained their disks for a longer time than typical of a young star. Our results suggest that binarity may be a key issue in understanding the lifetime of disks.

3.1 Preface

Spatially resolved studies of circumstellar disks surrounding nearby (d < 200 pc) pre-main sequence stars (e.g. Grady et al. 2000, Augereau et al. 2001, Mannings & Sargent 1997) demonstrated that protoplanetary disks are structures that extend up to several hundreds of AU, and that in the outer part of these disks (R > 50 AU) exists an important reservoir of cold gas. Optical spectroscopy studies of β Pictoris (Olofsson et al. 2001), a prototypical debris disk [1], unveiled the presence of small amounts of cold gas in keplerian rotation by the detection of spatially resolved Na I D emission at 5890 Å. Studies of the variability of the same Na I D line, but in absorption, towards the Herbig Ae star UX Ori (Grinin et al. 1994), revealed the existence of a significant amount of cold gas in a close to edge-on circumstellar disk.

The combined evidence of these works suggests that, if a background star is viewed through the disk of a nearby pre-main-sequence star, its spectra will present significant excess of absorption (with respect to its spectral type) in cold gas tracers such as Na I, K and Ca II. The detection of absorption excess combined with the apparent separation of the background source provides a lower limit for the extension of the gaseous disk. The amount of absorption excess allows to

[1] Observational evidence suggest that Debris Disks are almost gas free disks (e.g. Pascucci et al. 2006).

constrain the amount of gas in the circumstellar disk at a specific distance to the central star. The velocity shift of the spectral line informs about the dynamics of the gas in the disk at the distance proben.

With the idea of using the optical spectra of background sources for constraining the physical properties of the gas in the outer region of protoplanetary disks, we selected a sample of nearby Herbig Ae stars and T Tauri stars with close companions (separations < 1.5”), and obtained optical spectra of the companions with the optical spectrograph FORS2 at ESO-VLT. We discovered that the companions are not background sources. In fact, the companions are young emission-line pre-main sequence stars and they are most likely physically associated to the bright primary. Given that the companions are not background sources, the absorption lines detected could not be attributed unambiguously to the primaries gas disks. However, since the companions are close and physically associated with the primaries, this allowed us to constrain the ages of the Herbig Ae/Be primaries, and to realize that binarity could be an important factor in the longevity of the disks and the Herbig Ae/Be star phenomenon.

3.2 Introduction

Planets form in disks of gas and dust around stars in their pre-main-sequence phase. Given that our Sun is a single and isolated star, investigations have been biased towards the study of planet formation around similar objects. In contrast, statistical studies reveal that more than 50% of the solar-type main-sequence stars in the solar neighborhood are members of a binary or a multiple system (e.g., Duquennoy & Mayor 1991; for a recent review see Bonnell et al. 2007) and that the multiplicity fraction is significantly higher in pre-main-sequence stars (e.g., Reipurth & Zinnecker 1993; Pirzkal et al. 1997; for a recent review see Duchême et al. 2007). In addition, investigations of star-forming regions and young stellar clusters show that most stars form in groups, and searches for extrasolar planets demonstrate that giant gaseous planets do exist in binary and multiple systems (e.g., Konacki 2005; for a recent review see Desidera & Barbieri 2006).

How planetary systems form and evolve in binary and multiple systems is an important question that is starting to be addressed theoretically (e.g., Kley 2000, Nelson et al. 2003, Moriwaki & Nakawa 2004, Boss 2006, Quintana & Lissauer 2006). From the observational perspective, besides continuing the search for planets in multiple systems, one logical step after the numerous imaging surveys for multiplicity in pre-main sequence stars (e.g., Chelli et al. 1988; Reipurth & Zinnecker 1993; Ghez et al. 1993, 1997; Li et al. 1994; Leinert et al. 1993, 1997; Richichi et al. 1994; Simon et al. 1995; Pirzkal et al. 1997; Bouvier & Corporon 2001; Koresko et al. 2002; Kouwenhoven et al. 2005; Ratzka et al. 2005) is to better constrain the characteristics of the companions of nearby sources with resolved disks. Binary systems with disks may be the progenitors of the binary systems with planets. The study of these systems when they are very young and still posses a disk will allow us to unveil around which component planets are forming, or whether there can be such a thing as circumbinary planets. To attain such goals, the first steps are: to obtain further evidence that the companion is not a background object, to constrain the spectral type (mass) of the companion(s), and to derive an independent estimate of the system age.

In this chapter we describe an effort to characterize close ($r < 1.5$” in projection) visual companions to four nearby ($d < 200$ pc) pre-main-sequence stars surrounded by protoplanetary disks: the Herbig Ae/Be stars (HD 144432, HD 150193, KK Oph) and the T Tauri star S CrA. We seek to

Table 3.1: *Log of the observations. The first column lists the name of the primary. The second and third list the separation r in arcsec and the position angle P.A. in degrees of the companion with respect to the primary. T_{exp} refers to the integration time in each grism. Hα/cont is the Hα peak/continuum ratio in the primary. Max. contamination refers to the maximum level of contamination in the continuum in the companion's spectra (see §3.4.1). References: [PE04] Pérez et al. 2004, [PI97] Pirzkal et al. 1997, [BA85] Baier et al. 1985.*

Primary	r [arcsec]	P.A [°]	Ref	seeing ["]	airmass	T_{exp} [s]	Hα/cont	Max. contamination [%]
HD 144432	1.4	4 [a]	PE04	0.7	1.1	3×60	3.4	7
HD 150193	1.1	236	PI97	0.6	1.4	3×11	2.2	8
KK Oph	1.5	257	PI97	0.9	1.0	3×110	7.3	2
S CrA	1.4	157	BA85	0.6	1.1	1×110	19.3	2

[a] PA re-determined from a new analysis of the IRTF image shown in Pérez et al. (2004).

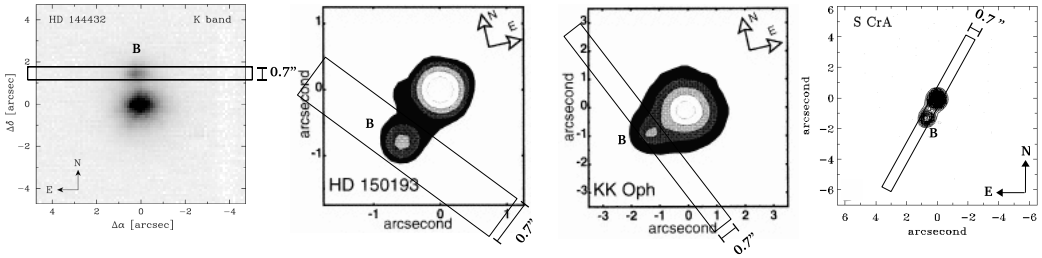

Figure 3.1: *Slit positions and the targets observed. The slits have the sizes scaled to the image obtained from the literature. References: HD 144432 [PE04], HD 150193 & KK Oph [PI97], S CrA (Reipurth & Zinnecker 1993).*

determine whether these companions are physically associated to the primary, or whether they are background sources. We derive the spectral type of the companions, place primaries and companions in the Herzsprung-Russell diagram (HRD) and show that in all cases these companions are physically associated with the primary. The chapter is organized as follows: In Section 3.2 the observations and the data reduction are described, in Section 3.3 the methods of spectra classification and luminosity determination are presented, and in Section 3.4 our results are discussed.

3.3 Observations & data reduction

3.3.1 Observations

During the night of 17 May 2005 we observed the companions to HD 144432, HD 150193, KK Oph and S CrA with the FORS2[2] optical spectrograph mounted on the VLT at Paranal Observatory in Chile[3].

The observations proceeded as follows: (1) The telescope was pointed to the primary and the

[2] http://www.eso.org/instruments/fors2

[3] The companions to HD 100456 A & B and the companions to HD 163296 A, B, C were observed the same night as well. The difference in brightness with the primary was too high for obtaining an adequate spectrum of the companions. The spectra obtained was completely dominated by the primary's spectrum.

instrument was rotated 90° with respect to the line joining primary and secondary. A first acquisition image was taken. (2) A blind offset in the direction of the secondary was performed and an image through the slit was taken. The blind-offsetting values were calculated based on the separation and position angle published in the literature (see Table 3.1). (3) Small adjustments (1-2 pixel) were performed in the pointing for ensuring that the companion was well centered on the slit. (4) Two science exposures were taken, one using the grism 1200R (wavelength range 5740-7230 Å, R≈2140) and another one with the grism 1028z (wavelength range 7660-9400 Å, R≈2560). In each grism exposure three integrations were executed, each in a different position on the CCD for avoiding errors due to the influence of bad pixels.

The slit was oriented perpendicular to the line connecting the primary and the secondary (see Fig. 3.1). Given the difference in brightness, a perpendicular slit orientation minimizes the amount of light of the primary that falls on the CCD - thereby greatly alleviating problems of dynamic range, saturation and electronic cross-talk.

In the case of S CrA (A&B), however, the slit was oriented in the direction of the line connecting the primary and secondary. The small difference in the brightness of the system components (1 mag) allowed us to obtain the spectra of primary (S CrA A) and secondary (S CrA B) simultaneously.

Integration times were calculated as a function of the estimated *V* magnitude of the companions. The slit width was selected as a function of (a) the astrometric accuracy of the position of the companion, (b) the separation of the sources and (c) the seeing conditions. This led to the choice of an 0.7" wide slit width.

3.3.2 Data reduction

In Table 3.1 we present a summary of the observations. To calibrate the data, at the end of the night we observed the spectro-photometric standard star HD 156026 using the same slit (0.7") and the two grims (1200R, 1028z). Lamp flatfields and lamp Ar-Xe arcs with the 0.7" slit for each of the two grims were also taken at the end of the night.

Raw data were reduced using standard techniques involving MIDAS, IRAF and IDL. Multiple exposures for one science target were reduced and extracted independently. The bias was determined in an homogeneous region in a dark exposure of zero seconds. Each flatfield frame was normalized after bias subtraction. A master flatfield was created by taking the median of all the flatfield frames. Each raw science frame was corrected for differences in the pixel gain by dividing by the master flatfield after the subtraction of the bias.

Each flatfield-corrected science frame was tilt corrected and simultaneously wavelength calibrated using the arc-lamp exposures. Standard IRAF routines were used for the tilt correction as described in the "IRAF User's Guide to Reducing Slit Spectra" by Massey et al. (1992). The sky lines and cosmic rays were subtracted from the tilt corrected frames before the spectral extraction. This procedure was particularly necessary for the case of S CrA (A&B), because the two sources overlapped in the spatial direction and the extraction algorithm required the selection of very small (2-4 pixels) background windows.

The extraction of the spectra of HD 150193 B, KK Oph B, HD 144432 B was performed in a straightforward manner, using the standard optimal-extraction algorithm EXTRACT/LONG implemented in MIDAS. In this method, two background windows and one extraction window are selected in the spatial direction of the spectra. The algorithm calculates the background cor-

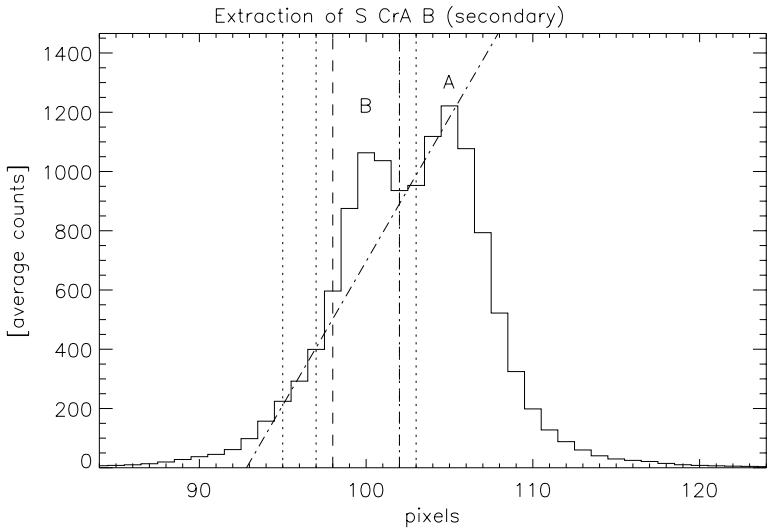

Figure 3.2: *Example of the extraction method in the case of S CrA A and S CrA B. Here we show a cut in the spatial direction of the spectra at an arbitrary wavelength. The PSF of the companion (left) overlaps with the PSF of the primary. In the figure, the vertical dashed lines represent the limits of the target extraction window (in this case the companion S CrA B) and the vertical dotted lines show the limits of the background windows. In the graph, the right limit of the extraction window and the left limit of the right background window overlap. The dot-dashed diagonal is the background fitted (see §3.3.1 for discussion). The first peak from the left is S CrA B (companion), the second is S CrA A (primary). The pixel scale is 1 pixel = 0.252".*

rection and performs the extraction, assigning different weights to each line where the spectrum is extracted. The final spectrum is the weighted sum of each contribution in the spatial direction. Identical results were obtained with the routine "apall" of IRAF. Finally, the individual wavelength-calibrated one-dimensional spectra from each exposure were added to obtain a final spectrum. Features present in only one of the exposures were considered reduction artifacts (e.g unfiltered cosmic rays) and were removed from the final combined spectrum.

In the case of the more complex reduction of S CrA (A&B) we developed an interactive IDL algorithm for extracting the spectra. The extraction procedure used the following steps: (a) the 2D frame is averaged in the wavelength direction and from the resulting spatial profile two background windows and one extraction window are chosen, (b) at each wavelength, the background is determined by a linear fit to the pixels lying in the background windows (chromatic background correction), (c) at each wavelength, the respective fitted background is subtracted to each pixel in the spatial direction, and (d) at each wavelength, all pixels in the extraction window are summed. An interactive routine was required because the best extraction demanded a careful tuning of the background and extraction windows. The lengths of the background and extraction intervals were changed pixel by pixel manually until the best signal to noise in the spectrum was obtained (~ 20). In Figure 3.2 we present an example of the extraction of S CrA B (companion). This procedure offered the best individual spectra of the sources. Nevertheless, we note that the flux fidelity is not conserved.

This method is optimized to obtain an optimal S/N ratio while preserving a low level of con-

tamination from a neighboring source when the PSF of two adjacent sources overlap. We tested the Gaussian deconvolution method for extracting the spectra. However, the results obtained (in terms of discerning the individual spectra), were not as good as the results obtained with straight-line fitting to the continuum. In particular the straight-line method was able to show that mostly all Paschen emission come from the primary S CrA A (see Fig. 3.3). We tested a third method consisting of mirroring the right wing of the PSF of the primary as an estimation of the background of the companion at each wavelength, and vice-versa. The spectra obtained for the primary and secondary were almost identical as the spectra obtained with the straight-line method. However, the straight-line method offered a better S/N ratio in the companion's spectra in the wavelength region 8800 - 9400 Å.

3.4 Results

3.4.1 Spectral classification

In Figure 3.3 we show the extracted spectra of the companions. In all the companions we detected H_α (6563 Å) in emission and Li I at 6708 Å in absorption. Ca II (8498, 8542, 8662 Å) in emission is detected in all the companions except for HD 144432 B. Details of important spectral features are illustrated in Figure 3.4. To determine the spectral type of the sources, we employed two complementary methods. First we applied the quantitative method of Hernandez et al. (2004). Then we compared the spectra with STELIB, a library of standard star spectra obtained with a similar spectral resolution (R≈2000; Le Borgne et al. 2003) [4].

The Hernandez et al. (2004) method is based on the measurement of the equivalent width of selected spectral features (photospheric in nature and less affected by activity-induced line emission) and assignment of a spectral type (or range of spectral types) to each spectral index measured. The combination of several spectral features narrows down the possible spectral type(s) to a range consistent with the multiple diagnostics. The method offers the advantage that when only very few lines are detected (and placing meaningful upper limits on the presence of others) it is possible to extract an accurate spectral type. This method is mainly useful for early type stars.

Calibration curves relating spectral types with equivalent widths of spectral features were computed by Hernandez et al. (2004). In the range covered by our observations the spectral features employed for spectral classification were : He I (5876 Å), Na I (5890 Å), Mn I (6015 Å), Ca I (6162 Å), TiO (6185 Å), CaH_2 (6385 Å), He I (6678 Å), TiO_3 (6720 Å), CaH_3 (6830 Å), CaH (6975 Å) and He I (7066 Å). The equivalent width measurement is presented in Table 3.2.

Effect of the veiling. The companions are found to be emission-line T Tauri stars. Active T Tauri stars are affected by veiling, a smooth "continuum" excess arising from the hot (T≈8000-10000 K) accretion spots. This excess decreases the equivalent width of all absorption features, potentially affecting the spectral typing using methods relying on quantitative measurements of the line strength. This smooth continuum can contribute significantly to the total flux (up to 50-70% in the red part of the spectrum), implying comparable reductions in the equivalent widths (Hartigan & Kenyon 2003). For the stars, for which we have detected many lines such as HD 144432 B, HD 150193 B, KK Oph B we can exclude the possibility of strong veiling. Large amounts of veiling would mean that different lines would yield to mutually exclusive spectral

[4] www.ast.obs-mip.fr/users/leborgne/stelib/index.html

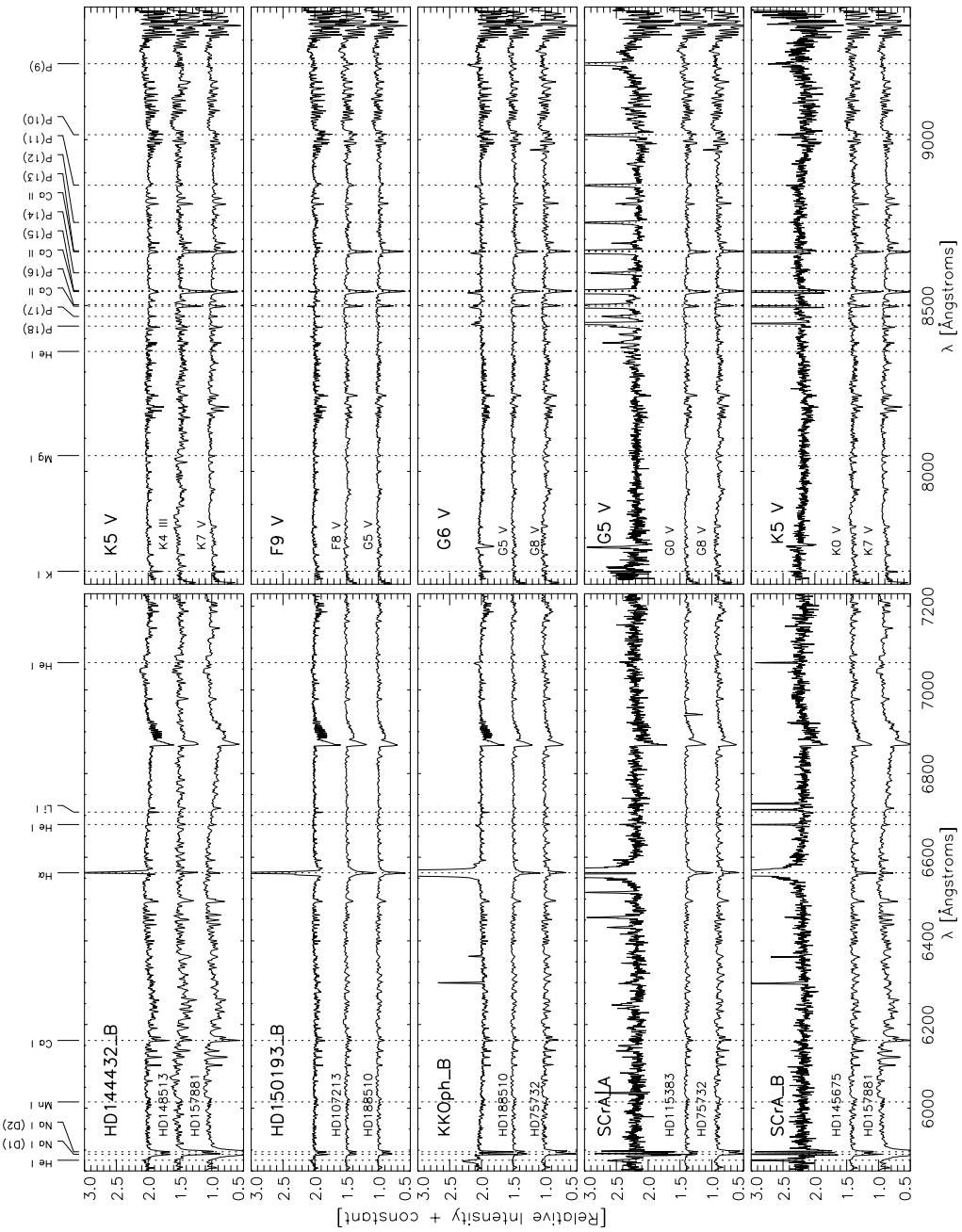

Figure 3.3: *Spectra obtained for the companions. The spectra in the left column were taken with the grism 1200R, the spectra in the right column with the 1028z grism. In each panel, we also show the spectra of standard stars from the STELIB spectral library for the range of consistent spectral types. The derived spectral type of the companion is indicated in the upper left part of the spectra in the right column. The spectra have been continuum-normalized with a second-order polynomial function.*

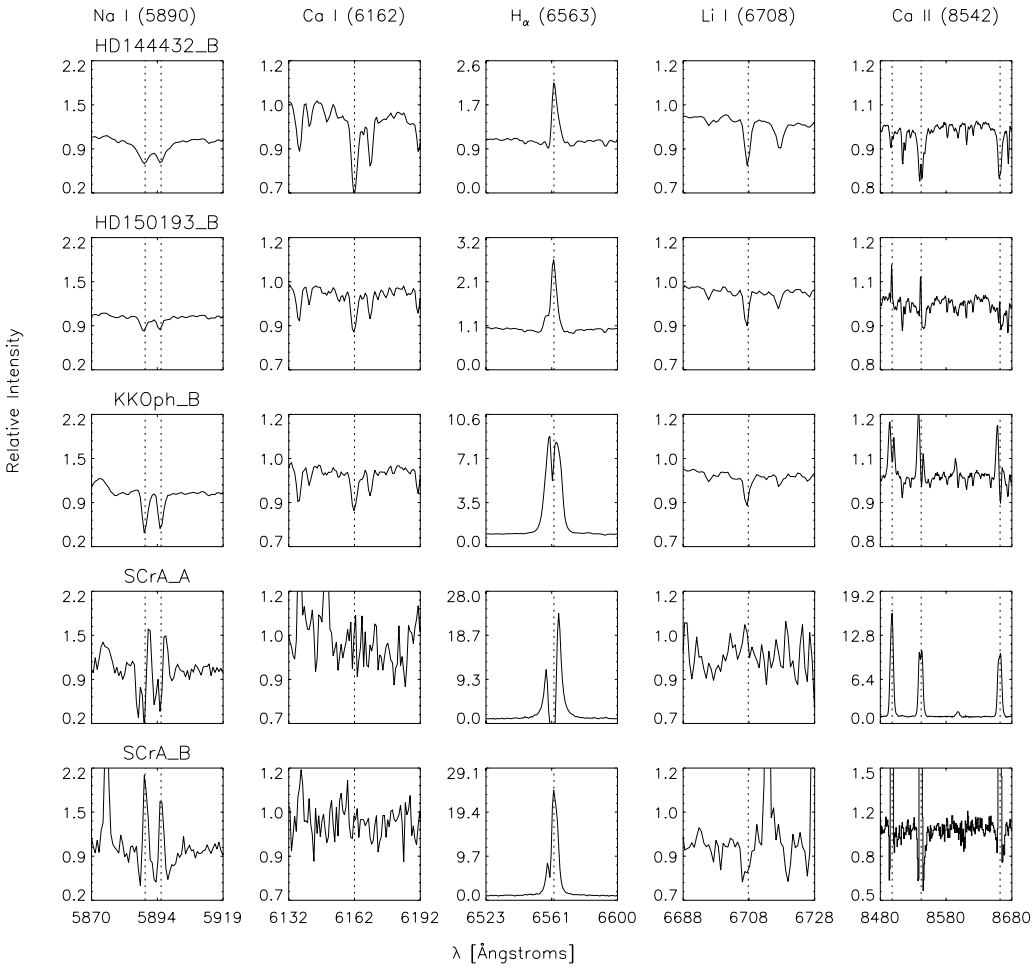

Figure 3.4: *Details of important spectral features (Na I D1 & D2, Ca I, H_α, Li I, Ca II) in the companion's spectra. Each row of panels represents the data for one star. The columns show each spectral feature.*

types. Since this effect is not observed in the three objects the veiling should be small (< 10%). The case of S CrA A&B is more complex since fewer lines are detected and the veiling effect limits the derivation of good upper limits of line strengths. However, non-detections combined with the detection of few photospheric absorption lines give a spectral interval in which the line can reach the measured strength regardless of the amount of veiling. Although error bars are larger, the determination of a range of spectral types is still possible.

The comparison with STELIB is a good additional method which is more accurate than the Hernandez et al. method for later spectral types (K and later), in which the quantitative evaluation of - often blended - absorption bands becomes difficult. For the direct comparison between our spectra and the STELIB spectra, the spectra were normalized by a second-order polynomial fit to the continuum. To perform the spectral classification, the depth of the absorption features and the overall shape of the spectra were compared to the templates.

Table 3.2: *Measurements of the equivalent widths (in Å) of important lines for the spectral classification of the companions. Negative values indicate that the line is in emission. Upper limits are given for spectral lines whose absence allows us to constrain the companion's spectral type.*

Line	λ [Å]	HD 144432 B	HD 150193 B	KK Oph B	S CrA A	S CrA B
He I	5876	-0.5 ± 0.1	-0.3 ± 0.1	-0.9 ± 0.1	-1.3 ± 0.4	-4.8 ± 0.4
Na I D1	5890	1.3 ± 0.1	0.6 ± 0.1	1.5 ± 0.1	0.5 ± 0.4	-0.8 ± 0.4
Na I D2	5896	1.2 ± 0.1	0.5 ± 0.1	1.3 ± 0.1	0.4 ± 0.4	-0.1 ± 0.4
Mn I	6015	<0.1	<0.1	<0.1	<0.4	<0.4
Ca I	6162	1.9 ± 0.1	1.0 ± 0.1	1.0 ± 0.1	<0.4	<0.4
TiO	6185	1.3 ± 0.1	<0.1	<0.1	<0.4	<0.4
CaH_2	6385	0.2 ± 0.1	<0.1	<0.1	<0.4	<0.4
H_α	6563	-2.6 ± 0.1	-5.6 ± 0.1	-80 ± 0.1	-96 ± 0.4	-127 ± 0.4
He I	6678	0.0 ± 0.1	<0.1	-0.3 ± 0.1	-0.8 ± 0.4	-2.0 ± 0.4
Li I (1)	6708	0.4 ± 0.1	0.3 ± 0.1	0.4 ± 0.1	<0.4	1.3 ± 0.4
TiO_3	6720	0.4 ± 0.1	0.2 ± 0.1	<0.1	<0.4	<0.4
CaH_3	6830	<0.1	<0.1	<0.1	<0.4	<0.4
He I	7066	<0.1	<0.1	-0.1 ± 0.1	<0.4	-1.2 ± 0.4
K I	7699	0.4 ± 0.1	0.2 ± 0.1	0.4 ± 0.1	<0.4	0.5 ± 0.4
Ca II	8498	0.0 ± 0.1	-0.4 ± 0.1	-1.4 ± 0.1	-54 ± 0.4	-10 ± 0.4
Ca II	8542	0.6 ± 0.1	-0.2 ± 0.1	-1.2 ± 0.1	-44 ± 0.4	-16 ± 0.4
Ca II	8662	0.6 ± 0.1	-0.1 ± 0.1	-0.9 ± 0.1	-42 ± 0.4	-14 ± 0.4
spectral type range		K4Ve - K7Ve	F8Ve - G5Ve	G5Ve - G8Ve	G0Ve - G9Ve	K0Ve - K7Ve
adopted spectral type		K5Ve	F9Ve	G6Ve	G5Ve	K5Ve

In Table 3.2 the spectral classification results are summarized. In Figure 3.3, the extracted spectrum for each companion is plotted together with comparison spectra of sources in the lower and upper spectral range of classification. The spectral type range deduced determines the range of effective temperatures. The error on T_{eff} is given by the range of possible spectral types (see Table 3.4).

Contamination from the primaries. The contamination of the companion's spectra by the primary was determined in the following way. In each 2D stellar spectrum, a cut in the spatial direction, averaged over 20 pixels in the dispersion direction, at the wavelength of H_α was extracted, and the total flux within the extraction window was measured. An analogue procedure was performed for a standard star frame obtained with the same slit (0.7") at a similar seeing (0.6"), taking care of scaling the standard star PSF so that it had the same high as the companion's PSF. Assuming that the seeing does not change significantly between the science and standard star observation, the maximum contamination in Hα is given by the excess of flux (in percentage) that the target's PSF has over the unresolved PSF from the standard star. To determine the maximum contamination in the continuum for each star, we divided the maximum contamination in Hα by the Hα peak/continuum ratio of each primary (see Table 3.1)[5]. The Hα peak/continuum ratio was obtained by rebinning the high-resolution spectra used in Acke et al. 2005 (HD 144432, HD 150193), van den Ancker, unpublished (KK Oph, S CrA) to R=2500. Our results are presented in Table 3.1. The contamination is always smaller than 10 %. In the following sections, we discuss in detail the spectra obtained for each companion.

[5]In the case of KK Oph the seeing of the standard star observation is 0.3" smaller. The maximum contamination is therefore smaller than the upper limit deduced

HD 144432 B

The spectrum of HD 144432 B shows a forest of metallic absorption lines characteristic of K type stars. Moderately strong Ca I at 6162 Å indicates that the star is later than K2. The strength of the Ca II lines at 8498, 8542 and 8662 Å indicates that HD 144432 B has a spectral type not later than K7. The presence of TiO bands around 7100 Å indicate that the star is mid-K type. The presence of K I absorption at 7698 Å indicates that the spectral type of HD 144432 B is later than a K4 star. The spectral range of HD 144432 B is, therefore, between K4 and K7. We adopt a spectral type K5Ve. H_α is observed in emission (EW≈-2.6 Å) and Li I at 6708 Å is detected. The spectral type range K4 to K7 is in agreement with the spectral type reported by Pérez et al. (2004).

HD 150193 B

The spectrum of HD 150193 is characterized by the presence of a forest of weak metallic lines between 5000 and 6000 Å. Weak Paschen absorption lines present in the spectra indicate that the star is of spectral type F. The strength of the Ca I line at 6162 Å indicates that the star is of early G type. H_α is detected in emission (EW≈-5.6 Å). Weak Ca II emission lines are observed inside weak Paschen lines. Lithium is detected in absorption (EW≈0.31 Å). Weak Mg I at 8047 Å is observed. Moderately strong Na I in absorption is detected (EW≈0.31 Å). Given that the star shows weak Paschen lines and metallic lines simultaneously, HD 150193 B should be a late F type star. Spectral types between F8 and G5 are consistent with the observed spectrum. Bouvier & Corporon (2001), using high resolution spectro-imaging and SED fitting, derived a K4 spectral type for HD 150193 B. However, in our spectra HD 150193 B does not show the strong spectral features characteristic of K-type stars (i.e strong Na I, Ca I, K I, and Ca II lines). We thus adopt a spectral type of F9Ve for HD 150193 B. Our data demonstrate that HD 150193 B is a T Tauri star, in agreement with the suggestion of Bouvier & Corporon (2001).

KK Oph B

KK Oph B shows weak metallic absorption lines. The strength of the Ca I line at 6162 Å, the weak Mg I line at 8047 Å and the absence of Paschen absorption lines indicate that KK Oph B is a G type star. Strong H_α in emission is observed (EW≈-80Å). Li I is detected in absorption. Double peaked Ca II at 8498, 8542 and 8662 Å is detected in emission. The range of spectral types obtained for KK Oph B is between G5 and G8. We conclude that KK Oph B is a G6Ve star. Recently, Herbig (2005) derived a K-type spectral class for KK Oph B based on spectro-photometry assuming an identical extinction for KK Oph A and KK Oph B. In §3.4.2 we will demonstrate that this is not be the case: the extinction for KK Oph B is larger than for KK Oph A. Herbig (2005) does report the presence of the Hα and Hβ lines in emission in KK Oph B, in agreement with our observations.

S CrA A & B

The spatially resolved individual spectra reveal that S CrA A and S CrA B are emission line stars. Primary and secondary show H_α in emission. S CrA A (primary) has a H_α double peaked profile, S CrA B (companion) has a single peaked profile with a small blue shifted peak (see Fig. 3.4). Ca

II in emission is present in both components. The Ca II emission in S CrA A (primary) is much stronger and broader than in S CrA B (companion). Strong Paschen *emission* (13-19) is observed only in the primary S CrA A. The Na I line is characterized by components in absorption and emission in both sources (see Fig. 3.4). Li I is detected *only* in S CrA B, where it is significantly broadened (probably due to rotational broadening). Li I is not observed in S CrA A, this is most probably due to the presence of strong veiling in the spectra of the source.

The spectral classification of S CrA A and S CrA B is challenging. Very few absorption lines are present in the spectrum of either component. In addition strong veiling is present in the spectrum. Our spectral classification is based on the absence of strong features that are characteristic of certain spectral classes.

First, given that broad Paschen *absorption* lines at 8000 Å are not present in the spectra, both components are not earlier than G. Second, the absence of strong TiO molecular bands at 6185, 6720, and 7100 Å, and CaH_2 (6385 Å) and CaH_3 (6830 Å) features, indicates that primary and companion are earlier than M. In the case of S CrA A none of the strong absorption lines characteristic of a K star are observed. The Ca I line at 6162 Å , the metallic lines between 6000 and 6600 Å , and the K I line at 7699 Å are absent. We conclude that S CrA A (primary) is most likely a G-type star. We assign a spectral range between G0 and G9, and adopt a G5Ve spectral type. In the case of S CrA B (companion) two features are observed, a weak K I line at 7699 Å (EW≈ 0.5 Å), three emission-filled Ca II absorption lines between 7000-8000 Å (see in Fig. 3.4 the 8542 and 8662 Ca II lines, where a narrow emission appears inside the core of the absorption line). The simultaneous presence of the K I and Ca II features indicate that S CrA B is very likely a K-type star. The presence of three *absorption* features at 8200 Å and at the position of P(18) and P(17), that are only seen in K-type stars (comparison with STELIB template), provide further evidence that S CrA B is of spectral type K. Given that the strong Ca I line at 6162 Å is absent in the spectra, S CrA B should be earlier than K7. We conclude that S CrA B is in the spectral range K0 - K7, and adopt a K5Ve spectral type.

Prato et al. (2003) observed S CrA A&B in the NIR. They mention that S CrA A is a K3 type star and S CrA B a M0 type star (from Krautter 1991) and reported the detection of CO bands at 2.3 μm. The spectra of S CrA A&B published by Prato et al. (Fig. 2), show that the NIR spectrum is virtually flat in both components and that none of the spectral features characteristic of G, K or M stars are present. Prato et al. estimated that the veiling in the NIR was high ($r_K \approx$ 2-3) [6]. We note that the optical spectrum provides better spectral diagnostics for the classification than NIR spectra, as in the optical range the photospheric contribution to the total system flux is expected to be stronger than in the near-IR. The discrepancy between Prato et al.'s spectral types and ours could be explained as the effect of the high NIR veiling.

3.4.2 Luminosity determination

For calculating the luminosity of the companions, their distance, visual magnitude, extinction and bolometric correction are required. Given that all the companions are emission line stars it is unlikely that they are field background objects. Since the companions are close (in projected distance) to the primaries, we assume that they are at the same distance.

The visual magnitudes V are available from the literature (see Table 3.3). To determine the visual extinction A_V, we calculated the R and I magnitudes from the total number of photons

[6] r_K is the ratio of the magnitude of the K-band excess to the photospheric flux of the star at 2.2 μm.

Table 3.3: *Magnitudes of the companion stars in V, K, R and I bands. References: Baier et al. 1985 [B85], Herbst & Shevchenko 1999 [HS99], Hillenbrand 1992 [HI92], Hipparcos catalogue [HIP], Kouwenhoven et al. 2005 [K05], Prato et al. 2003 [P03], Rositer 1955 [R55], Wycoff et al. 2006 [W06].*

STAR	literature				PSF spectrum	
	V[mag]	Ref	K[mag]	Ref	R[mag]	I[mag]
HD 144432 B	12.9±0.5	R55	9.0 ± 0.1	[a]	11.2 ± 0.2	10.1 ±0.2
HD 150193 B	12.3±0.2	HIP	7.9 ± 0.1	K05	10.9 ± 0.2	9.9 ±0.2
KK Oph B	13.0±0.3 [b]	HS94	8.1 ± 0.1	HI92 [c]	13.1 ± 0.2	11.7 ±0.2
S CrA A	11.0±0.2	B85,W06	6.56 ± 0.06	P03	14 ± 0.3 [d]	13.0 ± 0.3 [d]
S CrA B	12.0±0.2	B85,W06	7.27 ± 0.08	P03	14 ± 0.3 [d]	13.2 ± 0.3 [d]

[a] From the acquisition IRTF image published in Pérez et al. 2004.

[b] The combined brightness of KK Oph A&B varies on short (days–months) and long (decades) timescales. Herbig and Bell (1988) reported that in 1987 KK Oph B was 1 mag fainter than KK Oph A in the *V* band. To obtain the literature value of the *V* magnitude of KK Oph B, we used the photometry of KK Oph A in 1987 published in Herbst & Shevchenko (1999).

[c] Pirzkal et al. (1997) reported that the companion to KK Oph A is 2.5 mag fainter in the K band. Here we used the Hillenbrand et al. (1992) magnitude measurement (K = 5.64 mag) of KK Oph A for estimating K for the companion.

[d] The *R* and *I* magnitudes derived for S CrA A and B from the PSF are 1-2 magnitudes too faint to be consistent with the *V* and *K* magnitudes reported in the literature and the spectral type of the sources. We include them here to illustrate the difference in flux of $\sim$ 0.2 mag between S CrA A and B in the *R* and *I* bands.

received in the spectra, and derived $A_{\rm V}$ self-consistently using the $(V-R)_i$ and $(V-I)_i$ colours intrinsic to the spectral-type(s) assuming a standard galactic extinction law: $0.37A_{\rm V} = (R-I)_{obs} + (V-R)_i - (V-I)_i$ (Fluks et al. 1994).

For determining *R* and *I*, in the cases of HD 144432 B, HD 150193 B and KK Oph B, we used the following procedure: First, in a flat-fielded, background emission and cosmic-ray corrected science target exposure, the total number of photons inside the PSF in the wavelength band was counted (for *R* band we used the 1200R grism exposure and for *I* band the 1028z grism). The flux of the target F_{TARGET} was obtained normalizing the total number of counts by the frame's exposure time. Second, the flux of the standard star F_{STD} was derived applying the same procedure to a standard-star frame. The *R* or *I* magnitudes were estimated using the classical flux/magnitude relation: $M_{TARGET} = M_{STD} - 2.5 \times log(F_{TARGET}/F_{STD})$. We employed a PSF window 30 pixels-wide and used the star HD 156026 (V=6.3 mag, R=5.4 mag, I=4.8 mag, seeing at the time of observation 0.6") as photometric standard. The errors on the derivation of *R* and *I* are maximum 0.2 mag: 0.1 mag by photon noise and systematics and maximum 0.1 mag due to slit differences in the seeing between the target and standard star observations. In the three objects extinction towards the companion is larger than towards the primary.

The method used for the extraction of the spectra of S CrA A and S CrA B did not conserve the fidelity of the fluxes (cf §3.3.2). Therefore, a different approach was required for determining F_{TARGET} on these sources. The two-dimensional science frame was converted to one-dimension by summing the counts in the dispersion direction. Two Gaussians with the same FWHM were fitted to the double-peaked profile obtained. The relative area of each Gaussian normalized by the

Table 3.4: *Details of the calculation of the luminosity of the companions.The parameters T_{eff} and the luminosity log L of the primary are taken from the literature. A_V was deduced self-consistely from the $(V-R)$ and $(V-I)$ colors (see §3.4.2). References: Acke et al. 2004 [A04], van Boekel et al. 2005 [B05], Hillenbrand et al. 1992 [H92], Leinert et al. 1997 [L97], Reipurth & Zinnecker 1993 [RZ93].*

Star		SpT	log T_{eff} log [K]	d [pc]	A_V [mag]	$V_{Lit} - A_V$ [mag]	log L [$L_\odot$]	log $L_{adopted}$ [$L_\odot$]	Ref
HD 144432	A	A9IVe	3.87	145	0.17			1.0 ± 0.1	A04,B05
	B	K4Ve	3.66	145	1.4 ± 1.1	11.5 ± 1.2	-0.16 ± 0.5	-0.2 ± 0.5	
		K7Ve	3.61	145	0.9 ± 1.1	12.0 ± 1.2	-0.24 ± 0.5		
HD 150193	A	A2IVe	3.95	150	1.49			1.38 ± 0.1	H92,A04,B05
	B	F8Ve	3.79	150	1.9 ± 1.1	10.4 ± 1.1	0.15 ± 0.4	0.13 ± 0.4	
		G5Ve	3.76	150	1.8 ± 1.1	10.5 ± 1.1	0.11 ± 0.4		
KK Oph	A	A6Ve	3.92	160	1.6			1.3 ± 0.1	H92,L97
	B	G5Ve	3.76	160	2.8 ± 1.1	10.2 ± 1.1	0.32 ± 0.4	0.3 ± 0.4	
		G8Ve	3.74	160	2.8 ± 1.1	10.2 ± 1.1	0.30 ± 0.4		
S CrA	A	G0Ve	3.78	140	3.2 ± 1.6	7.8 ± 1.6	1.14 ± 0.6	1.1 ± 0.6	RZ93
		G9Ve	3.73	140	3.0 ± 1.6	8.0 ± 1.6	1.08 ± 0.6		
	B	K0Ve	3.72	140	2.9 ± 1.6	9.1 ± 1.6	0.67 ± 0.6	0.6 ± 0.6	
		K7Ve	3.61	140	1.9 ± 1.6	10.1 ± 1.6	0.53 ± 0.6		

exposure time determined the flux of each of the binary components. Using the flux/magnitude relation, the R and I magnitudes were calculated for each component. The R and I obtained are up to 2 mag too faint to be compatible with previous measurements of V and the spectral type of the sources. That may be due to the intrinsic variability of S CrA (A&B) (V=10.5 - 12.4 mag; de Winter et al. 2001). Although not adequate for absolute photometry, the estimates of R and I in S CrA A and S CrA B do allow relative photometry, and permit us to obtain an estimate of the visual extinction towards the sources. We find that the companion is $\approx 0.2 \pm 0.3$ magnitudes fainter than the primary in the R and I band.

The absolute magnitude M_V of the companions was derived from our estimation of A_V and V-band measurement from the literature. Given that the extinction-corrected visual magnitude estimate and the bolometric correction depend on the spectral type, we calculated the luminosity for the two extremes of the spectral range derived for each companion. The spectral type $(V-R)_i$ and $(V-I)_i$ colors, the bolometric correction and the effective temperature calibrations were taken from Table A5 of Kenyon & Hartmann (1995). The error in the luminosity is determined by the error in the M_V magnitude estimation and the range of the bolometric correction. The typical error in the determination of $\log(L/L_\odot)$ was 0.4 to 0.6. A summary of the calculation of the companions' luminosities is given in Table 3.4.

3.4.3 Primaries and companions in the HR diagram

With the estimates of the effective temperature T_{eff} and the luminosity L, we localized the primaries and their companions in the HR diagram (see Figure 3.5). To calculate the mass and the age of the systems, we used the theoretical evolutionary tracks of Palla & Stahler (1993). The parameters of the systems (masses and ages) are summarized in Table 3.5. The first column shows

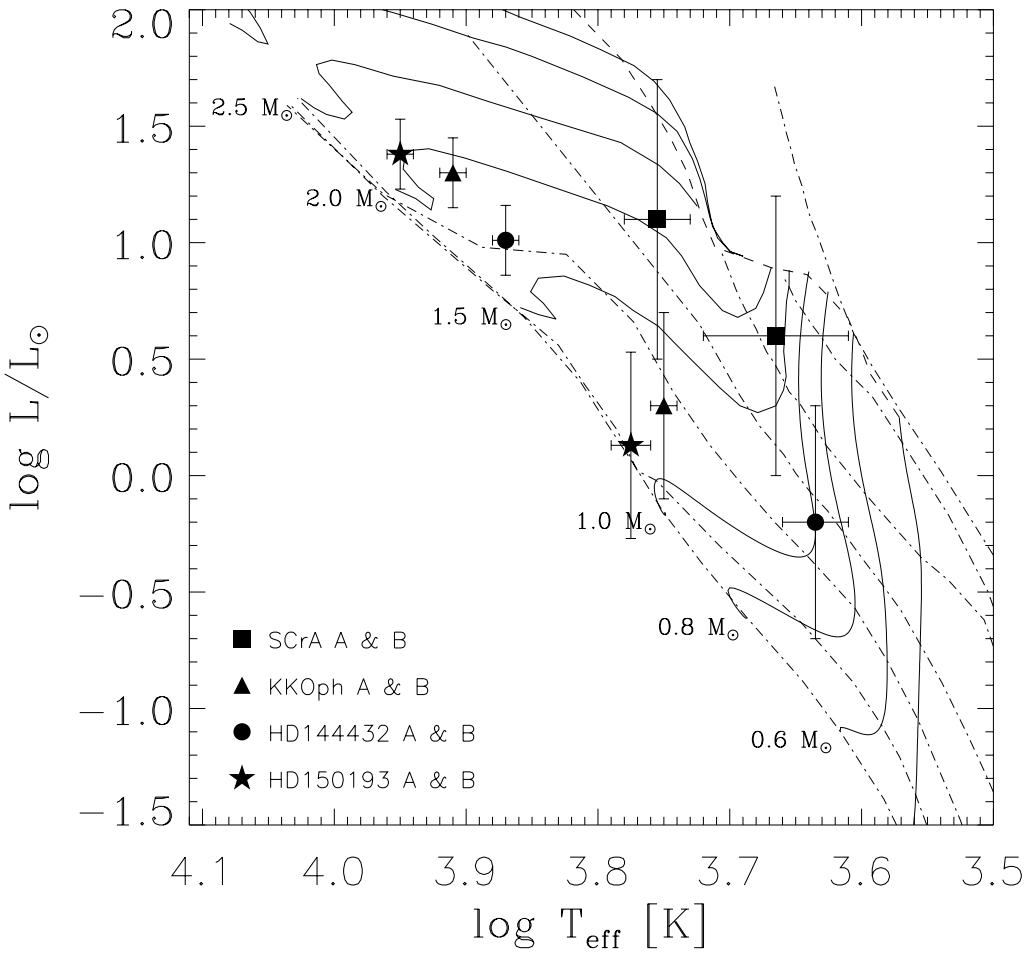

Figure 3.5: *HR diagram of the primaries and the companions. In each pair, the upper star is the primary and the lower one is the companion. The theoretical evolutionary tracks are from Palla and Stahler (1993). The primaries and companions are located on similar isochrones within the errors. The isochrones correspond to 0.1, 0.3, 1, 3, 10, 30 and 100 Myr respectively.*

the mass of each source; the second, the age range for each star. Primaries and companions are within the errors coeval objects. Assuming coevality, the system age (third column) is is the age interval that is *simultaneously* consistent with the age derived for the primary and for the companion. It is given by the 1-sigma confidence level interval of the age probability distribution obtained by multiplying the age probability distribution of the primary and companion (assuming symmetric Gaussians in the log(age) space).

Fukagawa et al. (2003) using photometry and the evolutionary tracks of Siess et al. (2000) derived a mass of 1.4 $M_\odot$ and age of 5 Myr for HD 150193 B. We demonstrated in §3.4.1 that HD 150193 B is a F8-G5 star and not a mid-K type star. Taking into account the uncertainly in the luminosity estimate, our spectral-type range rules out ages smaller than 10 Myr for HD 150193B.

Table 3.5: *Masses and ages derived for the companions and primaries from the HR diagram. The system age is the age interval that is simultaneously consistent with the age derived for the primary and the companion (see §3.4.3).*

Star		Mass [$M_\odot$]	Age [Myr]	System age [Myr]
HD 144432	A	1.6 ± 0.1	9^{+7}_{-2}	8^{+3}_{-1}
	B	1.0 ± 0.2	4^{+26}_{-3}	
HD 150193	A	2.0 ± 0.1	7^{+2}_{-1}	10^{+1}_{-1}
	B	1.2 ± 0.2	30^{+1000}_{-20}	
KK Oph	A	1.6 ± 0.1	7^{+2}_{-1}	$7^{+1}_{-0.5}$
	B	1.1 ± 0.2	12^{+18}_{-7}	
S CrA	A	2.2 ± 0.7	2^{+8}_{-1}	$2^{+0.5}_{-1}$
	B	1.3 ± 0.7	$1^{+3}_{-0.9}$	

3.5 Discussion

We obtained spatially resolved optical spectroscopy of the close companions to the Herbig Ae/Be stars HD 144432, HD 150193, KK Oph and the T Tauri star S CrA A. Our first objective was to find out whether the visual companions are physically associated objects or background sources. For answering this, we determined their spectral types. Using *V* photometry from the literature and estimated A_V values from our data, we determined their luminosities and their location in the HR diagram. The results of our observations are:
i) The spectra of all the companions are characterized by H_α in emission and in some cases also strong Ca II in emission.
ii) The spectra of the companions are characterized by Li I in absorption
iii) Several companions have early spectral types.
iv) Assuming the same distance, primaries and companions are in the pre-main-sequence zone of the HR diagram and – within the errors – they are localized on similar isochrones as their primaries.

Let us now address the question of whether the companions are physically associated with the primary. First, it is unlikely that the companions are background sources. Background sources usually do not have emission lines and in general are not early-type stars. Second, the companions are very likely young. HD 144432 B and KK Oph B are pre-main-sequence stars with masses < 1.2 $M_\odot$ and show Li I in absorption. Stars with masses smaller than 1.2 $M_\odot$ are expected to have photospheres significantly depleted in lithium by the time they reach the main-sequence (Stahler & Palla 2004). Therefore, the presence of Li I in HD 144432 B, KK Oph B combined with their location above the ZAMS indicate that they are young. In addition, KK Oph is an actively accreting T Tauri star (H_α EW≈ << -5 Å). HD 150193 B has about 1.2 $M_\odot$ and is located low in the HR diagram close to the ZAMS. In consequence, the detection of Li I is a less obvious sign

of youth. However, HD 150193 B is an early-type star (F9V) with accretion signatures (H_α and Ca II in emission) and X-ray emission (see below). Therefore, HD 150193 B seems still to be young. S CrA B ($M > 1.2\ M_\odot$) must be young because its position in the HR-diagram and its strong accretion signatures.

These results combined with the small projected separation from their primaries, *provide strong evidence that HD 144432 B, HD 150193 B and KK Oph B are physically associated T Tauri stars to Herbig Ae/Be primaries, and confirm that S CrA is a T Tauri binary*. KK Oph B and S CrA B are actively accreting T Tauri stars and are very likely surrounded by disks. HD 150193 B is an early-type T Tauri star with a low accretion rate, HD 144432 B is a weak-line T Tauri star without strong evidence for a disk. Follow up studies analyzing the proper motion of the objects, as reported in the case of HD 144432 A & B (Pérez et al. 2004), and HD 150193 A&B (Fukagawa et al. 2003) will be extremely useful to confirm that the systems are true binaries, and to derive their orbital parameters.

The presence of T Tauri companions physically associated with Herbig Ae/Be stars raises interesting questions concerning the potential of such objects to form planets and, in a more general sense, about the formation scenarios of the Herbig Ae/Be stars themselves.

Growing observational evidence for binary and multiple systems points towards "isolated" Herbig Ae/Be stars being the exception rather than the rule (e.g., Chen et al. 2006; Baines et al. 2006).

Let us now consider the X-ray emission. In our sample of Herbig stars, X-ray emission has been observed towards HD 150193 by ROSAT and Chandra [7]. Feigelson et al. (2003), Skinner et al. (2004) and Stelzer et al. (2006) imaged HD 150193 with Chandra and detected two X-ray sources: a faint X-ray northern source and a bright X-ray southern source. The nearly identical separation and position angle with respect to the IR image from Pirzkal et al. (1997), suggest a one-to-one correspondence between the two sources seen in the X-ray and IR images. Our observations show that the IR companion is a T Tauri star. This result provides further evidence that the X-ray bright source is HD 150193 B. In the case of the T Tauri star S CrA A&B, X-rays have been detected by ROSAT, XMM and Chandra. Chandra deep (160 ksec) data of the region show that the source emission appears to be only due to the primary (Forbrich et al. 2007).

Let us now move to the structure of protoplanetary disks. There are several potential effects of a companion. The Herbig Ae/Be stars HD 100453, HD 34700, HD 169142, MWC 1080, HD 35187, HD 141569 have no 10 μm silicate feature, and they all have companions. Chen et al. (2006) suggested that the lack of 10 μm silicate may be linked to the presence of close companions. Although further investigations are needed to establish whether Herbig stars that lack the 10 μm silicate feature show a higher binary frequency than stars with silicate feature, our observations do not support this as a general conclusion. All Herbig stars in our sample (HD 144432, HD 150193, KK Oph), do show silicate emission (Acke & van den Ancker 2004), yet they also show close companions (HD 144432 B, separation $\approx$ 200AU, HD 150193 B, separation $\approx$ 160AU, KK Oph separation $\approx$ 240AU). Some of our sources (HD 150193) are very similar in other properties (age, mass, distance to the companion) to sources in the Chen et al. sample (i.e HD 100453, separation $\approx$ 120 AU) . So we can find clear examples of sources with close companions which show evidence for the presence of relatively small dust grains in the surface layers of their protoplanetary disks, as well as sources with close companions in which these small

[7] KK Oph and HD 144432 have no reported X-ray detections.

dust grains are absent, either due to settling or grain coagulation. Other parameters than binarity must thus play a role in the processing of dust in the disks around Herbig Ae/Be stars.

Lets us now consider the influence of binarity on the disk's lifetime. Theoretically (e.g. Artymowicz and Lubow, 1994) and observationally (e.g. Bouwman et al., 2006), it has been suggested that in low-mass close (projected separation < 20 AU) T Tauri binaries, the disks have shorter lifetimes compared to single-star systems. Binarity may well be a key issue in Herbig stars too. In our sample (projected separation ≈ 200 AU), three of the four systems studied (HD 144432, HD 150193, KK Oph) have ages > 7 Myr, suggesting that they may have retained their disks for a much longer time than typical for a young star. Our sample is small, it does not represent a complete sample, and we should be cautious about extrapolating our findings. However, it could be that Herbig stars may retain their disks much longer than other young objects because of a companion's influence. Further research is required to determine if Herbig stars with close companions consistently retain their disks longer than isolated objects.

Another interesting point is the influence of the Herbig primary on the companion's disk lifetime. All our systems have a mass ratio of ≈0.6 and a similar separation, S CrA A&B is 2 Myr old and both stars show evidence for disks. KK Oph A&B is 7 Myr old and the companion is still an active accreting object. HD 144432 A&B is 8 Myr old and the companion is apparently disk free. HD 150193 A&B is 10 Myr old and the companion is a weak accretor. In our sample the companion's disk has dissipated after 8 Myr. As in the case of the Herbig primaries, our companions retained their disks longer than typical for a young star. Now, HD 150193 B at 10 Myr still has its disk and HD 144432 B (8 Myr) not. One important difference between HD 150193 B and HD 144432 B is that the former is more massive. We speculate that at similar primary/secondary ratio and separation (∼ 200 AU), the secondary may be more likely to retain its disk longer the higher its mass is. Studies with larger samples with a variety of mass ratios and separations are required to statistically test these trends.

Acknowledgements. A.C. is grateful to J.Hernandez for providing the calibration curves for spectral classification, and for discussions concerning the spectral classification of pre-main-sequence stars. A.C. would like to thank K.T. Hole and C. Grady for useful comments on the manuscript, and to J. Bouwman for helpful discussions. We are very grateful to the referee for comments and suggestions that helped to improve the paper. This research has made use of the SIMBAD database operated at CDS, Strasbourg, France.

3.6 References

Acke, B., & van den Ancker, M. E. 2004, A&A, 426, 151
Acke, B., van den Ancker, M. E., & Dullemond, C. P. 2005, A&A, 436, 209
Augereau, J. C., Lagrange, A. M., Mouillet, D., & Ménard, F. 2001, A&A, 365, 78
Artymowicz, P., & Lubow, S. H. 1994, ApJ, 421, 651
Baier, G., Keller, E., Weigelt, G., Bastian, U., & Mundt, R. 1985, A&A, 153, 278
Baines, D., Oudmaijer, R. D., Porter, J. M., & Pozzo, M. 2006, MNRAS, 232
Bonnell, I.A., Larson, R.B, Zinnecker, H., in Protostars and Planets V., Edited by B. Reipurth, D. Jewitt, and K. Keil. University of Arizona Press, Tucson, 2007
Boss, A. P. 2006, ApJ, 641, 1148
Bouvier, J., & Corporon, P. 2001, IAU Symposium, 200, 155

Bouwman, J., et al. 2006, ApJ Letters (in press)
Chelli, A., et al. 1988, A&A, 207, 46
Chen, X. P., Henning, Th., van Boekel, R., & Grady, C. A. 2006, A&A, 445, 331
de Winter, et al. 2001, A&A, 380, 609
Desidera, S., & Barbieri, M. 2006, A&A in press, arXiv:astro-ph/0610623
Duchême, G., et al. in Protostars and Planets V., Edited by B. Reipurth, D. Jewitt, and K. Keil. University of Arizona Press, Tucson, 2007
Duquennoy, A., & Mayor, M. 1991, A&A, 248, 485
Feigelson, E. D., Lawson, W. A., & Garmire, G. P. 2003, ApJ, 599, 1207
Forbrich, J., et al. 2007, A&A, 464, 1003
Fluks, M. A.,et al. 1994, A&As, 105, 311
Fukagawa, M., et al. 2003, ApJ, 590, L49
Ghez, A. M., Neugebauer, G., & Matthews, K. 1993, AJ, 106, 2005
Ghez, A. M., et al. 1997, ApJ, 481, 378
Grinin, V. P., et al. 1994, A&A, 292, 165
Hartigan, P., & Kenyon, S. J. 2003, ApJ, 583, 334
Hernández, et al. 2004, AJ, 127, 1682
Herbig, G. H., & Bell, K. R. 1988, Lick Observatory Bulletin, Santa Cruz: Lick Observatory.
Herbig, G. H. 2005, AJ, 130, 815
Herbst, W., & Shevchenko, V. S. 1999, AJ, 118, 1043
Hillenbrand, L. A., Strom, S. E., Vrba, F. J., & Keene, J. 1992, ApJ, 397, 613
Kley, W. 2000, IAU Symposium, 200, 211P
Kenyon, S. J., & Hartmann, L. 1995, ApJs, 101, 117
Konacki, M. 2005, Nature, 436, 230
Kouwenhoven,T. et al. 2005, A&A, 430, 137
Koresko, C. D. 2002, AJ, 124, 1082
Krautter, J. 1991, in Low-Mass Star Formation in Southern Molecular Clouds, ed. B. Reipurth (Garching: ESO), 127
Le Borgne, J.-F., et al. 2003, A&A, 402, 433
Leinert, C., et al. 1993, A&A, 278, 129
Leinert, C., Richichi, A., & Haas, M. 1997, A&A, 318, 472
Li, W., Evans, N. J., Harvey, P. M., & Colome, C. 1994, ApJ, 433, 199
Martín, E. L. 1998, AJ, 115, 351
Massey, P., Valdes F., Barnes, J. A User's Guide to Reducing Slit Spectra with IRAF, April 1992.
Mannings, V., & Sargent, A. I. 1997, ApJ, 490, 792
Moriwaki, K., & Nakagawa, Y. 2004, ApJ, 609, 1065
Nelson, R. P. 2003, MNRAS, 345, 233
Olofsson, G., Liseau, R., & Brandeker, A. 2001, ApJL, 563, L77
Palla, F., & Stahler, S. W. 1993, ApJ, 418, 414
Pascucci, I., et al. 2006, ApJ, 651, 1177
Pérez, M. R.,et al. A&A, 416, 647
Pirzkal, N., Spillar, E. J., & Dyck, H. M. 1997, ApJ, 481, 392
Prato, L., Greene, T. P., & Simon, M. 2003, ApJ, 584, 853
Quintana, E. V., & Lissauer, J. J. 2006, Icarus, 185, 1
Ratzka, T., Köhler, R., & Leinert, C. 2005, A&A, 437, 611

Reipurth, B., & Zinnecker, H. 1993, A&A, 278, 81
Richichi, A., Leinert, C., Jameson, R., & Zinnecker, H. 1994, A&A, 287, 145
Rossiter, R. A. 1955, Publ. Michigan Obs., 11, 1
Siess, L., Dufour, E., & Forestini, M. 2000, A&A, 358, 593
Simon, M., et al. 1995, ApJ, 443, 625
Skinner, S. L., Güdel, M., Audard, M., & Smith, K. 2004, ApJ, 614, 221
Stelzer, B., et al. 2006, ArXiv Astrophysics e-prints, arXiv:astro-ph/0605590
Stahler, S. W., & Palla, F. 2004. The Formation of Stars. Willey-VCH, p 600
van Boekel, R., et al. 2005, A&A, 437, 189
Weinberger, A. J., et al. 1999, ApJ, 525, L53
Wycoff, G. L., Mason, B. D., & Urban, S. E. 2006, AJ, 132, 50

Submitted to A&A as: A. Carmona, M.E van den Ancker, Th. Henning, Ya. Pavlyuchenkov, C.P. Dullemond, M. Goto, W.F-.Thi, J.Bouwman, and L.B.F.M. Waters – *"A Search for Molecular Hydrogen Emission from Protoplanetary Disks: Where is the Warm Gas?"*, Astronomy and Astrophysics, 2007.

Chapter 4

A Search for MIR Molecular Hydrogen Emission from Protoplanetary Disks

Abstract

We report on a sensitive search for mid-infrared molecular hydrogen emission from protoplanetary disks. We observed the Herbig Ae/Be stars UX Ori, HD 34282, HD 100453, HD 101412, HD 104237 and HD 142666, and the T Tauri star HD 319139 and searched for $H_2\ 0-0\ S(2)$ $(J = 4-2)$ *emission at 12.278 micron and* $H_2\ 0-0\ S(1)$ $(J = 3-1)$ *emission at 17.035 micron with VISIR, ESO-VLT's high-resolution mid-infrared spectrograph. None of the sources present evidence for molecular hydrogen emission at the wavelengths observed. Stringent* 3σ *upper limits to the integrated line fluxes and the mass of warm gas (T = 150, 300 and 1000 K) in the disks are derived. The disks contain less than a few tenths Jupiter mass of emitting gas at 150 K at most, and less than a few Earth masses of emitting gas at 300 K and higher temperatures. We compare our results to a Chiang and Goldreich (1997) two-layer disk model of masses 0.02* $M_\odot$ *and 0.11* $M_\odot$*. The upper limits to the disk's warm gas mass are smaller than the amount of warm gas in the interior layer of the disk, but they are much larger than the amount of mass expected to be in the surface layer. Two viable explanations may account for the non-detections of* H_2 *emission. First, if the two-layer approximation to the structure of the disk is correct, the non-detections are explained because the thermal* H_2 *flux levels from the surface layer are intrinsically low. Second, if the two-layer approximation is not adequate, then, the bulk of the mass of optically thin warm* H_2 *gas must be small. We discuss several scenarios for explaining the latter. We favor thermal decoupling between gas and dust or a localized gas/dust ratio significantly smaller than 100, that may be caused by the presence of a low-mass companion (such as a giant planet), as the most likely alternative explanations for the non-detection of warm gas in the sources.*

4.1 Introduction

Circumstellar disks surrounding low- and intermediate- mass stars in their pre-main sequence phase are the locations where planets presumably form. Such protoplanetary disks are composed of gas and dust. Their mass is dominated by gas (99%), specifically by molecular hydrogen (H_2), the most abundant gas species. The dust constitutes only a tiny fraction of the disk's mass. However, it is the main source of opacity. Consequently, most of what we know observationally about protoplanetary disks has been inferred from studies of dust emission and scattering (for recent reviews see Natta et al. 2007, Dullemond et al. 2007, Watson et al. 2007). To understand the structure and evolution of protoplanetary disks, it is necessary to study their gaseous content independently from the dust. For example, a basic physical quantity such as the disk's mass is conventionally deduced from dust continuum emission at millimeter wavelengths assuming a interstellar gas to dust ratio of 100 (e.g. Beckwith et al. 1990, Henning et al. 1994). If dust is

physically processed in the disk, as it should be in order to form planets, the gas to dust ratio must change as the protoplanetary disk evolves. The disk's dissipation time scale - another fundamental quantity required to disentangle between proposed giant planet formation scenarios (Pollack et al. 1996; Boss et al. 1998) - is deduced from observations in the thermal infrared continuum as well (Haisch et al. 2001, 2005). Although recent studies (e.g., Sicilia-Aguilar et al. 2006) suggest a parallel evolution of the dusty and gaseous components, it stills remain to be demonstrated that the gaseous disks disappear over the same time scale as the infrared excess.

The study of the disk's gas is based mostly on spectroscopy. A variety of disk's gas diagnostics have been observed from the UV to the millimeter (see reviews by Najita et al. 2007 and Dutrey et al. 2007). However, the only diagnostic that is able to probe the warm gas in the regions where giant planets are thought to form are the mid-infrared emission lines of H_2. Other gas diagnostics are either not sensitive to the total amount of gas (e.g. the near-IR H_2 and the NIR and (sub)-mm CO lines), or only measure the column of gas in the line of sight towards the star (all absorption line studies, e.g. H_2 lines in the UV). Such diagnostics do not probe the H_2 (bulk of the gas mass) directly, therefore being highly dependent on fractional abundances of the tracer in question and thus on the details of the disk chemistry. Finally, UV and near-infrared diagnostics only probe the innermost regions of the disk (R < 1 AU), and mm and sub-mm diagnostics are limited to probe the cold outermost regions of the disk (R >10 AU).

Molecular hydrogen is by far the most abundant molecular species in the disk. It remains optically thin up to high column densities (10^{23} cm^{-2}), it does not freeze out onto dust surfaces, it self-shields efficiently against photodissociation, and, most importantly, it permits the derivation of the warm gas mass without the recourse to uncertain conversion factors as the CO/H_2 ratio or the gas-to-dust ratio. Unfortunately, H_2 is one of the most challenging molecules to detect. Since H_2 is a homonuclear molecule, it lacks of a dipolar moment and its transitions are thus electric quadrupole in nature. The small Einstein coefficients characteristic of the quadrupole transitions imply that the emission features of H_2 are very weak, and, in the case of protoplanetary disks, the H_2 emission is to be detected on the top of a strong dust infrared continuum. In addition, practical observational challenges are to be faced. From the ground, the mid-infrared windows are strongly affected by sky and instrument background emission, and the H_2 transitions at 12 and 17 μm lie close to atmospheric absorption lines highly dependent on atmospheric conditions. The advent of high spectral resolution spectrographs mounted on larger aperture telescopes, allows for the first time the study of H_2 emission from the ground, but the search is still limited to bright targets. From space, the problems of atmosphere absorption are alleviated and the $J = 2 - 0$ feature at 28 μm is visible. But, the beam sizes are large and the spectral resolution of space mid-infrared spectrographs is notably low when compared to ground-based facilities.

Here we report on a sensitive search for molecular hydrogen emission from protoplanetary disks. We observed six southern nearby (d<400 pc) Herbig Ae/Be stars and one T Tauri star, employing VISIR[1], ESO's Very Large Telescope mid-infrared high-resolution spectrograph, and searched for H_2 $0-0\,S(1)$ ($J = 3 - 1$) emission at 17.035 μm and H_2 $0-0\,S(2)$ ($J = 4 - 2$) emission at 12.278 μm. Our objective is to derive the first unbiased measurements of the warm gas mass in the circumstellar disks of these stars. The chapter is organized as follows: in Section 4.2 we will present the sample studied, and the details of how the observations were performed. In Section 4.3 we will discuss the data reduction. In Section 4.4 we will deduce upper limits to

[1] http://www.eso.org/instruments/visir

Table 4.1: *Summary of the stellar physical properties and previous gas and dust observations. References: Acke et al. 2004 [A04], de Zeeuw et al. 1999 [D99], Hipparcos catalogue [HIP], van den Ancker et al. 1998 [V98], Piétu et al. 2003 [P03], Dent et al. 2005 [D05], Stempels & Gahm 2004 [S04]*

Star	Sp.T.	$\log(T_{eff})$ [log(K)]	$\log(L/L_{\odot})$ [log($L_{\odot}$)]	Ref	d [pc]	Ref	Age [Myr]	CO sub-mm	M_{DISK} [a] [M_J]	Group I/II [b]
UX Ori	A4IVe	3.92	1.68	A04	340	D99	5	D05	16	II
HD 34282	A3Vne	3.94	1.27	A04	400	P03	7	D05	100	I
HD 100453	A9Ve	3.87	0.90	A04	112	HIP	> 10	...	21	I
HD 101412	B9.5Ve	4.02	1.40	A04	160	D99	> 8	...	...	II
HD 104237	A4IVe+sh	3.92	1.54	A04	116	V98	2	...	7.8	II
HD 142666	A8Ve	3.88	1.13	A04	145	D99	6	D05	16	II
HD 319139 [c]	K5Ve+K7Ve	3.64+3.61	0.44	S04	145	D99	2 [d]	...	47 [e]	CTTS

[a,b] from Acke et al. (2004) and references therein. Group I: flared disks. Group II self-shadowed disks. CTTS: Classical T Tauri star.
[c] Spectroscopic binary of period 2.4 days [S04].
[d] We assume that both components have the same luminosity.
[e] Disk mass by Jensen et al. (1996) scaled to our adopted distance of 145 pc.

the H_2 fluxes, and using the optically thin approximation, we will derive upper limits to the mass of warm (150 - 1000 K) gas in the disks. In Section 4.5 we discuss our results in the context of the Chiang and Goldreich (1997) two-layer disk model. Finally, we summarize our results and conclusions in Section 4.6.

4.2 Observations

Target Selection. We selected a sample of well known nearby Herbig Ae/Be and T Tauri stars based on evidence of large disk reservoirs. The targets have either reported detections of cold CO gas at (sub)-mm wavelengths, or dust continuum emission at mm wavelengths. We choose stars with 12 μm continuum fluxes > 0.5 Jy (otherwise too faint for acquisition with VISIR) and < 25 Jy (hard to detect weak lines on top of a strong continuum).

The physical properties of the targets are compiled in Table 4.1. The second, third and fourth column summarize the spectral type, the effective temperature, and the luminosity from the literature. The distance of the observed stars appears in column six and its reference in column seventh. Ages derived from the H-R diagram employing the pre-main-sequence evolutionary tracks of Palla and Stahler (1993) are shown in the eighth column. Previous reports of CO emission at (sub)-millimeter wavelengths towards the targets are presented in column number nine. Reported disk masses derived from dust continuum emission at millimeter wavelengths are shown in column number ten. Finally, the group of each Herbig Ae/Be star disk, according to the classification scheme of Meeus et al. (2001), appears in column number eleven. Group I sources -flared disks- are sources with a rising mid-IR Spectral Energy Distribution (SED) and Group II sources -self-shadowed disks- are sources with a flat SED (Dullemond et al. 2002).

Observations. The sources were observed in the first semester of 2006 and 2007 with the VLT Imager and Spectrometer for the Mid-Infrared (VISIR), a combined imager and spectrograph designed for observations in the N ($\approx 8-13\,\mu$m) and Q bands ($\approx 6.5-24.5\,\mu$m) (Lagage et al. 2004) mounted at the ESO-VLT Melipal telescope in Cerro Paranal, Chile. The $H_2\ 0-0\ S(1)$ ($J = 3-1$) line at 17.035 μm was observed in the high-resolution long-slit mode with a 0.4 arcsec slit, giving a spectral resolution R $\approx$ 21000, or 14 km s^{-1}.

The $H_2\ 0-0\ S(2)$ ($J = 4-2$) line at 12.278 μm was observed in the high-resolution echelle

Table 4.2: *Summary of the observations.*

Star	λ [μm]	Date	U.T. [hh:mm]	$t_{\rm exp}$ [s]	Airmass [a]	$V_\oplus$ [b] [km s^{-1}]	Calibrator [c]		t_{exp} [s]	Airmass	
UX Ori	12.278	11 January 2006	02:28	3600	1.0 - 1.2	−15.94	HD 36167	(P)(F)	1000	1.1(P)	1.2(F)
	17.035	4 January 2007	01:54	3600	1.0 - 1.0	−13.50	HD 25025	(P)	600	1.0 (P)	...
HD 34282	12.278	10 January 2006	04:01	3600	1.0 - 1.5	−13.83	HD 36167	(P)(F)	1000	1.1(P)	1.7(F)
HD 100453	12.278	22 March 2006	07:27	3600	1.2 - 1.5	7.45	HD 89388	(P)(F)	600	1.5 (P)	2.0 (F)
	17.035	27 March 2006	06:26	3600	1.3 - 1.7	5.96	HD 89388	(P)	1000	1.5 (P)	...
HD 101412	12.278	30 March 2006	04:40	3600	1.2 - 1.4	6.82	HD 91056	(P)(F)	600	1.3 (P)	1.7 (F)
	17.035	30 March 2006	01:27	3600	1.3 - 1.2	7.02	HD 91056	(F)	1000	...	1.3 (F)
HD 104237	12.278	10 February 2006	05:43	3600	1.7 - 1.7	13.09	HD 92305	(P)(F)	600	1.7 (P)	1.8 (F)
	17.035	12 February 2006	06:36	3600	1.6 - 1.7	13.15	HD 92305	(F)	1000	...	1.8 (F)
HD 142666	17.035	28 February 2006	06:28	3600	1.1 - 1.0	24.06	HD 169916	(P)	1000	1.1 (P)	...
HD 319139	17.035	30 March 2006	08:30	3600	1.1 - 1.0	29.47	HD 169916	(P)	1000	1.2 (P)	...

[a] The airmass interval is given from the beginning to the end of the observations.
[b] $V_\oplus$ is the expected velocity shift of the spectra due to the reflex motion of the Earth around the Sun.
[c] The standard stars were observed previously (P) and/or immediately following (F) the science observations.

mode with a 0.4 arcsec slit, giving a spectral resolution R ≈ 20000, or 15 km s^{-1}. The total integration time in each line was 1h. The slit was oriented in the North-South direction. Sky background was subtracted by chopping the telescope by ∼8" in the direction of the slit. Asymmetrical thermal background of the telescope was subtracted by nodding the telescope by ∼8" in the direction of the slit as well. For correcting the spectra for telluric absorption and obtaining the absolute flux calibration, spectroscopic standard stars at close airmasses to that of the science targets were observed immediately preceding and following the 12 μm exposure, and preceding or following 17 μm exposure. Finally, we tried as much as possible to observe the stars at a moment of high velocity shift between the telluric absorption feature at 12.27 microns and the H_2 S(2) line. This effect is due to the reflex motion of the Earth around the Sun. A summary of the observations is presented in Table 4.2.

4.3 Data Reduction

VISIR raw data consists of a collection of data cubes, in which each data cube is associated to data taken in one nod position[2]. The odd planes in the data cube correspond to a half-chop cycle frame, the even planes correspond to the average of the difference of all preceding half-chop cycles (i.e. A_i=A_1-B_1+ A_2-B_2+...+A_i-B_i/i). The last plane corresponds to the average of all half-cycle difference images.

The first step in the data reduction process was to recover the individual half chop cycles frames from the data cube, and to guarantee that all of them have the same wavelength in the same row of pixels (in each 2D spectrum, the spatial direction is along the columns and the dispersion direction is along the rows). We proceeded as follows. In each 2D half-chop cycle frame, at the position of the target's spectrum, a cut with a size of 20 pixels in the spatial direction was made. From this cut, a spectrum of the atmospheric emission was obtained by the sum of the counts in the spatial direction. This atmospheric emission spectrum was rebinned by a factor of 50. Using as reference the atmospheric emission spectrum from the first half-chop cycle of the first nod, the offset that each half-chop cycle raw frame required for having the center of the sky emission

[2]The sequence of the observations is ABBA, where A and B correspond to two different nod positions.

lines at the same pixel position as the reference frame was determined. The offset was given by the difference between the center of the gaussian fitted to one sky emission line in the reference spectra, and the center of the gaussian fitted to the same sky line in the atmospheric emission spectrum of the half-chop cycle frame to be corrected. The typical offsets were a fraction of a pixel, and did not depend on the sky line used for reference. Then, each 2D raw half-chop cycle frame was rebinned by a factor 50 in the dispersion direction, and it was shifted -in the dispersion direction - by the offset found. Finally, the obtained 2D frame was rebinned to the original size of 256x256 pixels. This procedure corrected small differences in 2D half-chop cycles introduced by variations in the grating position within the instrument.

Thereafter, with the corrected half-chop frames, the VISIR data cubes were re-built and processed with the VISIR pipeline (Lundin 2006). Bad pixels were detected in the half-cycle frames when their number of counts exceeded the limit of 65000. They were cleaned by interpolation with neighboring pixels. In the long-slit mode (i.e., 17 μm data), the 2D frames were corrected for distortion, by interpolating the analytical optical distortion (see description in the VISIR user's manual, Siebenmorgen et al. 2006) and the value from the source pixels. The 2D frames in each nod position were created by averaging all the half-cycle difference images in the data cube. The nodding images were produced by averaging the image in the two nod positions A and (-B), and dividing the result by 2×DIT, where DIT is the Detector Integration Time [3]. The nodded images are jittered and were thus shifted and added to form the final combined image using the offsets stored in the FITS header.

The wavelength calibration was performed with the following procedure. The first half-cycle from the first nod position was "collapsed", producing a 1-dimensional spectrum of the atmosphere. The center (in pixels) of the atmospheric emission lines was determined by fitting gaussians to their profiles. The centers of the atmospheric emission lines were found by fitting gaussians to their profiles in a HITRAN model spectrum of Paranal's atmosphere emission (for details of the model, see Lundin 2006). The dispersion relation was found by a second degree polynomial fit between the centers of the atmospheric lines in the observed and model spectrum.

The spectrum at each wavelength was extracted from the 2D combined image by summing the pixels in the spatial direction inside the PSF. In the case of the long-slit 17 μm data, one spectrum was extracted for each of the nod positions present in the final 2D combined image. The final extracted spectrum is the sum of these three spectra. The telluric correction was performed by dividing the extracted spectra by the extracted spectra of the standard star. Small shifts (of a fraction of a pixel) on the spectra of the standard star in the wavelength direction were applied until the best signal to noise spectra (i.e. best telluric correction) was found. The spectral flux calibration was made multiplying the telluric-corrected science spectrum by a model spectrum (Cohen et al. 1999) of the standard star [4].

4.4 Results

In Figures 4.1 and 4.2 we present a summary of the obtained spectra. In the left panel, the atmosphere-corrected flux calibrated spectra in wavelength scale of km s^{-1} are shown. In the right panel, for reference, the normalized spectra of the science target and the standard star are

[3] The factor 2 is due to the fact that the on-source and the off-source images both contribute to the whole DIT.

[4] The catalogue of spectroscopic standard stars in the MIR is available at www.eso.org/VISIR/catalogue.

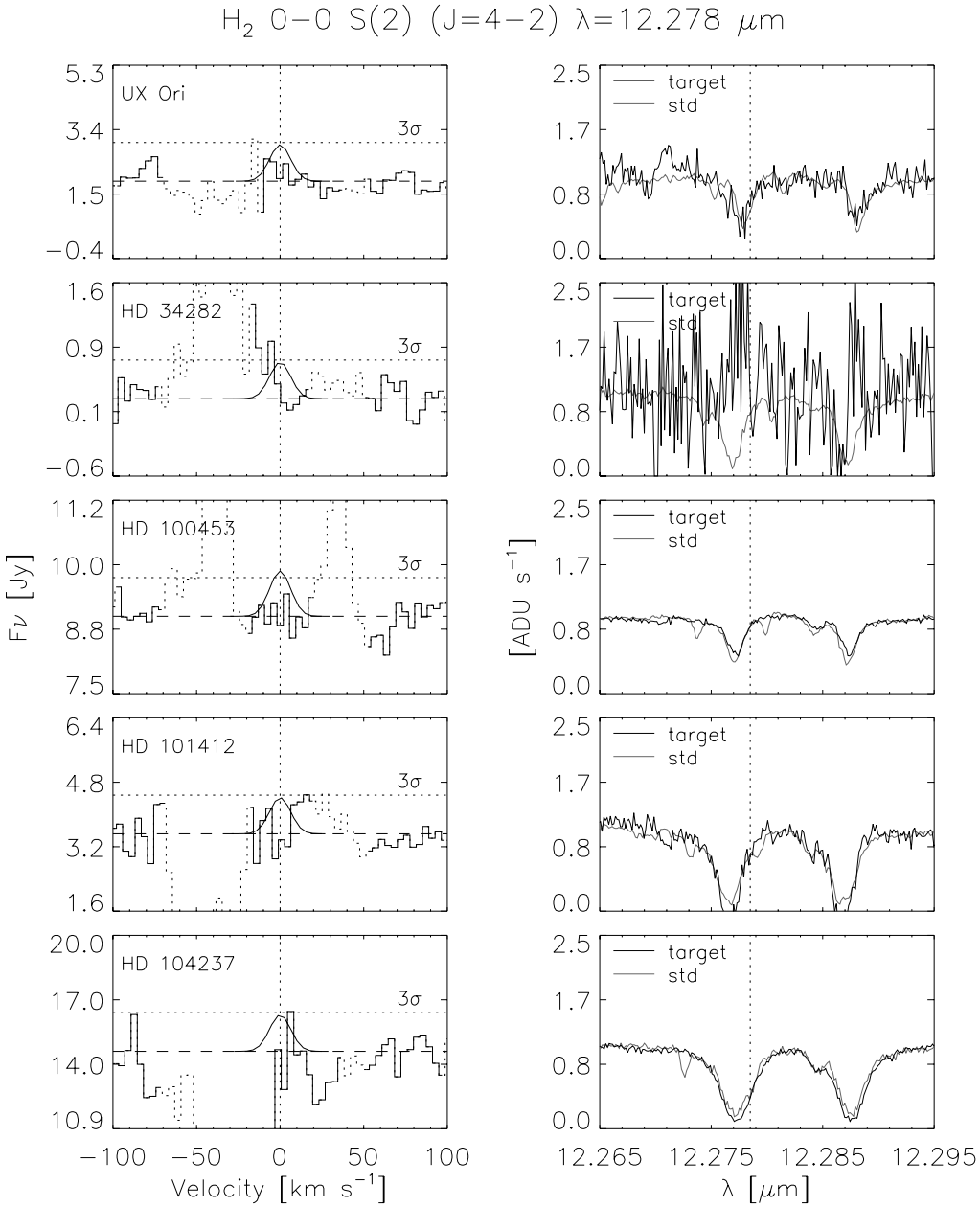

Figure 4.1: *Spectra obtained for the H_2 0–0 S(2) (J=4–2) line at 12.275 μm. The left panel shows a zoom to the -100 to 100 km/s interval of the atmospheric corrected spectra. The right panel shows the continuum normalized spectra of the standard star and the target before telluric correction. In the left planel, a Gaussian of FWHM = 15 km s^{-1} and integrated line flux equal to the line-flux upper limits obtained is overplotted. Dotted lines show spectral regions strongly affected by telluric or standard star absorption features. The spectra are not corrected for the radial velocity of the targets.*

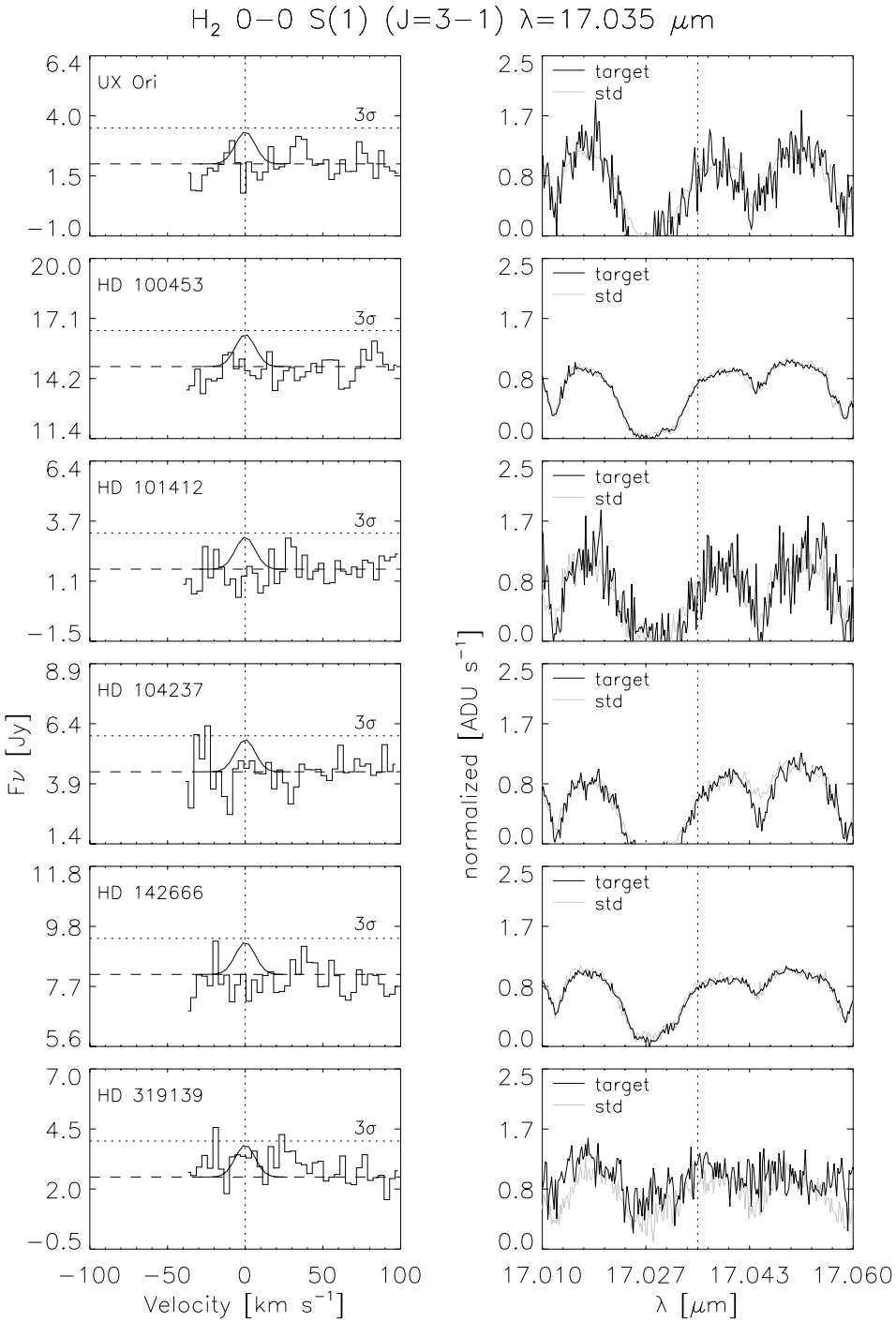

Figure 4.2: *Spectra obtained for the H_2 0–0 S(1) (J=3–1) line at 17.035 μm. The left panel shows a zoom in the -100 to 100 km/s interval of the atmospheric corrected spectra. The right panel shows the continuum normalized spectra of the standard star and the target before telluric correction. In the left planel, a Gaussian of FWHM = 15 km s^{-1} and integrated line flux equal to the line-flux upper limits obtained is overplotted. The spectra are not corrected for the radial velocity of the targets.*

Table 4.3: *Upper line flux limits derived*

	0–0 S(2) (J=4–2) 12.278 μm		0–0 S(1) (J=3–1) 17.035 μm	
	Continuum	Line Flux	Continuum	Line Flux
	F_ν	[$\times 10^{-14}$ ergs s^{-1} cm^{-2}]	F_ν	[$\times 10^{-14}$ ergs s^{-1} cm^{-2}]
Star	[Jy]	LW = 15 km s^{-1}	[Jy]	LW = 15 km s^{-1}
UX Ori	1.9 (1.1)	<1.4	2.0 (1.5)	<1.3
HD 34282	0.3 (0.4)	<0.5	...	...
HD 100453	9.0 (0.7)	<0.9	14.8 (1.7)	<1.5
HD 101412	3.5 (1.0)	<1.2	1.6 (1.6)	<1.4
HD 104237	14.6 (1.8)	<2.2	4.4 (1.5)	<1.3
HD 142666	...	...	8.0 (1.2)	<1.1
HD 319139	...	...	2.5 (1.5)	<1.3

displayed. None of the observed sources show evidence for H_2 emission at 12 or 17 μm.

Line flux upper limits. In the flux-calibrated science spectra, the standard deviation (σ) of the continuum flux was calculated in regions less influenced by telluric absorption, and close to the features of interest. In Figures 4.1 and 4.2, the horizontal dotted line shows the 3σ limits of the continuum flux derived. 3σ upper limits to the integrated line flux were calculated multiplying the 3σ flux times the instrument resolution line width[5] of 15 km s^{-1}. In Table 4.3, a summary of the upper flux limits is presented. In Figures 4.1 and 4.2 a Gaussian line of FWHM = 15 km s^{-1} and an integrated flux equal to the upper flux limit is overplotted on each observed spectrum.

Upper limits to the warm gas disk mass. Under the assumption that the H_2 emission is optically thin, that the emitting H_2 is in local thermodynamical equilibrium, and that the source size is equal to VISIR's beam size, we derived upper limits to the H_2 mass as a function of the temperature employing (Thi et al. 2001)

$$M_{\rm gas} = f \times 1.76 \times 10^{-20} \frac{F_{ul}\, d^2}{(hc/4\pi\lambda)\, A_{ul}\, x_u(T)} \;\; M_\odot, \tag{4.1}$$

here F_{ul} is the upper limit to the integrated line flux, d is the distance in pc to the star, λ is the wavelength of the transition, A_{ul} is the Einstein coefficient of the $J = u - l$ transition[6] and x_u is the population of the level u at the excitation temperature T in LTE; f is the conversion factor required for deriving the total gas mass from the H_2-ortho or H_2-para mass determined. Since $M_{\rm H_2} = M_{\rm H_2\,ortho} + M_{\rm H_2\,para}$, f=1+ortho/para for the S(2) line (a H_2-para transition) and f=1+1/(ortho/para) for the S(1) line (a H_2-ortho transition). The equilibrium ortho-para ratio at the temperature T was computed using (Takahashi et al. 2001)

$$ortho/para = \frac{3\sum_{odd}(2J+1)e^{-BJ(J+1)/T}}{\sum_{even}(2J+1)e^{-BJ(J+1)/T}} \;\; , \tag{4.2}$$

[5]The true line width is expected to be of a few km s^{-1}, narrower than the instrumental line width of 15 km s^{-1}.

[6]4.76×10^{-10} s^{-1} for the S(1) line $J = 3-1$ transition, 2.76×10^{-9} s^{-1} for the S(2) line $J = 4-2$ transition (Wolniewicz, Simbotin, & Dalgarno 1998).

Table 4.4: *Upper warm H_2 mass limits*

	Upper mass limits in $M_J \sim 10^{-3} M_\odot$					
	12 μm			17 μm		
Star	150 K	300 K	1000 K	150 K	300 K	1000 K
UX Ori	27.9	1.9×10^{-1}	1.2×10^{-2}	1.0	6.8×10^{-2}	2.0×10^{-2}
HD 34282	13.8	9.7×10^{-2}	6.0×10^{-3}	...	...	...
HD 100453	1.9	1.4×10^{-2}	0.9×10^{-3}	0.1	0.9×10^{-2}	2.5×10^{-3}
HD 101412	5.3	3.7×10^{-2}	2.3×10^{-3}	0.2	1.6×10^{-2}	4.8×10^{-3}
HD 104237	5.0	3.6×10^{-2}	2.2×10^{-3}	0.1	0.8×10^{-2}	2.3×10^{-3}
HD 142666	...	...	...	0.2	1.0×10^{-2}	3.1×10^{-3}
HD 319139	...	...	...	0.2	1.2×10^{-2}	3.7×10^{-3}

Table 4.5: *Physical parameters of prototypical Herbig Ae/Be stars and their disks after Chiang et al. (2001).*

Parameter	MWC 480 high-mass	HD 36112 low-mass
T_* [K]	8890	8465
R_* [$R_\odot$]	2.1	2.1
M_* [$M_\odot$]	2.3	2.2
L_* [$L_\odot$]	24.6	20.2
d [pc]	140	150
Σ_0 [g cm^{-2}]	8000	1000
a_0 [AU]	100	250
H/h	1.7	1.5
p	1.5	1.5
$M_{\rm DISK}$ [$M_\odot$]	0.11	0.02

employing B=87.6 K. In Table 4.4, we present our results.

The H_2 S(1) and S(2) line fluxes constrain the amount of emitting hot and warm H_2 gas. The disks contain less than a few tenths Jupiter mass of emitting gas at 150 K, and less than a few Earth masses of emitting gas at 300 K and higher temperatures. In Bitner we present the mass of gas as a function of the temperature derived from a S(1) and a S(2) line with a flux 10^{-14} erg s^{-1} cm^{-2} for a source at a distance of 140 pc.

We see that the S(1) line sets constraints for the mass of gas at temperatures 150 K $< T <$ 500 K. For higher temperatures the S(2) is a better tracer[7].

[7]For temperatures below 150 K the S(0) ($J = 2 - 0$) line at 28 μm provides better constraints to the gas mass than the S(1) line. However, as the Earth's atmosphere is completely opaque at these wavelengths, the S(0) line is only observable from space.

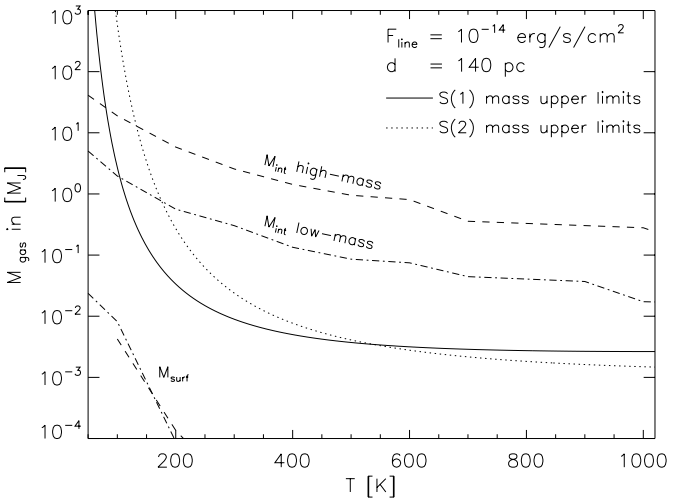

Figure 4.3: *Disk's gas mass limits derived from H_2 S(1) (solid line) and H_2 S(2) (dotted line) as a function of the temperature for a line flux upper limit of 10^{-14} ergs s^{-1} cm^{-2} for a source at a distance of 140 pc. Dashed and dot-dashed lines show the gas mass as function of the temperature for a Chiang and Goldreich (1997) optically thick two-layer model for a low-mass (0.02 $M_\odot$) and a high-mass (0.11 $M_\odot$) disk. $M_{\rm int}$ is the mass of the interior layer. $M_{\rm surf}$ is the mass of the surface layer.*

4.5 Discussion

4.5.1 Comparison with the gas mass of a 2-layer disk model

To understand the mass upper limits derived, we suppose that the disk has a two-layer structure (Chiang & Goldreich, 1997). In this disk model, the infrared excess in the SED is produced by the radiation of small dust grains in the superheated optically thin surface layer of the disk. In the interior layer, the gas is thermalized by the high extinction of the coexisting dust, the column densities of H_2 are larger than 10^{23} cm^{-2} and the optical depth is higher than one (see Figure 4.5). The interior layer is optically thick in both gas and dust even at mid-infrared wavelengths. Emission lines from an optically thick medium are only observable when there are temperature gradients. The hot uppermost layer can provide emission lines against the cold mid-plane.

Using a two-layer disk model implementation (CGplus, Dullemond et al. 2001) with physical parameters aimed to fit the SED of the prototypical Herbig Ae/Be stars (see Table 4.5 and Figure 4.4), we computed the expected amount of gas in the interior and surface layer as function of the temperature for disks of mass 0.11 $M_\odot$ (MWC 480) and 0.02 $M_\odot$ (HD 36112)[8]. In Figure 4.3 we present our results. The mass limits derived from the H_2 S(1) and S(2) line observations are smaller than the amount of warm gas in the interior layer, but much larger than the amount of gas in the surface layer. Figure 4.3 shows that the amount of gas in the upper layer is very small ($< 10^{-2}$ $M_J \sim 3M_\oplus$) and almost independent of the total mass of the disk.

[8]In our models no puffed-up inner rim was used. We employed a model with a truncation radius at T = 5000 K. We assumed that $T_{gas} = T_{dust}$ and a gas to dust ratio of 100. For disk-models with $T_{gas} \neq T_{dust}$ see for example, Kamp and Dullemond (2004), Nomura and Millar (2005) and Jonkheid et al. (2006).

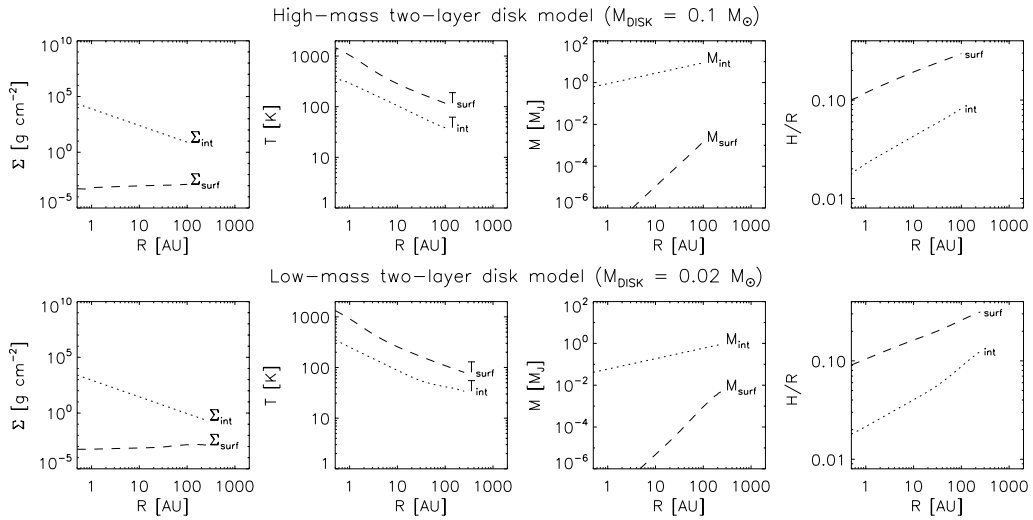

Figure 4.4: *Physical parameters of the two-layer disk model as a function of radius (R). Upper panels: high-mass disk model. Lower panels: low-mass disk model. The indices int and surf refer to the interior and the surface layer.* Σ *is the surface density, T the temperature, M the disk mass and H/R the scale height.*

4.5.2 Derivation of expected S(1) and S(2) H_2 emission from the two-layer disk model.

Our observations are one of the most sensitive efforts to date of H_2 emission from gas-rich protoplanetary disks (see Table 4.6)[9]. If the H_2 emission is only produced from the upper layer of the disk, as the two layer model suggests, we would like to find out which flux levels we could expect.

In the two-layer disk model, at each disk radius the H_2 emission from the surface layer has to be observed on the top of the optically thick continuum of the interior layer, and the optically thin continuum of the dust at the surface layer. The total intensity (line plus continuum) emitted at each radius (R) is given by

$$I_\nu(R) = B_\nu(T_{\rm int})e^{-\tau_{\nu_{\rm surf}}} + B_\nu(T_{\rm surf})(1 - e^{-\tau_{\nu_{\rm surf}}}). \quad (4.3)$$

Here $B_\nu(T_{\rm int})e^{-\tau_{\nu_{\rm surf}}}$ is contribution of the interior layer to the intensity. It is the black body emission $B_\nu(T_{\rm int})$ of the interior layer at temperature $T_{\rm int}$ seen through the surface layer optical depth ($\tau_{\nu_{\rm surf}} = \tau_{\nu_{\rm dust\,surf}} + \tau_{\nu_{\rm gas\,surf}}$) . The contribution of the surface layer is $B_\nu(T_{\rm surf})(1 - e^{-\tau_{\nu_{\rm surf}}})$. It is the optically thin emission of the gas and dust in the surface layer at temperature $T_{\rm surf}$.

The dust optical depth in the surface layer is given by

$$\tau_{\nu_{\rm dust\,surf}} = \kappa_{\nu_{\rm dust}} \Sigma_{\rm dust_{surf}}, \quad (4.4)$$

where $\kappa_{\nu_{\rm dust}}$ is the dust opacity per unit of mass[10] at the frequency ν, and $\Sigma_{\rm dust_{surf}}$ is the dust surface density in the surface layer of the disk.

[9] Spitzer observations of H_2 emission towards debris disks by Pascucci et al. (2006) are one order of magnitude more sensitive than our VISIR observations . However, the spectral resolution of Spitzer ($R \sim 700$) does not allow to reach similar sensitivities for young gas-rich disks because of the strong dust continuum emission at the H_2 emission wavelengths.

[10] We used the opacities by Laor & Draine (1993).

Table 4.6: *Observational efforts to detect H_2 emission from gas-rich protoplanetary disks. References: Bitner et al. 2007 [B07], Carmona et al. 2007 (this work) [C07], Sako et al. 2005 [S05], Sheret et al. 2003 [SR03], Richter et al. 2002 [R02], Thi et al. 2001 [T01].*

Instrument	$\lambda/\Delta\lambda$ at 17μm	LW [km s^{-1}]	beam [arcsec × arcsec]	flux & flux limits [$\times 10^{-14}$ erg s^{-1} cm^{-2}]	ref
VISIR	21000	14	0.4×0.4	<0.4	C07
COMICS	5000	60	0.6×0.4	<1.0 [a]	S05
TEXES	60000	5	2×2	<1.4 [b]	R02
	100000	3	0.4×0.4	1.1 [c]	B07
MICHELLE	15200	40	1×1	<6.7 [d]	SR03
ISO-SWS	2000	210	14×27	<0.8 – 40 [a,b,d]	T01

[a]The detection of H_2 S(1) in HD 163296, MWC863, CQ Tau and LkCa15 by Thi et al. 2001 was not confirmed by Sako et al. 2005.

[b]The detection of H_2 S(1) in CQ Tau and AB Aur by Thi et al. 2001 was not confirmed by Richter et al. 2002.

[c]Bitner et al. 2007 reported the detection of the H_2 S(1), S(2) and S(4) lines in AB Aur.

[d]The detection of H_2 S(1) in HD 163296, AB Aur and GG Tau by Thi et al. 2001 was not confirmed by Sheret et al. 2003.

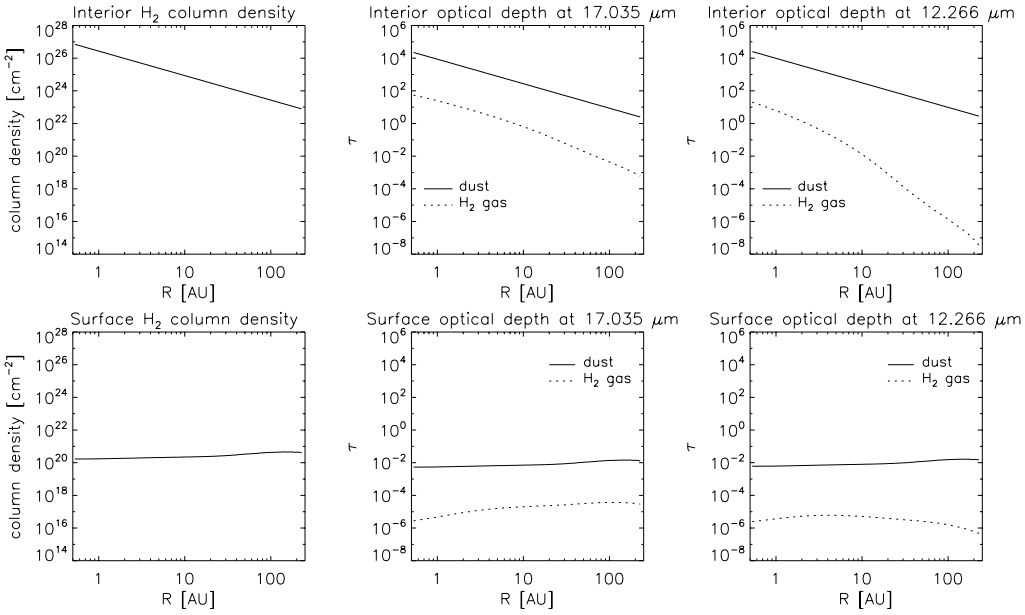

Figure 4.5: *Column density of H_2 and optical depth of H_2 and dust as a function of radius R for the interior (upper panels) and the surface layer (lower panels) in the two-layer low-mass disk model ($M = 0.02 M_\odot$). A factor ten higher values in the H_2 column density and optical depth of the interior layer are reached in the high-mass ($M = 0.11 M_\odot$) model.*

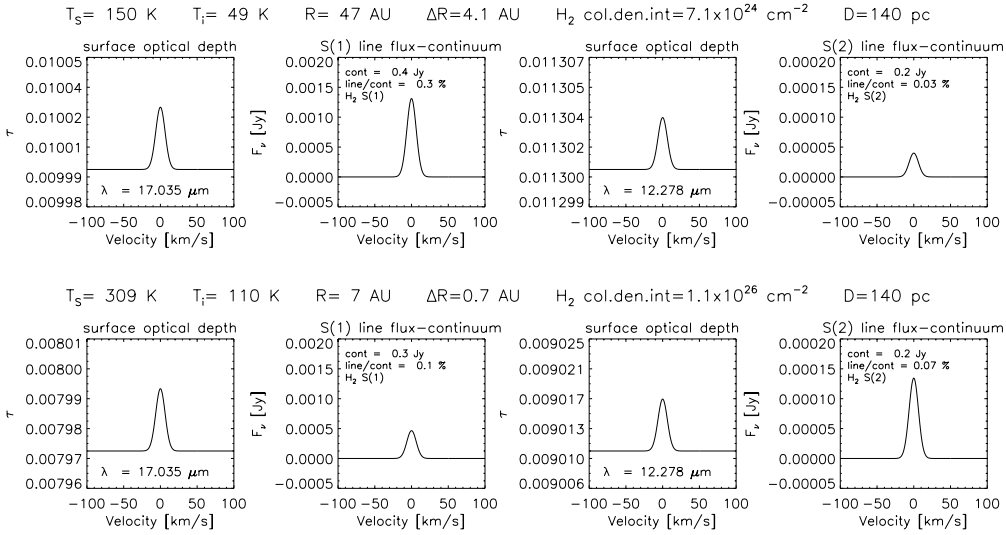

Figure 4.6: *Surface optical depth and predicted H_2 S(1) and S(2) emission line flux for the regions where the surface temperature (T_s) ~ 150K (upper panel) and ~ 300K (lower panel) in the two-layer high-mass disk model. T_i is the interior temperature. An instrumental line FWHM of 15 km s^{-1} was assumed.*

The H_2 gas optical depth in the surface layer at the frequencies ν in the vicinity of the H_2 line at frequency ν_0 is

$$\tau_{\nu_{\rm gas\,surf}} = \kappa_{\nu_{\rm line}} \Sigma_{\rm gas_{surf}} f_2, \tag{4.5}$$

with $\Sigma_{\rm gas_{surf}}$ being the gas surface density in the disk surface layer[11], and f_2 the conversion factor from the total gas surface density $\Sigma_{\rm gas_{surf}}$ to the H_2-ortho or H_2-para surface densities. Since $M_{\rm gas} = M_{\rm ortho} + M_{\rm para}$, then f_2=1/(1+ortho/para) for the S(2) line (a H_2-para transition) and f_2=1/(1+1/(ortho/para)) for the S(1) line (a H_2-ortho transition). The gas opacity per unit of mass ($\kappa_{\nu_{\rm line}}$) in the vicinity of the H_2 transition at frequency ν_0 is given by

$$\kappa_{\nu_{\rm line}} = \frac{1}{2m_{\rm p}} \frac{h\nu_0}{4\pi} (x_l B_{lu} - x_u B_{ul}) \phi_\nu. \tag{4.6}$$

Here x_l and x_u are the lower and upper level population of the transition $J = u - l$, B_{lu} and B_{ul} are the probabilities of absorption and emission given by

$$B_{ul} = \frac{c^2}{2h\nu_0^3} A_{ul}, \tag{4.7}$$

$$B_{lu} = \frac{g_u}{g_l} B_{ul}, \tag{4.8}$$

with A_{ul} being the Einstein coefficient of the $J = u-l$ transition and g_u and g_l the statistical weights ($2J + 1$ for para-H_2 and $6J + 3$ for ortho-H_2). We assumed that the gas is in LTE and derived the level populations using the Boltzmann equation. The line profile ϕ_ν is assumed Gaussian with a

[11] Here we assume that all the gas is H_2.

FWHM[12] equal to 15 km s^{-1}:

$$\phi_\nu = \frac{1}{\sigma_\nu \sqrt{\pi}} e^{\left(\frac{\nu-\nu_0}{\sigma_\nu}\right)^2}, \tag{4.9}$$

where $\sigma_\nu = (\nu_0/c) * \mathrm{FWHM}/\left(2\sqrt{\ln 2}\right)$. The expected flux $dF_\nu(R)$ (in Janskys) at each radius (R) in the disk is given by

$$\mathrm{d}F_\nu(R) = I_\nu(R)\mathrm{d}\Omega \times 10^{23} = I_\nu(R)\frac{2\pi R \mathrm{d}R}{d^2} \times 10^{23}, \tag{4.10}$$

with dΩ being the solid angle, and dR the width of the region at a distance R from the central object where the surface temperature is equal to T_{surf} and the interior temperature is equal to T_{int}. The distance to the source is d.

Figure 4.6 shows two examples of the surface optical depth ($\tau_{\nu_{\mathrm{surf}}}$) and the continuum subtracted S(1) and S(2) H_2 predicted line fluxes for the regions with surface temperature ~150 K (R ~47 AU upper panel) and ~300 K (R ~7 AU lower panel). We assumed for the calculation, a face-on high-mass disk model at a distance of 140 pc. The column density of H_2 in the interior layer of the disk is larger than 10^{23} cm^{-2}. The total optical depth peaks at the H_2 S(1) and S(2) rest wavelengths.

We see that the strength of surface optical depth at the line peak is less than 1% stronger than the surface optical depth in the continuum. Consequently, the peak line flux emitted by the region is much weaker that the continuum flux. In the region of T_s ~150 K, the H_2 S(1) peak line flux is 0.3% stronger than the continuum. In the case of the H_2 S(2) line, the peak line flux is only 0.03% stronger than the continuum. In the region at T_s ~300 K, the H_2 S(1) peak line flux decreased to be 0.1% stronger than the continuum and the H_2 S(2) peak line flux increased to be 0.7% stronger than the continuum.

The contribution to the total flux in each line varies as a function of the distance to the central source. Since at each radius, the surface layer's optical depth of dust and H_2 gas is much smaller than one (see Figure 4.5) Equation 4.3 can be approximated by [13]

$$I_\nu(R) = B_\nu(T_{\mathrm{int}})e^{-\tau_{\nu_{\mathrm{surf}}}} + B_\nu(T_{\mathrm{surf}})\tau_{\nu_{\mathrm{surf\,dust}}} + B_\nu(T_{\mathrm{surf}})\tau_{\nu_{\mathrm{gas\,surf}}}. \tag{4.11}$$

In this way, the contributions to I_ν by the interior layer $B_\nu(T_{\mathrm{int}})e^{-\tau_{\nu_{\mathrm{surf}}}}$, by the dust in the surface $B_\nu(T_{\mathrm{surf}})\,\tau_{\nu_{\mathrm{dust\,surf}}}$ and by the H_2 line $B_\nu(T_{\mathrm{surf}})\,\tau_{\nu_{\mathrm{gas\,surf}}}$ at the surface can be separated at each radius. Combining Equation 4.11 with Equation 4.10, we can disentangle the different contributions to the flux dF_ν as a function of the radius. In the left panels of Figure 4.7, we show the contributions, in percentage of the peak flux, by the interior layer (solid line), the dust in the surface (dashed lines) and the H_2 emission (dotted lines) as a function of the radius. Up to a few AU, the main source of continuum emission is the dust in the interior layer, at larger radii, the principal source of continuum emission is the superheated dust in the surface layer. The H_2 line contribution is always very small, typically less than 1% of the total continuum flux.

In the central panels of Figure 4.7, we show the evolution of line peak flux minus the continuum as a function of radius. In the case of the S(1) line the maximum contribution to the total flux is given by the region around 50-100 AU. In the case of the S(2) line the most important contribution to the line flux is made by material around 5-20 AU.

[12] We checked that the optical depth is smaller than one with a ϕ with thermal width $\sigma_{th} = \sqrt{kT_s/(2m_p)}$, therefore, ϕ could be assumed from the start with a width equal to the instrument resolution.

[13] Here we used the expansion $e^x \approx 1 + x$, valid if $x << 1$

The total expected flux from the disk is the sum of the contributions of each radius:

$$F_\nu = \int_{R_{in}}^{R_{out}} dF_\nu = \frac{2\pi}{d^2} \int_{R_{in}}^{R_{out}} I_\nu(R) R \, \mathrm{d}R \tag{4.12}$$

In the right panels of Figure 4.7, we present the total expected line from the disk. The line strength over the continuum is less than 0.05 Jy for the S(1) line and less than 0.005 Jy for the S(2) line. The total integrated flux of the line is of the order of 10^{-16} erg s^{-1} cm^{-2} for the S(1) line, and of the order of 10^{-17} erg s^{-1} cm^{-2} for the S(2) line. These line flux levels are below the sensitivity limits of our observations. *If the two-layer model is an adequate representation of the structure of the disk, the thermal flux levels of the H_2 emissions are intrinsically weak.*

We note that our H_2 line flux predictions from the two-layer model take only into account thermal excitation of the gas, therefore, show the minimum amount of expected flux. If additional excitation mechanisms, such as X-rays or UV heating, are taken into account, the line fluxes are expected to be higher. In radiative transfer models of the disk around the T Tauri star TW Hya by Nomura et al. (2005, 2007), the predicted H_2 S(1) and S(2) line fluxes are of a few 10^{-15} erg s^{-1} cm^{-2} and the line-to continuum flux ratios 10^{-5}. For a star at 140 pc these line fluxes translate to a few 10^{-16} erg s^{-1} cm^{-2}, consistent with our two-layer model. These theoretical H_2 line fluxes are still two orders of magnitude below the detection limits of our observations. In addition, the achievement of line-to continuum flux ratios $< 10^{-3}$ are a challenging task for present ground-based observations. In our observations, for example, the best line-to continuum ratio achieved is 10^{-1}.

Higher spectral resolution will improve the line contrast and make detecting the H_2 lines achievable. For example, recent work by Bitner et al. (2007) reports the detection of the H_2 S(1), S(2) and S(4) lines towards the Herbig Ae star AB Aur employing a spectral resolution $R \sim$100000. The H_2 line fluxes measured by Bitner et al. (2007) range from 0.5 to 1.5 10^{-14} erg s^{-1} cm^{-2}, line fluxes very similar to the flux limits of our VISIR observations. Bitner et al. (2007) point out that additional non-thermal heating mechanisms, such as X-rays or UV heating, are needed for explaining the H_2 lines observed.

4.5.3 The effect of the disk inclination

For simplicity on the discussion, until here we assumed that the disk is viewed pole-one. Now, if the disk is inclined an angle i, the line profile ϕ_ν used in Equation 4.6 will be doppler-shifted for each parcel of gas having a velocity component in the line of sight. For a parcel of gas located at radius R and at azimuth[14] θ, orbiting a star of mass $M_\star$, the doppler shift $\Delta\nu$ due to the Keplerian motion of the gas is

$$\Delta\nu = (\nu_0/c)\ sin(\theta) sin(i) \sqrt{\frac{GM_\star}{R}}, \tag{4.13}$$

with c being the speed of light. The doppler-shifted line profile $\phi_{\nu\ \mathrm{shifted}}$ will be

$$\phi_{\nu\ \mathrm{shifted}} = \frac{1}{\sigma_\nu \sqrt{\pi}} e^{\left(\frac{\nu - \nu_0 + \Delta\nu}{\sigma_\nu}\right)^2}. \tag{4.14}$$

Using Equation 4.14 instead of Equation 4.9 and employing Equations 4.3 to 4.8, the intensity $I(R, \theta, i)$ emitted by each parcel of fluid is calculated. The expected flux (in Janskys) emitted by

[14] We define θ=0 as the angle where the velocity component of the motion is 0 in the line of sight.

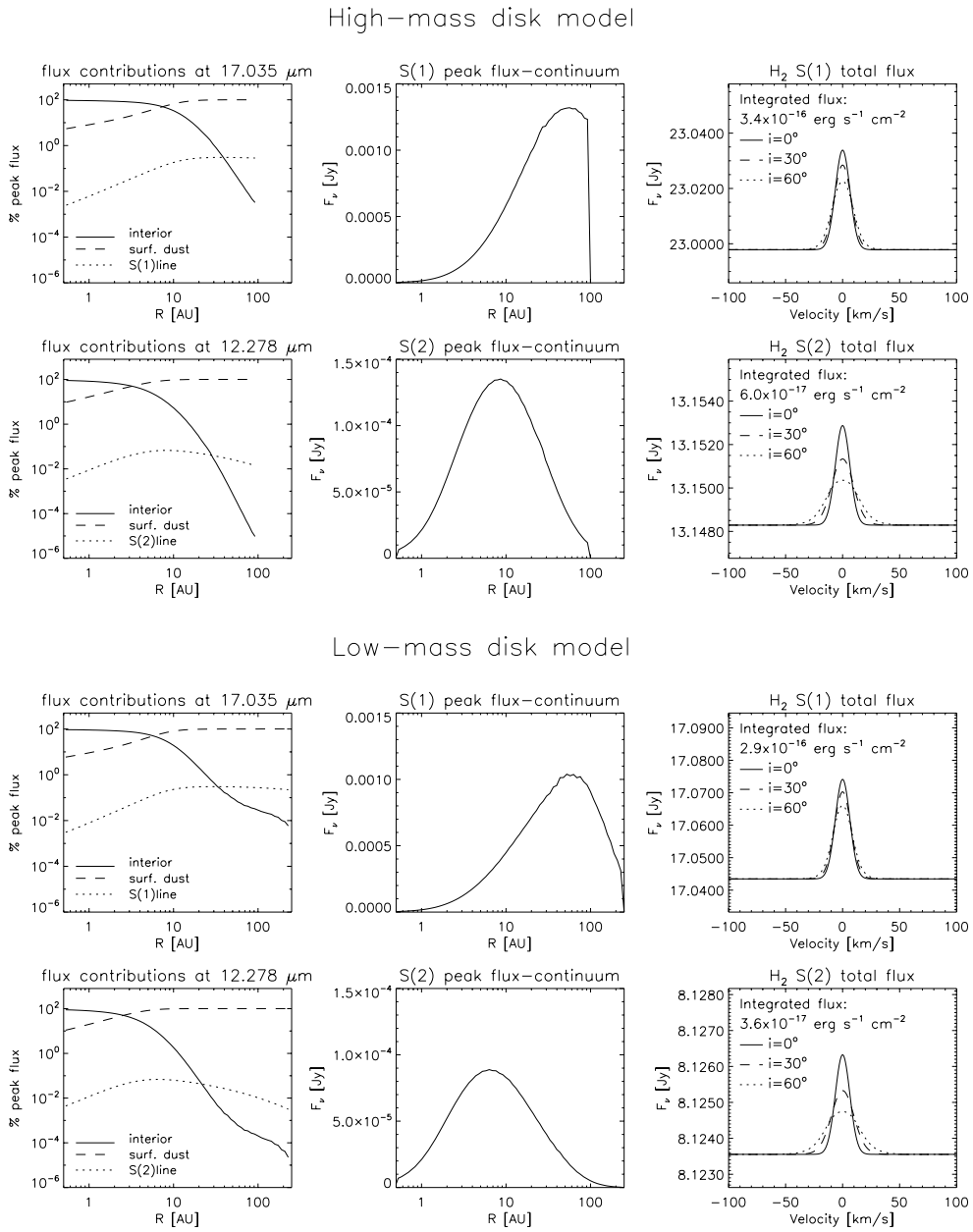

Figure 4.7: *Total S(1) and S(2) line fluxes for the two-layer high-mass disk model (upper six panels) and low-mass disk model (lower six panels). Left panels present the percentage contribution to the peak flux by the optically thick interior layer (solid), the optically thin dust in the surface layer (dashed) and the H_2 line (dots) as a function of radius for a pole-on disk (i=0°) . Central panels show the peak flux minus the continuum as a function of radius for pole-on disk. Right panels display the expected total H_2 line flux for three disk inclinations: pole-on (solid), i=30° (dashed) and i=60° (dotted).*

the parcel of fluid of dimensions $\mathrm{d}R \times R\,\mathrm{d}\theta$ will be given by

$$dF(R,\theta,i) = I(R,\theta,i)\,\frac{R\,dR\,d\theta}{d^2} \times 10^{23}. \tag{4.15}$$

Finally, the total emission by the disk is the sum of the contributions of all the fluid parcels

$$F_\nu = \int_{R_{min}}^{R_{max}} \int_0^{2\pi} dF_\nu = \frac{1}{d^2} \int_{R_{min}}^{R_{max}} \int_0^{2\pi} I(R,\theta,i)\,R\,dR\,d\theta \tag{4.16}$$

Here R_{min} and R_{max} are the inner and outer radius of the emitting region. Assuming that R_{min} = 0.5 AU and that R_{max} is the disk outer radius, we calculated the expected H_2 S(1) and H_2 S(2) line profiles for the high-mass and the low-mass disk at inclinations of 30 and 60 degrees. Our results are presented in the right panels of Figure 4.7. The net effect of the inclination is the broadening of the line and a decrease of the peak flux. The S(2) line is more affected than the S(1) line by the inclination. Since most of the material responsible for the S(1) and S(2) emission are located at distances larger than a few AU (see central panels of Figure 4.7) even at high inclinations the double peaked profile is not exhibited. This result suggest that higher temperature lines emitted at regions closer to the star (e.g., the S(3) line) are more suitable to investigate the inner-disk dynamics.

4.6 Summary and Conclusions

We observed a sample of nearby pre-main sequence stars with evidence for cold ($T < 50$ K) gas disk reservoirs and searched for emission of the warm gas with $T > 150$ K that is expected to be present in the inner region of these disks. None of the targets show any evidence for H_2 emission at 17.035 μm or at 12.278 μm. From the 3σ upper limits of the H_2 line fluxes, we found stringent upper limits to the mass of warm H_2 emitting gas. The disks contain less than a few tenths Jupiter mass of emitting gas at 150 K at most, and less than a few Earth masses of emitting gas at 300 K and higher temperatures.

Assuming that $T_{gas} = T_{dust}$ and a gas to dust ratio of 100, we compared our results to models of disks employing a Chiang and Goldreich (1997) optically thick two-layer disk model of masses 0.02 $M_\odot$ and 0.11 $M_\odot$. The upper limits to the disk's warm gas mass are smaller than the warm gas mass in the interior layer of the disk, but they are much larger than the amount of mass expected to be in the surface layer. The amount of mass in the surface layer is very small ($< 10^{-2}$ M_J) and almost independent of the total disk mass. We calculated the expected H_2 S(1) and H_2 S(2) line fluxes emitted from a two-layer disk for the low-mass and the high-mass cases assuming the sources at a distance of 140 pc, and LTE thermal emission. The predicted line fluxes of the two-layer disk model are of the order of $\sim 10^{-16} - 10^{-17}$ erg s^{-1} cm^{-2}, much smaller than the detection limits of our observations (0.4×10^{-14} erg s^{-1} cm^{-2}).

If the two-layer approximation to the structure of the disk is correct, we are essentially "blind" to most of the warm H_2 in the disk because it is located in the optically thick interior layer of the disk. Our non-detections are explained because of the intrinsically low thermal H_2 emission flux levels from the surface layer. Naturally, the two-layer disk model is only an approximation of the real structure of a protoplanetary disk. The puffed-up inner rim, which could be an important contributor to the H_2 emission, is not included in our models, and in reality there will be a smooth

transition zone between the disk's hot surface layer and the cool disk interior, which again could contribute significantly to the H_2 emission. A definitive interpretation of our results awaits the development of future more sophisticated models. However, independently of the model used, the observations clearly indicate that the bulk of optically thin warm H_2 gas must be small. In the following paragraphs, we explain several alternative scenarios that could be invoked for explaining our non-detections.

There is little warm gas because the gas/dust ratio changed globally in the disk. A possibility is to invoke a global change in the gas/dust ratio to explain the non-detection of warm gas. In this scenario the gas and dust are well mixed, but the amount of warm gas is so small that the emission levels are beyond our line flux sensitivity. For example, in the case of HD 104237 to reach the H_2 upper mass limits at T>200 K an optically thin low-mass disk requires a global gas/dust ratio < 30. However, the detections of CO emission at (sub)mm wavelengths for several of our targets indicate that large reservoirs of cold gas exist in the outer regions of their disks. If a change in the gas/dust ratio is responsible for the low levels of H_2 emission, it should be a local effect.

The gas and dust are thermally decoupled: the gas is there but most of it is cold. In this scenario, the stellar radiation is able to heat the dust grains efficiently, and the small superheated dust emission is observed in the MIR. If dust and gas are thermally decoupled, the gas is not heated as efficiently as the dust and very little warm gas is present. In other words, substantial amounts of gas are present in the inner disk, but we are not able to probe this in the H_2 transitions, because, the gas is too cold for emitting detectable flux levels in the MIR.

There is little warm gas, because the gas in the inner disk has been dissipated. A possible explanation for the low flux levels observed is that the gas/dust ratio in the inner region of the disk is much smaller than 100. A reduction of the gas/dust ratio in the inner disk could be explained as a consequence of disk dissipation. This explanation is interesting. However, the evaporation of small dust particles occurs before the gas is blown away. The observed targets do not present evidence for holes from the SED, this suggests that dust and gas are still present in the inner disk.

In the particular case of T Tauri star HD 319139 an alternative explanation is plausible. HD 319139 is a short period (2.4 days) spectroscopic binary. The non-detection of gas in the inner disk could be explained as the consequence of the inner disk truncation by the gravitational interaction of the binary pair (Artymowicz & Lubow, 1994).

There is little warm gas, because the gas in the inner disk has been cleared by a low-mass companion. One exciting possibility is that low amounts of warm gas in the inner disk observed are in fact the consequence of the formation of a giant planet. The giant planet itself would have most of the gas that was present in the inner disk. The accretion observed in the systems could be explained as material flowing across the gap. One limitation of this scenario is that we will expect to see no warm dust in the SED of the sources as a consequence of the gap. But the observed targets do not present evidence for holes in the SED. However, spectral features in the MIR and the SED can be still produced in the innermost part of the disk from small amounts of dust present in the remaining gaseous material that has not been accreted by the giant planet. We note that recently, indications for the presence of a planet in a disk, as required for this scenario, have been found in the Herbig Ae/Be star HD 100456 (Acke & van den Ancker 2006).

In summary, an optically thick disk where only the H_2 in the surface layer produce emission lines, thermal decoupling, or a localized gas/dust ratio much smaller than the canonical ISM value of 100, remain as viable explanations for the observed lack of warm gas emission in the circumstellar disks of the Herbig Ae/Be stars observed.

Acknowledgements. This research has made use of the SIMBAD database operated at CDS, Strasbourg, France. We would like to thank the staff of Paranal Observatory for performing our observations in service mode.

4.7 References

Acke, B., & van den Ancker, M. E. 2004, A&A, 426, 151
Acke, B., & van den Ancker, M. E. 2006, A&A, 449, 267
Alexander, R. D., Clarke, C. J., & Pringle, J. E. 2006, MNRAS, 369, 229
Artymowicz, P., & Lubow, S. H. 1994, ApJ, 421, 651
Beckwith, S. V. W., Sargent, A. I., Chini, R. S., & Guesten, R. 1990, AJ, 99, 924
Bitner, M. A., et al. 2007, ApJL, 661, L69
Boss, A. P. 1998, ApJ, 503, 923
Chiang, E. I., & Goldreich, P. 1997, ApJ, 490, 368
Chiang, E. I., et al. 2001, ApJ, 547, 1077
Cohen, M., Walker, R. G., & Witteborn, F. C. 1999, LPI Contributions, 969, 5
de Zeeuw, P. T., et al. 1999, AJ, 117, 354
Dent, W. R. F., Greaves,J. S., & Coulson, I. M. 2005, MNRAS, 359, 663
Dullemond, C. P., Dominik, C., & Natta, A. 2001, ApJ, 560, 957
Dullemond, C. P. 2002, A&A, 395, 853
Dullemond, C. P., Hollenbach, D., Kamp, I., & D'Alessio, P. 2007, in Protostars and Planets V., Edited by B. Reipurth, D. Jewitt, and K. Keil. University of Arizona Press, Tucson, 2007
Dutrey, A., Guilloteau, S., & Ho, P. 2007, in Protostars and Planets V., Edited by B. Reipurth, D. Jewitt, and K. Keil. University of Arizona Press, Tucson, 2007
Haisch, K. E., Jr., Lada, E. A., & Lada, C. J. 2001, ApJL, 553, L153
Haisch, K. E., Jr., Jayawardhana, R., & Alves, J. 2005, ApJL, 627, L57
Henning, T., Launhardt, R., Steinacker, J., & Thamm, E. 1994, A&A, 291, 546
Jensen, E. L. N., Mathieu, R. D., & Fuller, G. A. 1996, ApJ, 458, 312
Jonkheid, B., Kamp, I., Augereau, J.-C., & van Dishoeck, E. F. 2006, A&A, 453, 163
Kamp, I., & Dullemond, C. P. 2004, ApJ, 615, 991
Lagage, P.O. et al. 2004, The Messenger 117, 12.
Laor, A., & Draine, B. T. 1993, ApJ, 402, 441
Lundin, L.K. VLT VISIR Pipeline User Manual. VLT-MAN-ESO-19500-3852. 2006
Meeus, G., et al. 2001, A&A, 365, 476
Najita, J. R., Carr, J. S., Glassgold, A. E., & Valenti, J. A. 2007, in Protostars and Planets V., Edited by B. Reipurth, D. Jewitt, and K. Keil. University of Arizona Press, Tucson, 2007
Natta, A., Testi, L., Calvet, N., Henning, T., Waters, R., & Wilner, D. 2007, in Protostars and Planets V.,Edited by B. Reipurth, D. Jewitt, and K. Keil. University of Arizona Press, Tucson, 2007
Nomura, H., & Millar, T. J. 2005, A&A, 438, 923
Nomura, H., et al. 2007, ArXiv Astrophysics e-prints, arXiv:astro-ph/0702030.
Palla, F., & Stahler, S. W. 1993, ApJ, 418, 414
Pascucci, I., et al. 2006, ApJ, 651, 1177
Piétu, V., Dutrey, A., & Kahane, C. 2003, A&A, 398, 565

Pollack, J. B., et al. 1996, Icarus, 124, 62
Richter, M. J., Jaffe, D. T., Blake, G. A., & Lacy, J. H. 2002, ApJL, 572, L161
Sako, S., et al. 2005, ApJ, 620, 347
Sheret, I., Ramsay Howat, S. K., & Dent, W. R. F. 2003, MNRAS, 343, L65
Siebenmorgen, R.,L Pantin, E., Sterzik, M. VLT VISIR User Manual.
VLT-MAN-ESO-14300-3514. 2004
Sicilia-Aguilar, A., et al. 2006, AJ, 132, 2135
Stempels, H. C., & Gahm, G. F. 2004, A&A, 421, 1159
Takahashi, J. 2001, ApJ, 561, 254
Thi, W. F., et al. 2001, ApJ, 561, 1074
van Boekel, et al. 2005, A&A, 437, 189
van den Ancker, M. E., de Winter, D., & Tjin A Djie, H. R. E. 1998, A&A, 330, 145
Watson, A. M., Stapelfeldt, K. R., Wood, K., & Ménard, F. 2007, in Protostars and Planets V.,
Edited by B. Reipurth, D. Jewitt, and K. Keil. University of Arizona Press, Tucson, 2007
Wolniewicz, L., Simbotin, I., & Dalgarno, A. 1998, ApJS, 115, 293

4.8 Appendix. A study for the H2EX mission

At the time of writing, the European Space Agency (ESA) is studying the possibility of launching a satellite dedicated to the study of molecular hydrogen emission in the universe: H_2 Explorer (H2EX). H2EX is a 1.2 m telescope equipped with a mid-infrared fourier spectrograph that will be able to achieve a spectral resolution of $R \sim 20000$. It is designed for covering the 0-0 S(0), 0-0 S(1), 0-0 S(2) and 0-0 S(3) transitions of H_2 with a sensitivity limits (3σ) of 7×10^{-20}, 1.8×10^{-20}, 1.6×10^{-20} and 1.5×10^{-20} W m^{-2} for each line respectively. A fraction of telescope time will be dedicated to study young stellar objects and their circumstellar disks.

Using the models described in this chapter, we performed a study in which we calculated the amount of H_2 *thermal emission* in the 0-0 S(0) to 0-0 S(3) lines expected from optically thick disks around stars of spectral types B5 to M0. For the calculations we assumed a passive disk without puffed-up inner rim, of mass 40 M_J, size 250 AU, and a surface density power law exponent of -1.5. For stars of spectral types B5 to K0, we assumed a truncation radius at $T = 5000$K, for stars of spectral K1 to M0, we assumed a truncation radius at $T = 3000$K. Our results are summarized in Figure 4.8. We obtained that H2EX will be able to measure 0-0 H_2 S(1) thermal emission from disks located up to 250 AU for stars of spectral types B5 to F0. At 250 pc the 0-0 S(0), 0-0 S(2) and 0-0 S(3) H_2 lines will be only detectable for the hottest stars (B5 to A5). For stars located at 140 pc (Taurus), H2EX will be able to probe the disks of stars earlier than G5. Our model predictions are only of H_2 thermal emission, therefore, they are very conservative estimations of the expected H_2 line fluxes. If the molecular hydrogen is heated by an additional source (e.g by intense UV or X-rays), the line fluxes are expected to be one or two orders of magnitude higher.

Some of the sources that H2EX is expected to observe are transitional disks. We were interested into know what are the mass sensitivity limits that H2EX could reach in each of the lines assuming that the emission is optically thin. Employing equation 4.1, the mass upper limit for a line of flux F_{ul} from a source at a distance d of gas at temperature T can be found. Employing the H2EX sensitivity limits in each of the four 0-0 H_2 lines, we calculated the mass sensitivity limits

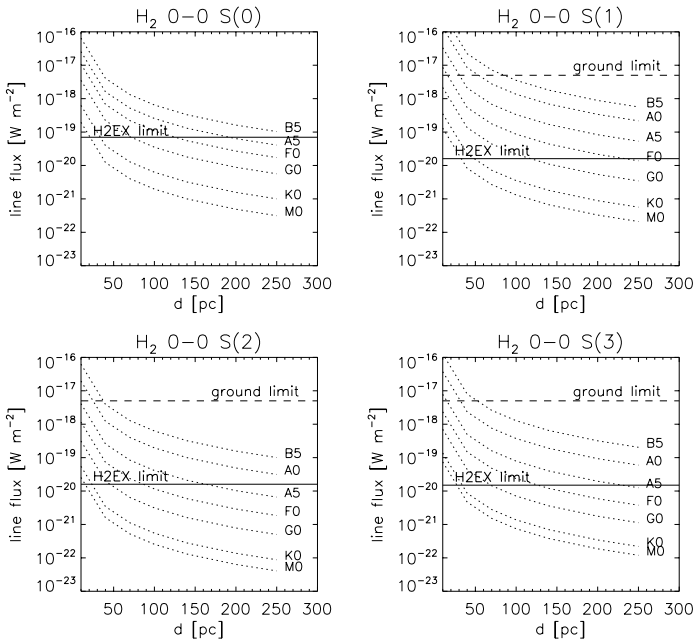

Figure 4.8: *Expected thermal 0-0 S(0), 0-0 S(1), 0-0 S(2) and 0-0 S(3) H_2 emission from a disk of mass 40 M_J and radius 250 AU surrounding stars of spectral types B5 to M0. The dashed horizontal line shows the ground sensitivity limits (~ 0.4 × 10^{-17} W/m^2). The continuos horizontal line displays the sensitivity limits of H2EX.*

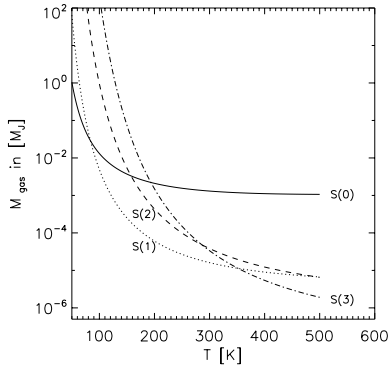

Figure 4.9: *H2EX mass sensitivity limits of optically thin H_2 gas as a function of temperature for a source distant 140 pc.*

as a function of temperature for a source located at 140 pc. Our results are presented in Figure 4.9. We found that for gas colder than 50K, observations of the H_2 S(0) line will be the most sensitive. For gas at temperatures between 50 and 350K, the H_2 S(1) line will be the most sensitive line. For gas warmer than 350K, the H_2 S(3) line will provide better sensitivity. H2EX will be able to probe 10^{-4} M_J of gas at 150 K, 10^{-5} M_J of gas at 300 K and 10^{-6} M_J of gas at 500 K.

Submitted to A&A as: A. Carmona, M.E van den Ancker, Th. Henning, M. Goto, D. Fedele, and B.Stecklum –
"Molecular Hydrogen Emission in the CTTS LkHα 264 and the debris disk 49 Cet", Astronomy and Astrophysics, 2007

Chapter 5

NIR Molecular Hydrogen Emission in the CTTS LkHα 264 and the debris disk 49 Cet

Abstract

We report on the first results of a search for molecular hydrogen emission from protoplanetary disks using CRIRES, ESO's new VLT Adaptive Optics high resolution near-infrared spectrograph. We observed the classical T Tauri star LkHα 264 and the debris disk 49 Cet, and searched for $v = 1 - 0$ *S(1)* H_2 *emission at 2.1228 μm,* $v = 1 - 0$ *S(0)* H_2 *emission at 2.2233 μm and* $v = 2 - 1$ *S(1)* H_2 *emission at 2.2477 μm. The* H_2 *line at 2.1218 μm is detected in LkHα 264 confirming the previous observations by Itoh et al. (2003). In addition, our CRIRES spectra reveals the previously undetected* H_2 *line at 2.2233 μm in LkHα 264. The detected lines coincide with the rest velocity of LkHα 264. They have a FWHM of ∼20 km* s^{-1}*. This is strongly suggestive of a disk origin for the lines. These observations are the first simultaneous detection of* $v = 1 - 0$ *S(1) and* $v = 1 - 0$ *S(0)* H_2 *emission from a protoplanetary disk. The emission is spatially unresolved. The enhanced spatial resolution of CRIRES constrains the* H_2 *emitting region to the inner 50 AU of the disk. The* H_2 *line at 2.2477 is not present in LkHα 264. 49 Cet does not exhibit* H_2 *emission in any of the three observed lines. We derive stringent limits for the mass of* H_2 *at* $T \sim 1500$ *K in the inner disks of LkHα 264 and 49 Cet. There are a few lunar masses of emitting* H_2 *in the inner 1 AU of LkHα 264, and less than a tenth of a lunar mass in the inner disk of 49 Cet. The measured 1-0 S(0)/1-0 S(1) and 2-1 S(1)/1-0 S(1) line ratios in LkHα 264 indicate that the* H_2 *emitting gas is at a temperature lower than 2000 K and that the* H_2 *is most likely thermally excited by UV photons. The* $v = 1 - 0$ *S(1)* H_2 *line in LkHα 264 is single peaked. Modeling of the shape of the line suggests that the disk should be seen close to face-on (*$i < 35^o$*). A comparative analysis of the physical properties of classical T Tauri stars in which the* H_2 $v = 1 - 0$ *S(1) line has been detected and non-detected indicates that the presence of* H_2 *emission is correlated with the magnitude of the UV excess and the strength of the Hα line. The lack of* H_2 *emission in the NIR spectra of 49 Cet and the absence of* H_α *emission suggest that the gas in the inner disk of 49 Cet has dissipated. These results combined with previous detections of* ^{12}*CO emission at sub-mm wavelengths indicate that the disk surrounding 49 Cet should have an inner hole. We favor inner disk dissipation by inside-out photoevaporation, or the presence of an unseen low-mass companion as the most likely explanations for the lack of gas in the inner disk of 49 Cet.*

5.1 Introduction

The discovery of extrasolar planets in the previous decade triggered an increasing interest in the physical mechanisms behind the process of planet formation. Many recent efforts have been directed to the study of disks surrounding pre-main-sequence stars. Observational and theoretical evidence suggests that planets are forming in these disks. To observationally determine

Table 5.1: *Stellar physical properties.*

Star	Sp.T.	T_{eff} [K]	d [pc]	Age [Myr]	CO sub-mm	$M^{\dagger}_{disk}$ [M_J]	object
LkHα 264	K5Ve[a]	4350[b]	300[c]	2[d]	...	85[a]	CTTS
49 Cet	A1V[e]	9970[b]	61[f]	20[g]	^{12}CO $J = 3-2$[h] $J = 2-1$[i]	0.4[j]	debris disk

[a] Itoh et al. (2003b). [b] Kenyon & Hartmann (1995). [c] Straižys et al. (2002). [d] Jayawardhana et al. (2001). [e] From Chen et al. (2006). [f] Hipparcos catalogue. [g] Zuckerman & Song (2004). [h] Dent et al. (2005) [i] Zuckerman et al. (1995). [j] Thi et al. (2001) and Bocklée-Morvan et al. (1995).

$^{\dagger}M_{disk}$ refers to the total mass in the disk deduced from mm observations.

the physical structure and dynamics of the gas and dust in protoplanetary disks is of paramount importance for understanding the process of planet formation.

In the inner 1 AU of protoplanetary disks, intense UV or X-ray heating can bring the gas temperatures to a few thousand Kelvin. At these high temperatures, ro-vibrational transitions of H_2 are excited and a rich spectrum of H_2 lines in the near-infrared is expected to be produced. The study of H_2 quiescent ro-vibrational emission[1] towards pre-main-sequence stars with disks offers the opportunity to address the question of the presence of hot gas in the disk, by probing the temperature and density in the innermost regions where terrestrial planets are expected to form. For example, the H_2 $\nu = 1-0$ S(1) line at 2.1218 μm (one of the strongest H_2 ro-vibrational lines) is sensitive to a few Lunar masses of gas. Therefore, the absence of the line would be strongly suggestive of little or no hot gas in the systems.

In this chapter we present the first results of a sensitive search for near-infrared H_2 emission from protoplanetary disks using CRIRES, ESO's new VLT near-infrared high-resolution spectrograph. We searched for the H_2 $\nu = 1-0$ S(1) line at 2.1218 μm, H_2 $\nu = 1-0$ S(0) line at 2.2233 μm and H_2 $\nu = 2-1$ S(1) line at 2.2477 μm, towards LkHα 264, a classical T-Tauri star with previously reported detections of the $\nu = 1-0$ S(1) line by Itoh et al. (2003), and 49 Cet, a debris disk with evidence of a large reservoir of cold gas at sub-mm wavelengths (Dent et al. 2005, Zuckerman et al. 1995). We confirm the detection of H_2 emission at 2.1218 μm in LkHα 264, and announce, for the first time, the detection of H_2 emission at 2.2233 μm from a disk (LkHα 264). We report the non-detections of H_2 emission at 2.2477 μm in LkHα 264, and at 2.1218, 2.2233 and 2.2477 μm in 49 Cet.

The remainder of this chapter is organized as follows. We start with a description of the observations and the data reduction. In Section 5.3 we present our results and calculate the mass limits for the hot ($T \sim 1500$ K) H_2 in the systems. In Section 5.4, based upon the measured 1-0 S(0)/1-0 S(1) and 2-1 S(1)/1-0 S(1) line ratios in LkHα 264, we determine the excitation mechanism of the observed H_2 emission. By modeling of the shape of the $\nu = 1-0$ S(0) H_2 line, we derive constraints for the inclination of the disk around LkHα 264, and finally we discuss the disk properties of the stars in which H_2 emission has been detected and the prospects for future investigations. Our conclusions are presented in Section 5.5.

[1] By quiescent emission we mean emission at the rest velocity of the star. H_2 emission can also be produced by shocked gas associated with outflows. However, in such a case the emission is expected to be doppler shifted more than 20 km s^{-1} with respect to the rest velocity of the star.

Table 5.2: *Summary of the observations.*

Star	λ [μm]	Date	UT [hh:mm]	t_{exp} [s]	Airmass	seeing [arcsec]	Calibrator [a]	t_{exp} [s]	Airmass	seeing [arcsec]
LkHα 264	2.1218	8 Nov 2006	06:25	720	1.4	1.2	HIP 13327	160	1.3	0.9
	2.2233, 2.2477	8 Nov 2006	06:52	720	1.4	1.0	HIP 13327	160	1.3	0.9
49 Cet	2.1218	9 Nov 2006	02:38	240	1.1	0.8	HIP 8497	40	1.0	1.2
	2.2233, 2.2477	9 Nov 2006	03:07	240	1.2	0.7	HIP 8497	40	1.0	1.2

[a] Spectrophotometric standard stars were observed immediately following the science observations.

5.2 Observations

We obtained high-resolution ($R \sim 45000$)[2] near-infrared spectra of LKHα 264 and 49 Cet, on 2006 November 8-9, using the ESO-VLT cryogenic high-resolution infrared echelle spectrograph CRIRES (Käufl et al. 2004), mounted on ESO's UT1 "Antu" 8m telescope atop Cerro Paranal Chile, during the CRIRES science-verification phase. CRIRES uses a mosaic of four Aladdin III InSb arrays providing an effective 4096 x 512 detector array in the focal plane. Adaptive Optics (MACAO - Multi-Applications Curvature Adaptive Optics) was used to optimize the signal-to-noise ratio and the spatial resolution. The science targets were used as natural guide stars.

Our observations were performed using a 46" long, 0.4" wide, north-south oriented slit, resulting in instrumental velocity resolution of 6.6 km s^{-1}. The observations were made by nodding the telescope 10" along the slit. To correct for bad pixels and decrease systematics due to the detector, a random jitter smaller than 2" was added to the telescope in addition to the nodding offset at each nodding position. For the telluric correction spectrophotometric standard stars at similar airmass to the science target were observed immediately following the science observations.

The observations were performed employing the wave-ID 27/1/n and the wave-ID 25/-1/n, providing a spectral coverage from 2.0871 to 2.1339 μm and from 2.2002 to 2.2552 μm respectively. To obtain the wavelength calibration, observations of an internal Th-Ar calibration lamp with 3x30 second exposures were executed immediately following the target and standard star spectroscopy observations at each wave-ID setting. A summary of the observations is provided in Table 5.2.

5.2.1 Data Reduction

The data was reduced using the CRIRES pipeline and the ESO/CPL recipes. In each chip, the chopped raw image frames at each nodding position were flat-field corrected, then combined and averaged, thereby correcting for the sky-background (i.e. $A = (A_1 - A_2 + ... + A_{n-1} - A_n)/n$). The resulting frames at each nodding position were corrected for jittering using the jitter information from the fits headers. Image pairs in the nodding sequence (AB) were subtracted and averaged resulting in a combined frame ($F_{combined} = (A - B)/2$), thereby correcting for instrument thermal emission. The ensemble of combined frames were stacked in one single 2D frame.

The spectrum was extracted by summing the number of counts inside the PSF in the dispersion direction in the 2D spectrum. The absolute wavelength calibration was obtained by cross-correlation with the Th-Ar lamp frame taken immediately after the science exposure. The wave-

[2]The spectral resolving power of our CRIRES observations was determined by the FWHM of the Gaussian fit of an unresolved skyline. A $\lambda/\Delta\lambda \sim 45000$ at 2.12 μm corresponds to a resolution of ~6.6 km s^{-1}. This FWHM is sampled on 5 pixels of the CRIRES detector.

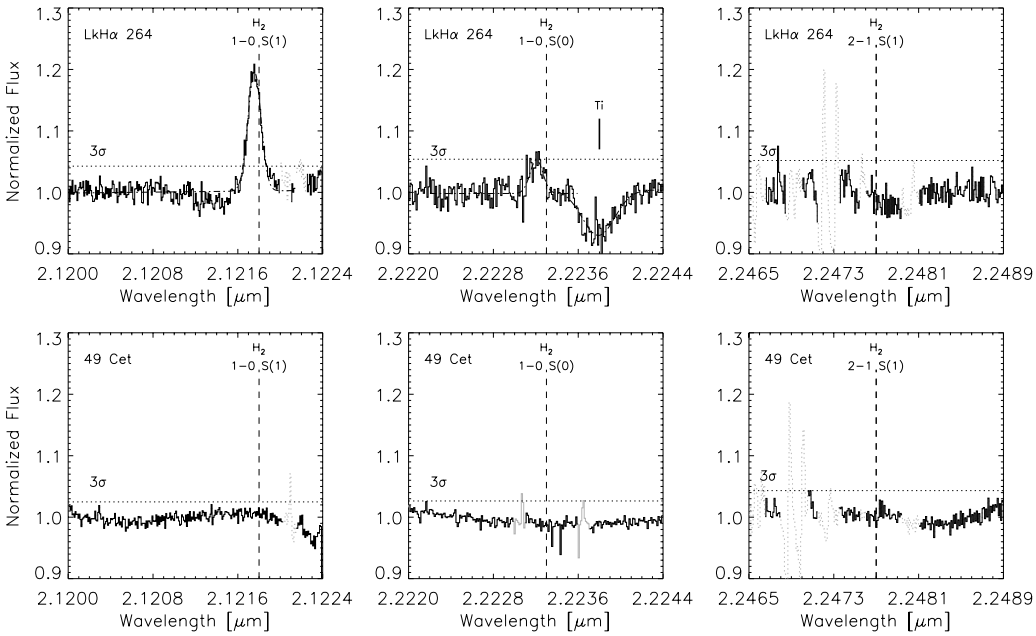

Figure 5.1: *CRIRES spectra of LkHα 264 (upper panels) and 49 Cet (lower panels) in the regions of the H_2 ν=1-0 S(1), H_2 ν=1-0 S(0) and H_2 ν=2-1 S(1) emission lines. The H_2 ν=1-0 S(1) and the H_2 ν=1-0 S(0) lines are detected in LkHα 264. A photospheric Ti feature at 2.2238 μm is observed in LkHα 264. The gaussian fits to the detected lines are illustrated in dash-dot lines. The H_2 ν=2-1 S(1) line is not present in LkHα 264. In the case of 49 Cet none of the three H_2 features are present in emission or absorption. Horizontal dotted lines show the 3σ continuum flux limits. The spectra is not corrected for $v_{\rm LSR}$ of the star. Regions of poor telluric correction are in gray-dotted lines in the spectra.*

length calibration was done for each chip independently. The one-dimensional spectrum was divided by the exposure time t_{exp} (see Table 5.2).

To correct for telluric absorption, the one-dimensional extracted science spectrum was divided by the one-dimensional extracted spectrum of the standard star. The standard star spectrum was corrected for differences in air-mass and air-pressure with respect to the science target spectrum employing the method described by Carmona et al. (2005). Small offsets of a fraction of a pixel in the wavelength direction were applied to the standard star spectrum until the best signal-to-noise in the corrected science spectra was obtained.

Absolute flux calibration was found by multiplying the telluric corrected spectrum by the flux of the standard star at the wavelengths observed. The flux of the standard star in the K band was found from the *K* magnitude of the standard star using Vega as the reference star[3]. The absolute flux calibration is accurate at the 20% level. The principal source of uncertainty is the imperfections in the telluric correction.

[3]The flux of Vega in the K band used is 4.14×10^{-10} W m^{-2} μm^{-1} (Cox, 2000).

5.3 Results

We present in Figure 5.1 the normalized spectra of LkHα 264 and 49 Cet. LkHα 264 exhibits H_2 $\nu = 1-0$ S(1) emission at 2.1228 μm and the H_2 $\nu = 1-0$ S(0) feature at 2.2233 μm. Our observations confirm the previous detections of the H_2 $\nu = 1-0$ S(1) line reported by Itoh et al. (2003). In contrast to Itoh et al. (2003) the H_2 $\nu = 1-0$ S(0) line is detected in our CRIRES spectra of LkHα 264. The H_2 $\nu = 2-1$ S(1) line is not seen in LkHα 264. The Si line at 2.1210 μm reported by Itoh et al. (2003) is not confirmed by our CRIRES spectrum. We observe Ti absorption lines at 2.2217 and 2.2238 μm of FWHM of 48.9 km s^{-1} and EW 0.2 Å. These lines are gravity sensitive, and would suggest that the underlying photosphere is of a late KV star (see e.g. Greene & Lada 2002) in agreement with the spectral type K5Ve of LkHα 264 . The broadening of the lines indicates a $v \sin i$ of 40 km s^{-1} in LkHα 264. In the case of 49 Cet none of the three H_2 features are present in emission or absorption. The spectrum does not exhibit photospheric absorption features. We summarize our results in Table 5.3.

5.3.1 Upper flux limits to H_2 emission in 49 Cet

3σ upper limits for the integrated line flux of the observed H_2 lines in 49 Cet were determined by calculating the standard deviation of the continuum flux in the vicinity of the H_2 features and multiplying 3 times the standard deviation (see horizontal dotted lines in Figure 5.1) times the FWHM of a CRIRES unresolved line ($4.95 \times 10^{-5}\mu$m). They are reported in Table 5.3. The continuum is spatially unresolved. The mean PSF FWHM measured in the continuum is 3.7 and 6.0 pixels for the spectrum at 2.12 and 2.22 μm respectively. Using the CRIRES pixel scale of 0.086 arcsec/pixel, we obtain a PSF FWHM of 0.3" and 0.5" for each spectrum. At the distance of 49 Cet (61 pc), that corresponds to 20 and 31 AU respectively. We conclude that the size of the continuum-emitting region of 49 Cet has an upper limit of 20 AU.

5.3.2 Molecular Hydrogen Emission in LkHα 264

The central wavelength the of the $\nu = 1-0$ S(1) H_2 emission in LkHα 264 was measured to be 2.121757 ± 0.000005 μm by a Gaussian fit. Assuming an error on the wavelength calibration of ~1.0 km s^{-1} (1 pixel), it corresponds to a velocity shift of -6.0 ± 1.0 km s^{-1}. At the time of the observations the velocity correction[4] due to the motion of the Earth was +0.4 km s^{-1}. The velocity shift is therefore -5.6 ± 1.0 km s^{-1}, in agreement with the center of the line of -5.1 ± 1.2 km s^{-1} by Itoh et al. (2003) and the rest velocity of the star of -5.9 ± 1.2 km s^{-1} by Itoh et al. (2003) and -4.2± 2.5 km s^{-1} by Hearty et al. (2000). Our observations confirm that the H_2 emission observed is coincident with the rest velocity of the star. The detected H_2 $\nu = 1-0$ S(1) emission line is symmetric. The FWHM of the line is 20.6 ± 1 km s^{-1}. The Equivalent Width (EW) of the line is -0.32 ± 0.01 Å, and the integrated line flux is 3.0×10^{-15} erg s^{-1} cm^{-2}. The observed line is 10 km s^{-1} narrower and slightly fainter than the line observed by Itoh et al. (2003). The line flux observed is within the range of 1 to 7×10^{-15} erg s^{-1} cm^{-2} line fluxes reported towards other classical T Tauri stars (Weintraub et al. 2000, Bary et al. 2003).

The H_2 $\nu = 1-0$ S(0) feature at 2.2233 μm is detected with a 3σ level confidence (see Figure 5.1). Employing a Gaussian fit, the central wavelength of the line found is 2.22321 ± 0.00005

[4]We employed the rvcorrect function of IRAF to calculate the velocity shift.

Table 5.3: *H_2 Line fluxes and upper limits measured*

		LkHα 264			49 Cet		
		1-0 S(1) 2.1218 μm	1-0 S(0) 2.2233 μm	2-1 S(1) 2.2477 μm	1-0 S(1) 2.1218 μm	1-0 S(0) 2.2233 μm	2-1 S(1) 2.2477 μm
Continuum	[ergs s^{-1} cm^{-2} μm^{-1}]	9.2×10^{-11}	1.5×10^{-10}	1.6×10^{-10}	3.5×10^{-9}	1.7×10^{-9}	1.5×10^{-9}
3σ	[ergs s^{-1} cm^{-2} μm^{-1}]	4.2×10^{-12}	8.2×10^{-12}	1.0×10^{-11}	1.0×10^{-10}	1.8×10^{-10}	3.1×10^{-10}
Flux[a]	[ergs s^{-1} cm^{-2}]	3.0×10^{-15}	1.0×10^{-15}	$< 5.3\times10^{-16}$	$< 5.4\times10^{-15}$	$< 8.9\times10^{-15}$	$< 1.6\times10^{-14}$
Mass H_2 at 1500 K[b]	[$M_\odot$]	5.6×10^{-8}	...	...	$< 4.2\times10^{-9}$	...	...

[a] For the calculation of upper limits, we assumed that the FWHM of the line is 6.6 km s^{-1}.
[b] Mass calculated using Eq. 1, T=1500 K and LTE conditions.

μm. This corresponds to a velocity shift of -12 ± 7 km s^{-1} which is in agreement with the velocity shift found in the $v = 1-0$ S(1) line. The error in the determination of the center of the $v = 1-0$ S(0) line is larger because the line is detected with a much smaller confidence level. The FWHM of the line is 19.8 ± 1 km s^{-1}. The EW of the line is -0.07 ± 0.01 Å, and the integrated line flux is 1.0×10^{-15} erg s^{-1} cm^{-2}. This line flux is smaller than the previous upper limits by Itoh et al. (2003) demonstrating the improvement on sensitivity reached by CRIRES.

The H_2 $v = 1-0$ S(1) emission is spatially unresolved. The mean PSF FWHM in the continuum measured is ≈4.2 pixels. Using the CRIRES pixel scale of 0.086 arcsec/pixel and a distance of 300 AU for LkHα 264, we obtain a PSF FWHM of ≈0.36" indicating that the $v = 1-0$ S(1) line is produced in the inner 50 AU of the LkHα 264 disk. The H_2 $v = 1-0$ S(0) emission is also spatially unresolved. The mean PSF FWHM in the continuum measured is ≈ 0.58" (6.8 pixels) corresponding to an upper limit of 90 AU for the H_2 $v = 1-0$ S(0) emitting region. The very similar FWHM of the H_2 $v = 1-0$ S(0) and the H_2 $v = 1-0$ S(1) (∼ 20 km s^{-1}) suggests that the gas responsible for the H_2 emission is located in similar regions of LkHα 264. Since both H_2 lines are spatially unresolved, and both lines presumably come from the same region, we conclude that the H_2 emitting region should be in the inner 50 AU of the LkHα 264 disk.

Employing a similar approach as described for 49 Cet, we derived an upper limit for the flux of 5.3×10^{-16} erg s^{-1} cm^{-2} for the H_2 $v = 2-1$ S(1) feature at 2.2477 μm in LkHα 264. Assuming an error of 20% in the flux calibration of the spectra, the 1-0 S(0)/1-0 S(1) line ratio is 0.33 ± 0.1 and the 2-1 S(1)/1-0 S(1) line ratio is <0.2. These line ratios are consistent with the line ratios of a gas at LTE at a temperature cooler than 2000 K (Mouri et al. 1994).

5.3.3 Mass of hot H_2 in LkHα 264 and 49 Cet

Assuming optically thin emission and a source size equal to the beam size of the telescope, the mass of hot H_2 gas in $M_\odot$ was determined from the $v = 1-0$ S(1) line flux employing (Bary et al. 2003, Thi et al. 2001)

$$M(\mathrm{H_2})_{v=1-0\,S(1)} = 1.76\times10^{-20}\frac{4\pi F_{ul} D^2}{E_{ul} A_{ul}\,\chi_{v,J}(T)} \tag{5.1}$$

with F_{ul} being the $v = 1-0$ S(1) line flux or the flux upper limit, D the distance in pc to the source, E_{ul} the energy difference in ergs between the levels u and l of the transition (9.3338×10^{-13} ergs), A_{ul} the Einstein coefficient ($A_{10} = 2.09\times10^{-7}$ s^{-1}) and $\chi_{v,J}(T)$ the level populations at temperature T of the H_2 gas at the upper level v, J of the transition (Bary et al. 2003). Under LTE

conditions at 1500 K, $\chi_{\nu,J}(T) = 5.44 \times 10^{-3}$. In LkH$_\alpha$ 264 the mass of hot gas is $\approx 5.6 \times 10^{-8} M_\odot$ (~1.5 M_{Moon}). Since the flux observed by our CRIRES observations is 50% lower to that reported by Itoh et al. (2003) the derived mass is ≈ 50% lower. Using the same set of equations, the upper limit to the mass of H_2 at T =1500 K obtained for 49 Cet is $4.2 \times 10^{-9} M_\odot$ (~0.1 M_{Moon}). If the origin of the emission is not thermal, for example in the case of excitation by UV-fluorescence or X-ray pumping, the level populations are smaller than at LTE and the mass limits larger.

Comparing the disk masses deduced from observations of dust continuum at mm wavelengths (see Table 5.1) with the gas mass probed by the $\nu = 1-0$ S(1) H_2 line (see Table 5.3), we can observe that the amount of gas that is probed by the $\nu = 1-0$ S(1) H_2 line is very small with respect to the total amount of gas in the disk. For LkHα 264 and 49 Cet the $\nu = 1-0$ S(1) H_2 line probes as little as 10^{-5} of the total amount of gas. Bary et al. (2003) suggest that a conversion factor of $10^7 - 10^9$ could be used for deducing the total mass of the gas from the masses obtained from the $\nu = 1-0$ S(1) H_2 line. Applying such a conversion factor for LkHα 264 we obtain a total disk mass of 0.5 to 50 $M_\odot$ and for 49 Cet a total disk mass of < 0.04 to 0.4 $M_\odot$. In the case of 49 Cet the deduced mass is in agreement with mm observations. In the case of LkHα 264 the total mass deduced is much too high to be consistent with the mass obtained from observations at mm wavelengths. In addition, the estimate is unrealistic since the disk would have fragmented due to its high mass.

5.4 Discussion

5.4.1 The excitation mechanism of the H_2 line in LkHα 264

H_2 emission can be the result of thermal (collisions) and non-thermal (radiative decay from excited electronic states) excitation mechanisms. In the thermal case, the gas is heated either by shocks, X-rays or UV-photons. In this case, the H_2 spectrum is characterized by a single excitation temperature typically between 1000 and 2000 K. In the non-thermal case, the electronic excitation results from the absorption of a UV photon in the Lyman-Werner band (912-1108 Å) or the collisions with a fast electron due to X-ray ionization.

The first step in our analysis is to determine whether the H_2 emission observed in LkHα 264 originates in an outflow (shock excited emission) or in a disk. The small velocity shift, the line shape (well reproduced by a disk model, see §5.4.2), and the fact that the emission is spatially unresolved are not in favor of shock excited H_2. An additional strong argument against shock excitation of H_2 is that LkHa 264 does not exhibit [OI] forbidden emission at 6300 Å (Cohen and Kuhi 1979); a classical signature of outflows in T Tauri stars. The lack of this line indicates that in LkHα 264 the outflow is not present or at least that it is very weak. We conclude that the H_2 emission observed in LkHα 264 originates very likely in a disk.

The thermal and non-thermal excitation mechanisms are distinguishable on the basis of line ratios (Mouri et al. 1994 and references there in). With Figure 3b of Mouri et al. (1994), we find that the measured 1-0 S(0)/1-0 S(1) (0.33 ± 0.1) and the 2-1 S(1)/1-0 S(1) (<0.2) line ratios in LkHα 264 are consistent with thermal emission of a gas cooler than 2000 K. If the distribution of errors is assumed Gaussian, then a 3σ error of 0.1 in the 1-0 S(0)/1-0 S(1) ratio implies that there is a 90% probability that 1-0 S(0)/1-0 S(1) > 0.28. Therefore, the most likely scenario is that the H_2 emitting gas is at a temperature cooler than 1000 K and that the H_2 is thermally excited by UV

photons[5]. LkHα 264 is also an X-ray source (Hearty et al. 2000). Nevertheless, given the line 1-0 S(0)/1-0 S(1) ratio measured, the probability that the heating mechanism is X-ray excitation is less of 1% (1-0 S(0)/1-0 S(1) < 0.23). The conclusion that the H_2 observed emission is very likely due to UV-photons is supported by the fact that LkHα 264 has a strong UV excess ($U - V = -0.46$, Bastian & Mundt 1979).

5.4.2 The inclination of the disk around LkHα 264

The spectral resolution of CRIRES ($\approx$ 6.6 km s^{-1}) and the thermal width of a 1500 K line ($\approx$ 2.4 km s^{-1}) are significantly smaller than the FWHM of 20 km s^{-1} of the H_2 lines observed in LkHα 264. Therefore, the line width must be linked to the dynamics of the gas in the region that is emitting the line. If the molecular hydrogen emission in LkHα 264 originates in a disk, the shape of the line allows us to constrain the region where the emission is produced if the inclination is known, or to constrain the inclination of the disk if the region where the emission is produced is given.

Implementing the two-layer Chiang and Goldreich (1997) disk model code CG plus (Dullemond et al. 2001), we modeled the disk around LkHα 264. As inputs for the model we used, a disk without a puffed-up inner rim with an inner truncation radius at T = 3000 K, a disk size of 250 AU, a mass of 85 M_J, a density power law factor of -1.5 and a luminosity of 0.53 $\log(L/L_\odot)$ for LkHα 264. The luminosity was determined from the spectral type K5V (T_{eff} = 4350 K), using a distance of 300 pc, a V magnitude of 12 mag, an extinction A_V = 0.5 mag (Itoh et al. 2003) and a bolometric correction of -0.72 (Kenyon and Hartmann, 1995). We found that the regions of the disk with a surface layer at $T_s < 1500$ K are located at $R > 0.1$ AU.

Prescribing a mass of 0.8 $M_\odot$ for LkHα 264 (found by its location in the HR diagram employing the evolutionary tracks of Palla and Stahler 1993), an H_2 emitting region from 0.1 to 10 AU, and assuming that the intensity I of the H_2 line is described by a power law according to the radius $I_{H_2}(R) = I_0\ R^\alpha$ (α being a negative number) we calculated the expected line profile produced by the inclined disk. We proceed as follows. Suppose there is a parcel of gas situated at a radius R of width dR and angular size dθ that emits a line intensity $I_{H_2}(R)$ with a profile ϕ_ν, in a disk inclined at an angle i surrounding a star of mass $M_\star$ at a distance D from the Earth. The doppler shift $\Delta\nu$ of a line at frequency ν_0 emitted by the parcel of fluid is given by

$$\Delta\nu = \frac{\nu_0\ sin(\theta)sin(i)}{c}\sqrt{\frac{GM_\star}{R}}, \tag{5.2}$$

with c being the speed of light. Assuming that the line profile ϕ_ν is gaussian, the doppler shifted line profile $\phi_{\nu\ \mathrm{shifted}}$ emitted by the parcel of fluid is

$$\phi_{\nu\ \mathrm{shifted}} = \frac{1}{\sigma_\nu\sqrt{\pi}} e^{\left(\frac{\nu-\nu_0+\Delta\nu}{\sigma_\nu}\right)^2}, \tag{5.3}$$

where $\sigma_\nu = (\nu_0/c) * \mathrm{FWHM}/\left(2\sqrt{\ln 2}\right)$. The FWHM (in km s^{-1}) in strict terms is the thermal broadening of the line, however, for the purpose of calculating of the observed profile by the instrument, we assumed the FWHM to be the resolution of the spectrograph (in our case 6.6 km

[5]Itoh et al. (2003) employing upper limits to the 1-0 S(0) emission suggested that the 1-0 S(0)/1-0 S(1) is smaller than 0.26 for LkHα 264. We detect the 1-0 S(0) line and find that most likely this line ratio is higher than 0.28.

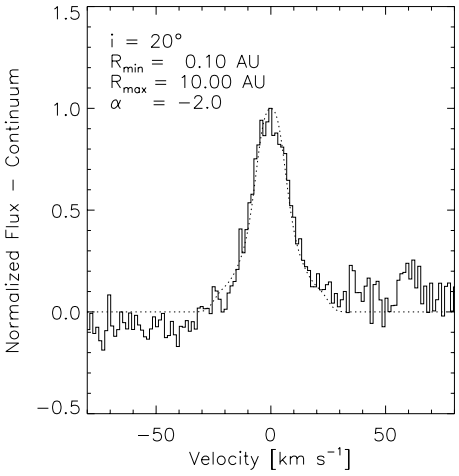

Figure 5.2: *Best model fit for the H_2 ν 1 − 0 S(1) line detected in LkHα 264 assuming that the emission originates in a circumstellar disk. $R_{\rm min}$ and $R_{\rm max}$ are the inner and outer radius of the emitting region. α is the power law exponent of the intensity $I(R) \propto R^{\alpha}$.*

s^{-1}). The flux emitted by the parcel of fluid is therefore

$$dF_{\rm H_2}(R,\theta) = I_{\rm H_2}(R)\,\phi_{\nu\ \rm shifted}\,\frac{R\,dR\,d\theta}{D^2}, \tag{5.4}$$

and the total emitted line flux is the sum of the contributions of all the fluid parcels

$$F_{\nu\ \rm H_2} = \int_{R_{min}}^{R_{max}} \int_0^{2\pi} dF_{\rm H_2}. \tag{5.5}$$

Here, R_{min} and R_{max} are the inner and outer radius of the region responsible for the emission. For our calculation we assumed that R_{min} = 0.1 AU, R_{max} = 10 AU, I_0 = 1 and D = 300 pc. The results are weakly dependent on the selection of a larger R_{max} since the intensity I decreases rapidly as a function of radius. R_{min} is 0.1 because is the radius at witch the temperature starts to be cooler than 1500 K in the surface of the LkHα 264 disk. The resulting synthetic line profile was scaled in such way that the peak flux of the synthetic line is equal to the peak flux of the line (minus continuum) observed. The α exponent of the intensity as a function of radius was assumed to be equal to -3, -2 and -1 for each set of models.

With the inclination i being the only free parameter, we manually changed its value for each value of α until we found a good fit for the line. If the inclination selected was too large, a double peaked profile was obtained, if it was too small, the velocity wings and the width of the line obtained were too narrow. Thus, only a small interval of inclinations fit the line profile for each value of α. We found that for reproducing the observed line profile, the inclination of the disk should be close to face-on, from 8° to 35° for α power law exponents ranging from -3 to -1 respectively. In Figure 5.2 we present the best fit found: an inclination of 20° and $\alpha = -2$.

Table 5.4: *Physical properties of classical T Tauri stars in which a search was done for H_2 $\nu = 1-0$ S(1) emission.*

Star	Class	Sp.T.	EW Hα [Å]	A_V [mag]	$(U-V)_{obs}$ [mag]	$(U-V)_{dered}$ [mag]	$(U-V)_{ex}$ [mag]	log L_X [erg s^{-1}]	M_{disk} [M_J]	Ref. H_2
				Detections						
LkHα 264	CTTS	K5 Ve	85	0.52	-0.46	-0.74	-2.92	29.7	85[q]	1,2
TW Hya	CTTS	K7 Ve	220	0.18[a]	0.86	0.8[a]	-1.8[a]	30.3	1.4[r]	3
GG Tau Aa	CTTS	K7 Ve	40	3.20[a]	2.73	1.0[a]	-1.6[a]	29.4	290[p]	3,6
GG Tau Ab	CTTS	M0.5 Ve	40	0.72[a]	1.42	1.0[a]	-1.5[a]	29.4	290[p]	3,6
LkCa 15	CTTS	K5 Ve	13	0.64	1.98[a]	1.6[a]	-0.5[a]	<29.6[e]	10[s]	3,6
AA Tau[b]	CTTS	K7-M0 Ve	37	0.93	0.9[c]	0.4	-2.2[d]	29.6[e]	21[p]	6
CW Tau[b]	CTTS	K3 Ve	135	2.34	1.46[c]	0.15	-1.65	30.5[l]	<15[p]	6
UY Aur[b]	CTTS	K7 Ve	73	1.05	0.92[f]	0.33	-2.18	<29.4[e]	0.9[t]	6
GM Aur[b]	CTTS	K7-M0 Ve	97	0.14	1.5[g]	1.4	-1.2[d]	<29.7[e]	60[p]	6
CS Cha	CTTS	K5 Ve	13	0.06[i]	1.72[i]	1.68	0.49	30.2[v]	21[w]	7
ECHA J0843.3-7905	CTTS	M3.2 Ve[x]	111[z]	<0.1[ac]	[ad]	...	...	<28.5[aa]	[ae]	8
				Non-Detections						
CD -33°7795	CTTS	M1.5Ve	15[m]	0.07[n]	2.39[n]	2.35	-0.33	30.6	<0.1[u]	5
IP Tau	CTTS	M0 Ve	30	...[y]	2.04[y]	2.04[y]	0.63	29.5	5[t]	3
IQ Tau[b]	CTTS	M0.5 Ve	8	0.77	0.93	0.49	-2.17	<29.5	40[p]	3
V836 Tau	CTTS[h]	K7 V	9[h]	0.71[i]	2.71[i]	2.31	-0.21	29.8	40[t]	3
RECX 5	CTTS	M4.0 Ve[x]	9[z]	<0.1[ac]	[ad]	...	...	29.0[ab]	[ae]	8
RECX 9	CTTS	M4.5 Ve[x]	12[z]	<0.1[ac]	[ad]	...	...	28.4[ab]	[ae]	8

References : (1) Carmona et al. 2007 (this work); (2) Itoh et al. (2003b); (3) Bary et al. (2003); (4) Bary et al. (2002); (5) Weintraub et al. (2000); (6) Shukla et al. (2003); (7) Weintraub et al. (2005); (8) Ramsay Howat & Greaves (2007).
Notes: [a] Average value from Table 5 of Bary et al. (2003); [b] Spectral Type, Hα EW and A_V from Cohen & Kuhi (1979); [c] Varsavsky (1960); [d] Average between the excess of the two spectral types; [e] Neuhäuser et al. (1995); [f] Mendoza (1966); [g] Bastian & Mundt (1979); [h] Given the Hα EW by Herbig & Bell (1988), we classified the source as CTTS ; [i] Herbig & Bell (1988); [j] Quadruple system (Soderblom et al. 1998); [k] Mermilliod (1986); [l] XEST data by Güdel et al. (2007); [m] Craig et al. (1997); [n] Gregorio-Hetem et al.(1992); [p] Beckwith et al. (1990); [q] Itoh et al. (2003b); [r] Weinberger et al. (2002); [s] Qi et al. (2003); [t] Osterloh & Beckwith (1995); [u] Jayawardhana et al. (1999), Weinberger et al. (2004) and Uchida et al. (2004) do not find evidence for infrared excess in the source, here we adopt the lower limit on the disk's masses of Osterloh & Beckwith (1995) as upper limit for the disk's mass. [v] Costa et al. (2000); [w] Lommen et al. (2007); [y] ROTOR data (Grankin et al. 2007) gives an E($B-V$) of -0.74 which is more than a magnitude off from that of Herbig & Bell (1988). Maybe there is some long-term evolution of this system that changes its colors on a long time scale. We worked with the $U-V$ ROTOR color but did not correct for redenning when calculating the $U-V$ excess; [x] Luhman & Steeghs (2004); [z] Jayawardhana et al. (2006); [aa] Lawson et al. (2002); [ab] Mamajek et al. (1999); [ac] Lyo et al. (2004); [ad] No U photometry published; [ae] No 1.3 mm continuum flux published.

5.4.3 H_2 NIR ro-vibrational emission in LkHα 264 and other T Tauri disks

The interest of measuring the H_2 in disks is high. It is crucial to constrain the properties of the gas in the terrestrial planet forming region of the disk. However, the detections of ro-vibrational H_2 emission from disks are relatively scarce compared to the large number of pre-main-sequence stars with gas-rich disks that are known. So far the ν =1-0 S(1) line has been detected in few classical T Tauri stars (CTTS): TW Hya, GG Tau A, LkCa 15 (Weintraub et al. 2000, Bary et al. 2002, 2003), AA Tau, CW Tau, UY Aur, GM Tau (Shukla et al. 2003), CS Cha (Weintraub et al. 2005), ECHAJ0843.3-7905 (Ramsay Howat & Greaves 2007) and LkHα 264 (Itoh et al. 2003, Carmona et al. 2007), and in four weak-lined T Tauri stars (WTTS): DoAr 21 (Bary et al. 2003), V773 Tau (Shukla et al. 2003), Sz33 and Sz 41 (Weintraub et al. 2005). Our CRIRES observations show for the first time the simultaneous detection of the $\nu = 1-0$ S(1) and $\nu = 1-0$ S(0) H_2 emission from a protoplanetary disk. Since the detections are not very numerous, it would be useful to know if the T Tauri stars with detected H_2 near-infrared ro-vibrational emission are peculiar objects.

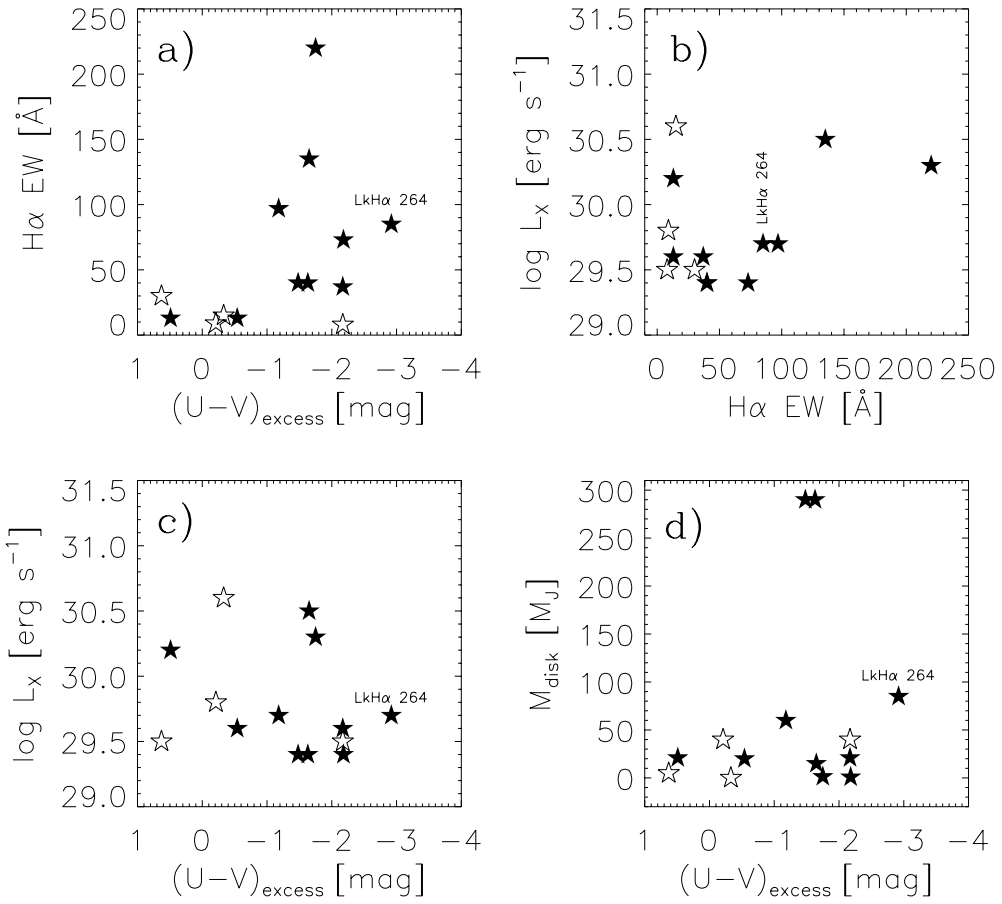

Figure 5.3: *Physical properties of classical T Tauri stars in which a search was done for the H_2 $\nu = 1-0$ S(1) line. Filled stars represent detections, non-filled stars represent non-detections. (a) Hα Equivalent Width versus $(U-V)_{\rm excess}$. (b) logL_X [erg s^{-1}] versus Hα Equivalent Width. (c) logL_X [erg s^{-1}] versus $(U-V)_{\rm excess}$. (d) M_{disk} versus $(U-V)_{\rm excess}$.*

In the case of H_2 emission detected in WTTS, DoAr 21 and V773 Tau are among the brightest X-ray WTTS (see Table 1 and 4 of Bary et al. 2003 and for V773 Tau the XEST data of Güdel et al. 2007)[6].

In the case of CTTS, such a correlation is not apparent. In Table 5.4, we summarize some important physical properties of the CTTS in which a search was done for H_2 $\nu = 1-0$ S(1) emission[7]. We list properties related to the accretion process such as the Hα emission EW and the

[6]log L_X of V773 Tau is 31.0 erg s^{-1}. The star is a quadruple system (Duchême et al. 2003). The K-type binary is is expected to widely dominate in X-rays (Audard, private communication).

[7]At the time of writing, non-detections have been only reported in Weintraub et al. (2000) and Bary et al. (2003). In

$U-V$ excess. In addition, we present the X-ray luminosity and the disk's mass deduced from mm observations reported in the literature. For the calculation of the $U-V$ excess, we first determined the $U-V$ dereddened color employing the visual extinction A_V assuming an interstellar medium extinction law ($A_U = 1.56A_V$). Thereafter we subtracted from the $U-V$ dereddened color the $U-V$ color intrinsic to the spectral type of the source by Johnson (1966). In the case of multiple spectral types for a source, we selected their average value.

With the intention of unveiling empirical correlations between the physical properties of the sources and the detectability of the H_2 $\nu = 1-0$ S(1) line, employing the data collected in Table 5.4, we created a series of plots relating the physical properties of the sources (see Figure 5.3).

Two possible mechanisms of excitation have been proposed as responsible for the H_2 emission in disks: X-ray and UV excitation. We observe in Figure 5.3 (panels b and c) that in the case of the CTTS there is no clear correlation between the X-ray luminosity and the detectability of the H_2 line. We have sources with faint X-ray luminosity and H_2 detections (e.g. CW Tau) and sources with relatively high X-ray luminosity but without H_2 detections (e.g. CD -33°7795)[8]. In addition, in several sources with X-ray luminosities smaller than that of V836 Tau (a non-detection) the H_2 line has been detected. We conclude that X-ray excitation could play a role in the heating of the gas, but that in the case of CTTS studied so far, it seems to not be the dominant factor in the excitation of H_2 emission.

The second source for the excitation of H_2 emission is UV photons. UV photons are produced in large quantities during the accretion process. The $U-V$ excess and the Hα emission are considered standard signatures of accretion in T Tauri stars. In Figure 5.3a we show the H_α EW vs the $U-V$ excess. We observe that the higher the $U-V$ excess and the stronger the Hα line are, the higher the number of sources with H_2 detections. The non-detections are situated in the area of small H_α EW and low $U-V$ excess. *This result suggests that the higher the accretion rate in the systems is, the higher the probability of exhibiting the $\nu = 1-0$ S(1) H_2 line* . For example the only object exhibiting H_2 2.12 μm emission in the η Chamaeleontis cluster is ECHA J0843.3-7905, a source with strong Hα emission and high accretion rate ($10^{-9} M_\odot$ yr^{-1}, Lawson et al. 2004). We should note that there are detections of the H_2 line in two objects (CS Cha and LkCa 15) that are located in the region of the Hα vs $U-V$ excess diagram where three non-detections are situated. In the case of CS Cha, the cause of the emission is probably the high X-ray luminosity. However, in the case of LkCa 15 another mechanism should be responsible for the H_2 emission, as this source has only an upper limit for the X-ray luminosity. It is also interesting to realize that there is a non-detection in a source (IQ Tau) that has a strong $U-V$ excess. However, IQ Tau exhibits a very small Hα EW.

Our CRIRES target, LkHα 264, is one of the sources with the strongest $U-V$ excess in the sample. With respect to other physical characteristics (H_α EW, disk mass and X-ray luminosity), LkHα is a "normal" source. Therefore, it is likely that in LkHα 264 UV photons are chiefly responsible for the H_2 emission. This conclusion is supported independently by the measured 1-0 S(0)/1-0 S(1) and 2-1 S(1)/1-0 S(1) line ratios as previously discussed.

Concerning the disk mass and the detectability of the H_2, there is no apparent correlation

the cases of the observations by Shukla et al. (2003) and Weintraub et al. (2005) only the names of the stars in which H_2 was detected are published.

[8]Note that in the case of CD -33°7795, it could be argued that there is no detection because there is no disk: this source does not show infrared excess (Jayawardhana et al. 1999; Weinberger et al. 2004; Uchida et al. 2004). However the source does exhibit Hα in emission Craig et al. (1997) and $U-V$ excess.

between them. H_2 detections and non-detections are present in the disk mass range from 1 to 40 M_J. In summary, LkHα 264 and the CTTSs in which H_2 emission has been detected share typical physical properties of classical T Tauri stars. Therefore, in the near future, we expect to see more detections of the H_2 near-infrared lines to come out of high-resolution spectrographs on a routine basis.

5.4.4 49 Cet disk

Optical spectroscopy of 49 Cet basically shows the spectrum of an A-type main sequence star. 49 Cet does not exhibit Hα in emission, and does not present UV excess in its Spectral Energy Distribution (SED). 49 Cet, therefore, is very likely not accreting. In the JHK bands the colors of 49 Cet do not differ significantly with respect to the JHK colors of an A1V star. However, in the mid- and far-infrared (i.e 25, 60 and 100 μm) 49 Cet exhibits emission in excess of photospheric levels, thereby revealing the existence of a circumstellar disk. Recent analysis of sub-arcsec mid-infrared imaging of 49 Cet by Wahhaj et al. (2007) suggests that the bulk of the mid-infrared emission comes from very small grains ($a \sim 0.1$ μm) confined between 30 and 60 AU from the star, and that most of the non-photospheric flux is radiated by an outer disk of large grains ($a \sim 15$ μm) of inner radius $\sim$ 60 AU and outer radius 900 AU. In their analysis Wahhaj et al. (2007) conclude that the most likely scenario is that the inner 20 AU is strongly depleted of dust.

Zuckerman and Song (2004) proposed an age of 20 Myr for 49 Cet, an age in which the gaseous disk is expected to have already dissipated. However, Zuckerman et al. (1995) and Dent et al. (2005) observed CO $J = 2-1$ and $J = 3-2$ emission towards 49 Cet, thereby revealing the existence of a reservoir of cold gas. Dent et al. (2005) modeled the double peaked CO $J = 3-2$ emission and proposed that the line is emitted from a compact disk of outer radius ~17 AU inclined at 16^o or a disk of outer radius ~50 AU but inclined at 35^o. Thi et al. (2001) claimed the detection of the pure rotational 0-0 S(0) H_2 emission at 28 μm in 49 Cet, but recent more sensitive *Spitzer* IRS observations by Chen et al. (2006) did not confirm the detection of the line.

The detection of CO emission in the sub-mm and the apparent existence of a dust gap in the interior of the 49 Cet disk pose the question whether gas still exists within the inner disk (R < 20 AU). The upper limit on the flux of the H_2 ro-vibrational lines in 49 Cet derived from our CRIRES data set stringent constraints on the amount of hot gas in the inner disk of 49 Cet (R < 1 AU): 49 Cet has less than a tenth of lunar mass of gas at T~1500 K. Our observations give additional support to the hypothesis that the disk of 49 Cet has an inner hole. The lack of H_α in emission and the non-detection of pure rotational and ro-vibrational emission of warm and hot H_2 in 49 Cet indicate that 49 Cet may have an inner hole in gas as well. This result supports the idea that gas and dust are dissipated on the same time scale in the inner disk (Sicilia-Aguilar et al. 2006), and is strongly suggestive that the disk disappears inside-out.

One interesting question to address is the possible mechanism of disk dissipation. It has been suggested (Alexander et al. 2005, 2006) that inside-out photoevaporation occurs very rapidly in a time scale of a few 10^5 years once the phenomenon is triggered after a disc life time of few million years. A challenge to this scenario is the presence of CO in the outer disk. Once the photoevaporation starts in the inner part of the disk, the entire gaseous disk should dissipate in a very short time frame as well (Alexander et al. 2006). Therefore, one puzzling aspect in this scenario is the reason why the outer gas remains in the system. An alternative scenario is to assume the presence of a sub-stellar companion to explain the lack of gas in the inner disk.

This explanation has the advantage that formation of a gas rich outer disk is a natural outcome of the planet formation process. Giant planets are thought to form in the inner 20 AU of the disk and the outer disk disappears later once the planets have been formed. We note that indications for the presence of a planet in a disk, as required for this scenario, have recently been found in a precursor of a 49-Cet type star, the Herbig Ae/Be star HD 100456 (Acke & van den Ancker 2006). The existence of low mass companion(s) as an explanation for the lack of gas and dust in the inner disk of 49 Cet is a suggestive idea that, given the relative closeness of the target ($d \sim 61$ pc), it will be possible to test with future high-contrast imaging facilities such as SPHERE at ESO-VLT.

5.5 Conclusions

We observed the classical T Tauri star LkHα 264 and the debris disk 49 Cet and searched for ro-vibrational $\nu = 1-0$ S(1) H_2 emission at 2.1218 μm, $\nu = 1-0$ S(0) H_2 emission at 2.2233 μm, and $\nu = 2-1$ S(1) H_2 emission at 2.2477 μm, using CRIRES ($R \sim 6.6$ km s^{-1}) at ESO-VLT. We confirmed the detection of the $\nu = 1-0$ S(1) H_2 line in LkHα 264 at the rest velocity of the star. The line found has a flux of 3.0×10^{-15} ergs cm^{-2} s^{-1}, and a FWHM of 20.6 km s^{-1}. In addition, the enhanced sensitivity of CRIRES allowed the observation of the previously undetected $\nu = 1-0$ S(0) H_2 line in LkHα 264. The line has a flux of 1.0×10^{-15} ergs cm^{-2} s^{-1}, and a FWHM 19.8 km s^{-1}. The very similar FWHM of the two H_2 lines detected suggests that the emitting gas is located in similar regions in the disk. Both lines are spatially unresolved. The measured mean PSF's FWHM ($\approx$ 0.36") in the H_2 1-0 S(1) spectrum indicates that the H_2 emitting region is located in the inner 50 AU of the disk assuming a distance of 300 pc for LkHα 264. The measured 1-0 S(0)/1-0 S(1) (0.33 $\pm$ 0.1) and the 2-1 S(1)/1-0 S(1) (<0.2) line ratios in LkHα 264 indicate that the H_2 emitting gas is at a temperature lower than 2000 K and that the H_2 is most likely thermally excited by UV photons. The measured line ratios suggest that X-ray excitation plays only a minor role in the heating of the emitting H_2 in LkHα 264. The flux of the $\nu = 1-0$ S(1) H_2 line in LkHα 264 implies that there are a few lunar masses of hot H_2 gas in the inner disk of LkHα 264. The $\nu = 1-0$ S(1) H_2 line in LkHα 264 is single peaked. Modeling of the $\nu = 1-0$ S(1) line shape indicates that the disk is close to face-on ($i < 35^{\circ}$). The best model fit suggests that the disk of LkHα 264 is inclined 20°, for an H_2 emitting region extending from 0.1 to 10 AU with a power law relation of the intensity as a function of radius with exponent $\alpha = -2$.

A comparative analysis of the physical properties of classical T Tauri stars in which the H_2 $\nu = 1-0$ S(1) line has been detected versus non-detected shows that there is a higher chance of observing the H_2 near-infrared lines in CTTS with a high $U-V$ excess and a strong Hα line. This result suggests that there is a higher probability of detecting the H_2 $\nu = 1-0$ S(1) line in systems with high accretion. In contrast to weak-lined T Tauri stars, there is no apparent correlation between the X-ray luminosity and the detectability of the H_2 $\nu = 1-0$ S(1) line in classical T Tauri stars. Taken as a group, LkHα 264 and the CTTS in which the H_2 emission has been detected exhibit typical properties of classical T Tauri stars. Therefore, we expect NIR ro-vibrational H_2 lines from T Tauri disks to be detected on a routine basis in the near future.

The non-detection of any of the three H_2 lines in 49 Cet puts stringent constraints on the amount of gas in the inner disk. From the upper limit for the flux of the $\nu = 1-0$ S(1) H_2 line we deduced that less than a tenth of lunar-mass of gas is present in the inner 1 AU of the disk surrounding 49 Cet. The lack of H_2 ro-vibrational emission in the spectra of 49 Cet, combined

with non detection of pure rotational lines of H_2 (Chen et al. 2006) and the absence of Hα emission suggest that the gas in the inner disk of 49 Cet has dissipated. These results together with the previous detection of ^{12}CO emission at sub-mm wavelengths (Zuckerman et al. 1995; Dent et al. 2005) point out that the disk of 49 Cet should have a large inner hole, and it is strongly suggestive of theoretical scenarios in which the disk disappears inside-out. We favor inner disk dissipation by inside-out photoevaporation, or the presence of an unseen low-mass companion(s) as most likely explanations for the lack of warm gas in the inner disk of 49 Cet.

Acknowledgements. This research has made use of the SIMBAD database operated at CDS, Strasbourg, France. A.C. would like to thank R. Mund for helpful discussions concerning outflows in T Tauri stars, M. Audard for kindly providing XEST X-ray luminosities of several sources, G. van der Plas for calculations of the rotational broadening of absorption lines, and C. Fallscheer for comments to the manuscript. Special thanks to the CRIRES science-verification team for executing the observations in Paranal and for their support in the data-reduction process.

5.6 References

Acke, B., & an den Ancker, M. E. 2006, A&A, 449, 267
Alexander, R.D., Clarke, C.J., Pringle, J.E.,MNRAS, 358, 283
Alexander, R.D., Clarke, C.J., Pringle, J.E.,MNRAS, 369, 229
Bary, J. S., Weintraub, D. A., & Kastner, J. H. 2002, ApJL, 576, L73
Bary, J. S., Weintraub, D. A., & Kastner, J. H. 2003, ApJ, 586, 1136
Bastian, U., & Mundt, R. 1979, A&AS, 36, 57
Beckwith, S. V. W., Sargent, A. I., Chini, R. S., & Guesten, R. 1990, AJ, 99, 924
Bockelé-Morvan, et al. 1995, in Circumstellar Dust Disks and Planet Formation, ed. R. Ferlet & A. Vidal-Madjar (Gif sur Yvette: Editions Frontiéres).
Carmona, A., van den Ancker, M. E., Thi, W.-F., Goto, M., & Henning, T. 2005, A&A, 436, 977
Chen, C. H., et al. 2006, ApJS, 166, 351
Chiang, E. I., & Goldreich, P. 1997, ApJ, 490, 368
Cohen, M., & Kuhi, L. V. 1979, ApJs, 41, 743
Costa, V. M., Lago, M. T. V. T., Norci, L., & Meurs, E. J. A. 2000, A&A, 354, 621
Cox, A. N. 2000, Allen's astrophysical quantities, 4th ed. Publisher: New York: AIP Press Springer, 2000. Edited by Arthur N. Cox.
Craig, N., Christian, D. J., Dupuis, J., & Roberts, B. A. 1997, AJ, 114, 244
Dent, W. R. F., Greaves, J. S., & Coulson, I. M. 2005, MNRAS, 359, 663
Duchêne, G., Ghez, A. M., McCabe, C., & Weinberger, A. J. 2003, ApJ, 592, 288
Dullemond, C. P., Dominik, C., & Natta, A. 2001, ApJ, 560, 957
Gregorio-Hetem, et al. 1992, AJ, 103, 549
Grankin, K. N., et al. 2007, A&A, 461, 183
Greene, T. P., & Lada, C. J. 2002, AJ, 124, 2185
Güdel, M., Padgett, D. L., & Dougados, C. 2007, in Protostars and Planets V., Edited by B. Reipurth, D. Jewitt, and K. Keil. University of Arizona Press, Tucson, 2007
Hearty, T., Hernández, M., Alcalá, J. M., Covino, E., & Neuhäuser, R. 2000, A&A, 357, 681
Herbig, G. H., & Bell, K. R. 1988, Lick Observatory Bulletin, Santa Cruz: Lick Observatory
Itoh, Y., et al. 2003, ApJL, 586, L141

Itoh, Y., Sugitani, K., Ogura, K., & Tamura, M. 2003b, PASJ, 55, L77
Jayawardhana, R., et al. 1999, ApJL, 521, L129
Jayawardhana, R., et al. 2001, ApJL, 550, L197
Jayawardhana, R., et al. 2006, ApJ, 648, 1206
Johnson, H. L. 1966, ARA&A, 4, 193
Käufl, H.U. et al. 2004, SPIE, 5492, 1218
Kenyon, S. J., & Hartmann, L. 1995, ApJS, 101, 117
Lawson, W. A., et al. 2002, MNRAS, 329, L29
Lawson, W. A., et al. 2004, MNRAS, 351, L39
Lommen, D., et al. 2007, A&A, 462, 211
Luhman, K. L., & Steeghs, D. 2004, ApJ, 609, 917
Lyo, A.-R., et al. 2004, MNRAS, 347, 246
Mamajek, E. E., Lawson, W. A., & Feigelson, E. D. 1999, ApJL, 516, L77
Mendoza V., E. E. 1966, ApJ, 143, 1010
Mermilliod, J. C. 1986, Bulletin d'Information du Centre de Donnees Stellaires, 31, 185
Neuhaeuser, et al. 1995, A&A, 297, 391
Osterloh, M., & Beckwith, S. V. W. 1995, ApJ, 439, 288
Palla, F., & Stahler, S. W. 1993, ApJ, 418, 414
Qi, C., Kessler, J. E., Koerner, D. W., Sargent, A. I., & Blake, G. A. 2003, ApJ, 597, 986
Ramsay Howat, S. K., & Greaves, J. S. 2007, ArXiv e-prints, 705, arXiv:0705.4601
Richter, M. J., Jaffe, D. T., Blake, G. A., & Lacy, J. H. 2002, ApJL, 572, L161
Rydgren, A. E., & Vrba, F. J. 1981, AJ, 86, 1069
Sako, S., et al. 2005, ApJ, 620, 347
Sicilia-Aguilar, et al. 2006, AJ, 132, 2135
Sheret, I., Ramsay Howat, S. K., & Dent, W. R. F. 2003, MNRAS, 343, L65
Shukla, S. J., Bary, J. S., Weintraub, D. A., & Kastner, J. H. 2003, Bulletin of the American Astronomical Society, 35, 1209
Soderblom, D. R., et al. 1998, ApJ, 498, 385
Straižys, ernis, K., Kazlauskas, A., & Laugalys, V. 2002, Baltic Astronomy, 11, 231
Thi, W. F., et al. 2001, ApJ, 561, 1074
Uchida, K. I., et al. 2004, ApJs, 154, 439
Varsavsky, C. M. 1960, ApJ, 132, 354
Wahhaj, Z., Koerner, D. W., & Sargent, A. I. 2007, arXiv:astro-ph/0701352
Weinberger, A. J., et al. 2002, ApJ, 566, 409
Weinberger, A. J., Becklin, E. E., Zuckerman, B., & Song, I. 2004, AJ, 127, 2246
Weintraub, D. A., Kastner, J. H., & Bary, J. S. 2000, ApJ, 541, 767
Weintraub, D. A., Bary, J. S., Kastner, J. H., Shukla, S. J., & Chynoweth, K. 2005, Bulletin of the American Astronomical Society, 37, 1165
Zuckerman, B., Forveille, T.,& Kastner, J.H. 1995, Nature, 373, 494
Zuckerman, B., & Song, I. 2004, ApJ, 603, 738

Chapter 6

Conclusion and Perspectives

The discovery of excess of infrared emission over photospheric levels in young-stellar objects, that took place more than two decades ago, opened the way for observational studies of protoplanetary disks. Since then we have considerably advanced the observational understanding of these disks by the study of dust emission. However, it is undoubtedly frustrating that the molecular gas, the chief constituent of the disk, escaped observational scrutiny. The increased sensitivity and spatial resolution of (sub)-mm telescopes in the early nineties allowed the study of the cold gas in the outer disk ($R > 50$ AU). Those studies empirically demonstrated that disks are indeed disks, that they are rotating, and opened the basis for the study of the disk's chemistry. Unfortunately, we believe that in the outer disk a planet can hardly form. A new technological development, the advent of a new generation of high-resolution infrared spectrographs in the late nineties, opened the possibility of studying the warm gas in the inner disk, the region in which we believe planets form. Motivated by the beginning of operations of VISIR [1] and the expected arrival of CRIRES[2], we decided in fall 2003 to dedicate my PhD thesis to the undertaking of the first steps in the exploitation of this new instrumentation, and study the gas in the disks of nearby southern Herbig Ae/Be stars and T Tauri stars. At the end of this adventure, it is now time to summarize what we learned during the project, to describe open questions in the field, and discuss the possibilities that present and future instrumentation offer for the study of gas in disks.

In our first project, the search for CO 4.7 μm ro-vibrational emission with ISAAC, the non-detections of the lines and the stringent upper limits to line fluxes derived, suggested that Herbig Ae/Be stars, despite their similarities in dust emission, are not a homogenous group concerning inner disk gas properties. Recent efforts with NIRSPEC at Keck[3] and CSHELL at NASA IRFT[4] reveal an increasing of number of Herbig Ae/Be and T Tauri stars exhibiting CO 4.7 μm emission. Larger samples are helpful to start the deduction of definitive conclusions concerning the frequency of CO 4.7 μm emission in young stellar objects and, most importantly, about the way in which warm CO emission correlates with the physical properties of the disk and its central star. In this respect, important progress needs to be done in the theoretical area. So far, most of the analysis has been concentrating on the construction of rotational diagrams, the deduction of excitation temperatures of the gas and fitting of double peaked profiles for constraining the disk inclination. However, more advanced modeling is required to better analyze the observations and deduce meaningful constraints in structure in the inner disk.

In the area of the study of CO 4.7 μm emission from disks, an important step was done recently by combining the power of high resolution-spectroscopy and the enhanced spatial resolution of-

[1] ESO's new VLT mid-infrared high-resolution spectrograph
[2] ESO's new VLT near-infrared high-resolution spectrograph
[3] Brown et al. 2005. PPV conference poster.
[4] Brittain et al. 2007, ApJ, 659, 685.

fered by adaptive optics (AO). Goto et al. (2006)[5] using IRCS at Subaru observed the Herbig Ae star HD 141569 and spatially resolved the CO 4.7 μm emission. They found the wonderful doppler shifted, spatially resolved line profile characteristic of a disk in keplerian rotation. These kinds of studies need to be done in a larger number of sources in order to obtain a global picture of the gas dynamics in the regions where giant planets form. In this respect, CRIRES at ESO-VLT, with its high spectral resolution and AO equipment, is an invaluable tool for the study of protoplanetary disks, the advancement of knowledge, and the competitiveness of European Astronomy.

Moving on to our second project, FORS2 optical spectroscopy of close companions to Herbig Ae/Be stars. Our original aim was to probe the outer gas of disks of Herbig Ae stars by measuring absorption lines superimposed into the spectra of close visual "background" stars. The spectra revealed that in fact the close companions are young T Tauri stars, which are very likely physically associated with the Herbig primary. Given this discovery, the absorption lines detected could not be attributed unambiguously to the gas disks surrounding the primaries. This project gave us the invaluable experience of trying to obtain the spectra of a faint object close (ρ <1.5") to a very bright one. This endeavor proved to be challenging even for a 8 m class telescope. From this project I learned much about the practical riddles of spectra classification of young stellar objects and introduced me to the complex problem of the age determination of stars of early spectral types. This project taught us that multiplicity is a very serious thing to be addressed in future studies of planet formation. We live, if we can say, happily in our single star Solar System, but if we want to understand planet formation in context of the galaxy, we should perhaps start to add the multiplicity dimension to our studies.

Besides the fact that very few companions to Herbig Ae stars have been studied until now, in this project we found that the companions are older than the age that was previously attributed to the primary. Since it is very likely that the companion is coeval with the Herbig star primary, we argued that the age of the systems need to be higher than 7 Myr and one case even older than 10 Myr. This result confirms that disks can last longer than the canonical 5 to 6 Myr found in studies of clusters of young stellar objects, and invites us to investigate the influence that multiplicity has in the disk's life time. This project was a beautiful example of the scientific enterprise. We designed and performed an experiment aiming to answer one question, and we ended up discovering something new and opening many new questions awaiting an answer.

Concerning the future of the multiplicity studies in young stellar objects, I consider that the next step to be done after the numerous imaging surveys that have been published is to begin to perform follow-up statistical investigations of the way in which the physical properties of circumstellar (and circumbinary disks) are correlated with multiplicity. It would be great to find the answer to questions such as: does the separation and mass ratio influence the disk dissipation time scale in PMS binaries? does the disk dissipate in a similar time scale for both components? or alternatively, which component is more likely to retain its disk longer? is the accretion rate of the components of a binary star correlated with the mass ratio? how does the accretion rate evolve with time? do binaries present an accretion behavior different than that of single stars? at a given age, how does the dust evolution depend on the mass of the central object? are the dust properties of the circumstellar disk strongly affected by a close companion? and if so, how does this depend on the binary separation and mass ratio? what are the dynamics of the gas in the inner region of a close (separation <40 AU) binary system? Is the gas orbiting in Keplerian motion ? what fraction

[5]Goto et al. 2006, ApJ, 652, 758.

of debris disks and transitional objects are binary ? is this fraction higher for single stars?. Present instrumentation at any major observatory is able to provide the spatial resolution and sensitivity that is required to try to answer these questions observationally. There is a lot of room for progress in the study of multiplicity in young stellar objects.

Let us now move to our third project. The search of molecular hydrogen emission from nearby Herbig Ae/Be stars with VISIR. This project was aimed to probe the disk's gas mass in the zone where giant planets are expected to form. This measurement being of paramount importance to constrain planet formation scenarios, we invested a significant amount of effort and telescope time. We were allocated 44 hours in Period 76 (40% executed) and 4 extra hours in Period 78 to exploit the capabilities of VISIR to derive the first unbiased measurements of warm gas mass in the disk. We searched for H_2 pure-rotational emission at 12μm and 17μm in a sample of carefully selected nearby Herbig Ae stars. In each line we integrated one hour on source (almost two hours of real time), we took care of observing the targets at high velocity shift with respect to the atmospheric emission, and requested good atmospheric conditions for the observations to be executed. We also took the time to observe spectrophotometric calibration stars before and after each science exposure to obtain a good correction of the atmosphere. Finally, we employed VISIR, a state of the art high resolution mid-infrared spectrometer. In summary, we did, perhaps, the best we could to achieve the detection of MIR H_2 emission from disks. However, H_2 pure rotational emission is absent in the sources studied. The exquisite sensitivity of VISIR permitted to deduce the most stringent limits to the mass of optically thin warm gas of protoplanetary disks to date. The disks contain less than a few tenths of Jupiter mass of emitting H_2 at 150 K at most, and less than a few Earth masses of emitting gas at 300 K and higher temperatures. How this can be? why is the mass of optically thin H_2 gas so low?. These are excellent questions that plunged us in the modeling of the H_2 emission from disks.

Our very first calculations were done assuming that the disk inner regions are optically thin in the mid-infrared. In this case, disks were expected to have at least a few Jupiter masses of emitting warm gas. Since the observations constrained so tightly the amount of warm gas in the disk, a more detailed calculation was required. We employed the Chiang and Goldreich disk model, a two-layer optically thick disk model widely used for fitting spectral-energy distributions, to set the disk's structure and calculated the amount of H_2 thermal flux expected. In this disk model only the superheated surface layer emits. The interior layer is optically thick in dust and gas even at mid-infrared wavelengths. We found that the predicted line fluxes are of the order of $\sim 10^{-16}$ – 10^{-17} erg s^{-1} cm^{-2}, much smaller than the detection limits of our observations (0.4×10^{-14} erg s^{-1} cm^{-2}). The synthetic spectra also showed us that an improvement on the signal to noise of one order of magnitude to detect the H_2 0-0 S(1) line at 17μm (0.01 Jy in a continuum $\sim$ 20 Jy), and of three orders of magnitude to detect the H_2 0-0 S(2) line at 12μm (0.001 Jy in a continuum $\sim$ 17 Jy) are required. These results explained naturally our non-detections. They showed us that *if the two-layer approximation to the structure of the disk is correct, we are essentially "blind" to most of the warm H_2 in the disk because it is located in the optically thick interior layer*. In addition, we learnt that most of the flux of H_2 0-0 S(1) line at 17μm comes from a region located between 50 and 100 AU in Herbig Ae disks, and if we are to probe the giant planet formation region, we should aim to detect the H_2 0-0 S(2) line at 12 μm because most of this line is emitted around 10 AU . The same kind of models in T Tauri stars, showed us that the emission in these sources is one to two orders of magnitude fainter than in Herbig Ae disks. The good news is that in such sources, the H_2 0-0 S(1) line at 17μm probes a region around 10 AU.

If the thermal H_2 emission from the two-layer model is so faint, and if the emission only comes from the surface of the disk, this poses an interesting question is it hopeless to study mid-infrared H_2 emission from disks?, No. We have hopes. Firstly, thermal emission is the most pessimistic scenario. We know that the inner disk is irradiated by intense UV photons and X-rays. They can excite H_2 emission in the upper layers of the disk with flux levels much higher than thermal emission (for example recently MIR emission of hot H_2 has been observed towards the Herbig Ae star AB Aur). Secondly, naturally, the two-layer disk model is only an approximation of the real structure of a protoplanetary disk. The puffed-up inner rim, which could be an important contributor to the H_2 emission, is not included in our models, and in reality there will be a smooth transition zone between the disk's hot surface layer and the cool disk interior, which again could contribute significantly to the H_2 emission. Thirdly, protoplanetary disks are not optically thick all their life. When the rocky cores that will form future giant planets are formed and they are accreting the gas from the disk, the disk is expected to have evolved to an optically thin disk. Therefore, a rich ensemble of optically thin transition disks is awaiting a sensitive study of H_2 MIR emission. In addition, when a giant planet has been formed and it is migrating, it opens a gap where the disk could become optically thin, and H_2 emission from this region is expected. Finally, new missions such as the H_2 Explorer (H2EX) are expected to be launched in the future. High resolution (R ~20000) mid-infrared spectrographs in orbit, will not be constrained by the atmosphere emission problem that we face in ground MIR observations. Such space observatories will be able to study large samples of pre-main-sequence stars in clusters of different ages, and teach-us about the evolution of gas in disks as a function of time.

Let us move now to fourth project, the search for near-infrared H_2 emission from the T Tauri star LkHα 264 and the debris disk 49 Cet. This project was done in the frame of the science verification of the ESO's new near-infrared spectrograph CRIRES. Our aim was to test the instrument in a well known target in which the H_2 1-0 S(1) emission was already detected (LkHα 264) and explore H_2 emission in 49 Cet, a very interesting transitional disk. Lets start by discussing the case of LkHα 264. The previously reported H_2 1-0 S(1) emission at 2.1218 μm was successfully confirmed by our CRIRES spectra. In comparison to previous efforts, CRIRES was able to achieve a 12σ detection of the line using a relatively short exposure (60 s). But not only that, CRIRES was able to detect for the first time the H_2 1-0 S(0) line at 2.2233 μm from a disk. We attained a 3σ detection of a line of 1×10^{-15} erg s^{-1} cm^{-2} with a exposure time of 60 s in a source of K magnitude 8.9. In addition, our CRIRES observation set meaningful upper-limits to the H_2 2-1 S(1) line at 2.2477 μm. These results display the improvement achieved with high-resolution spectroscopy. From the the measured 1-0 S(0)/1-0 S(1) (0.33 ± 0.1) and the 2-1 S(1)/1-0 S(1) (<0.2) line ratios in LkHα 264, we learnt that the H_2 emitting gas is at a temperature lower than 2000 K and that the H_2 is most likely thermally excited by UV photons. The measured line ratios indicated us that X-ray excitation plays only a minor role in the heating of the emitting H_2 in LkHα 264. The H_2 FWHM of both lines measured is ~20 km s^{-1}, by modeling of the line profile shape we were able to constrain the inclination of the disk in LkHα 264 to be close to pole-on ($i < 35^{o}$). Finally, a comparative analysis of the physical properties of classical T Tauri stars in which stars in which a search was done for H_2 $\nu = 1-0$ S(1) line indicated that: (1) the presence of H_2 emission is correlated with the magnitude of the UV excess and the strength of the Hα line. (2) the CTTS in which H_2 emission has been detected share typical physical properties of classical T Tauri stars. Therefore, in the near future, *we expect to see more detections of the H_2 near-infrared lines to come out of high-resolution spectrographs on a routine basis*. H_2 NIR infrared emission from disk's is an

important tool for studying the gas in the terrestrial planet zone of protoplanetary disks. In the case of 49 Cet, a debris disk in which CO emission in the (sub)-mm revealed the presence of a cold gas reservoir, no emission was observed in any of the three H_2 observed lines. Our CRIRES observations allowed us to derive stringent limits to the mass of H_2 at $T \sim 1500$ K in the inner disk of 49 Cet, there is less than a tenth of a lunar mass in the inner disk of 49 Cet. The lack of H_2 ro-vibrational emission in the spectra of 49 Cet, combined with non-detection of pure rotational lines of H_2 and the absence of Hα emission suggest that the gas in the inner disk of 49 Cet has a gas inner hole. The study of gas NIR emission from disks is very promising for the coming years. However, for attaining meaningful conclusions the study of statistically representative samples is needed. Therefore, the combined effort of several facilities in large survey programs should be envisaged in the future.

Our ISAAC, CRIRES and VISIR projects taught us that a great amount of information can be learnt when the lines are detected, but also when meaningful limits are set to non-detections. For example, in the cases of H_2 emission in the MIR and CO emission at 4.7μm we learnt that the amount of optically thin warm gas in the disk must be small, otherwise the lines would have been detected. In the case of our CRIRES search for H_2 emission in the NIR, we learnt from the study of detection and non-detections of the H_2 $\nu = 1 - 0$ S(1) line in classical T Tauri stars, that the H_2 emission is correlated with accretion, but that there is no a clear correlation with the X-ray luminosity in contrast to weak lined T Tauri stars. In the case of 49 Cet, the thigh limits to the mass of hot gas in the disk show us that the disk most likely have an inner hole. In summary, *the combined analysis of detections and non-detections cases is required to understand the environment of sources studied and identify the most relevant physical processes behind an observational diagnostic*.

After having described the four projects that constitute this thesis, and having briefly discussed future perspectives in each of them, let us now discuss some additional possibilities for future studies of gas in disks. We discussed in the introduction, that Hα in emission is a very reliable indicator of gas in the disk. The width of this line (> 100km/s) reveals the presence of accretion. An important fraction of young sources without JHK excess have MIR infrared excess ($\lambda > 8\mu$m) and present accretion related Hα up to small EW (few Å). It would be interesting to survey Hα emission with high resolution optical spectroscopy, in a large unbiased sample of sources with and without JHK excess in clusters of different ages. The objective would be to deduce an independent disk's life time estimate from the gas. In the coming years, great advances will be achieved in (sub)-mm instrumentation. From space, the satellite Herschel will be operating very soon. Herschel will search for an important number of molecules from protoplanetary disks with an unprecedented sensitivity. The results of these observations will play a vital part in our understanding of the chemistry of protoplanetary disks. From the ground, it is foreseen in the near future to attain significant improvements in the sensitivity and spatial resolution. Planned updates of IRAM-Plateau de Bure Interferomenter, and the sub-mmm array (SMA) will allow to study in great detail the emission of cold gas in the outer disk. In a few years with the start of operations of the Atacama Large Millimeter Array (ALMA), we will be able to prove the cold gas in the mid-plane up to distances of 10 AU. ALMA observations of the disk's mid-plane combined with infrared diagnostics of the upper warm layers of the disk, would allow us for the first time to constraint observationally the structure of protoplanetary disk. A long list of exciting research is in front us, so, let's go and write some good proposals!

Acknowledgments

First of all, I would like to thank to my supervisors, Dr. Mario van den Ancker and Prof. Dr Thomas Henning, for their careful guidance during my PhD. Special thanks to Miwa Goto, Kees Dullemond and Yaroslav Pavlyuchenkov collaborators and friends for fruitful discussions and help during these years. My warmest thanks to my colleagues at ESO (Garching) and the MPIA (Heidelberg) for the wonderful time and support. I would like to acknowledge the staff at ESO; without their hard work, none of these observations would be possible.